https://dx.doi.org/10.1016/j.progpolymsci.2020.101289

An elegant coupling: Freeze-casting and versatile polymer composites

Jie Yang[a], Wei Yang[c,*], Wei Chen[a,b,*], Xiaoming Tao[a,*]

[a] Research Centre for Smart Wearable Technology, Institute of Textiles and Clothing, The Hong Kong Polytechnic University, Hung Hom, Kowloon, Hong Kong 999077, P. R. China

[b] The Hong Kong Polytechnic University Shenzhen Research Institute, Shenzhen 518057, P. R. China

[c] College of Polymer Science and Engineering, Sichuan University, State Key Laboratory of Polymer Materials Engineering, No. 24 South Section 1, Yihuan Road, Chengdu 610065, Sichuan, P. R. China

ABSTRACT

The innovations of materials science and modern technologies are boosting the prosperity of polymer composites in various emerging multi-disciplinary fields. Cooperating with the conventional and emerging processing methods, the freeze-casting (ice-templating) technique is attracting interest in the assembling of three-dimensional structural materials (3D-SMs) accompanying the growth of ice crystals. These unique 3D-SMs with isotropic, cellular, lamellar and radially aligned structures have enabled to fabricate multifunctional polymer composites as diverse as mechanically reinforced materials, electrically conductive materials, thermally conductive materials, thermally insulating materials, adsorbents, energy-related materials, biomaterials, and many more. Herein, the working principles and methodologies of ice-templating strategy and its recent advances in shaping and structuring of 3D-SMs and production of corresponding multifunctional polymer composites are summarized. Finally, directions and prospects lying ahead are highlighted, involving the structure designs, processing routes and potential applications. Freeze-casting has manifested responsibilities for producing advanced functional composites. What is it being prepared to do?

KEYWORDS: Freeze-casting, Ice-templating principles, Three-dimensional structural materials, Multifunctional polymer composites

* Corresponding authors

E-mail: weiyang@scu.edu.cn (W. Yang), weii.chen@polyu.edu.hk (W. Chen), xiao-ming.tao@polyu.edu.hk (X. Tao).

Contents

Abbreviations: 0D, zero-dimensional; 1D, one-dimensional; 2D, two-dimensional; 3D-SMs, three-dimensional structural materials; AAM, aligned-acrylamide; AgNW, Ag nanowire; AlN, aluminum nitride; ANF, aramid nanofiber; BN, boron nitride; BNNS, BN nanosheet; CE, cyanate ester; CB, carbon black; CF, carbon fiber; CNT, carbon nanotube; CuNWs, copper nanowires; CV, crystal violet; CVD, chemical vapor deposition; dB, decibel; DMSO, dimethyl sulfoxide; EDS, energy-dispersive spectrometry; EMI, electromagnetic interference; GF, Gauge Factor; HA, hydroxyapatite; HNTs, halloysite nanotubes; IC, indigo carmine; IL, ionic liquid; IPA, isopropanol alcohol; MB, methylene blue; MG, methylene green; MMA, methyl methacrylate; NR, neutral red; PA, polyampholyte; PAA, polyacrylic acid; PAAm, polyacrylamide; PANI, polyaniline; PCL, polycaprolactone; PCMs, phase change materials; PDA, polydopamine; PDMS, polydimethylsiloxane; PEDOT:PSS, poly(3,4-ethylenedioxythiophene)-polystyrene sulfonate; PEG, polyethylene glycol; PEO, poly(ethylene oxide); PI, polyimide; PEI, polyethyleneimine; PLGA, poly(lactic-co-glycolic acid); PMMA, poly(methyl methacrylate); PNIPAm, poly(N-isopropylacrylamide); PPy, polypyrrole; PU, polyurethane; PVA, poly(vinyl alcohol); PVDF, polyvinylidene fluoride; P(VDF-TrFE), poly(vinylidene fluoride-trifluoroethylene); PZT, zirconate titanate; RB, rhodamine B; rGO, reduced graphene oxide; SE, shielding effectiveness; SEM, scanning electron microscopy; SiCMW, SiC microwire; SiCNW, SiC nanowire; SSE, specific SE; TBA, tert-butyl alcohol; TPI, *trans*-1,4-polyisoprene; TCE, thermal conductivity enhancement; THF, tetrahydrofuran; TIMs, thermal interface materials; TPU, thermoplastic polyurethane; UGA, unidirectional graphene aerogel; WPU, water-borne polyurethane; XRD, X-ray diffraction; Y-TZP, yttria-stabilized tetragonal zirconia polycrystals.

1. Introduction

With the innovations of materials science, polymer composites have become one of the most important functional materials for advanced modern and future technologies in coating, automotive, aerospace, energy and medical applications, predominantly due to their light weight, low cost, good processability, and large tunability in macroscopic properties (mechanical, optical, electrical, thermal, and transport properties).[1, 2] The introduction of functional materials into a polymer matrix can induce drastic changes in the target properties of polymer composites,[3] which can be dated back to the period when functional fillers were incorporated into rubber matrix to manufacture toughed automobile tires.[4, 5] The functional fillers include early clay,[6] carbon black (CB)[7, 8] and fashionable low-dimensional materials as well as three-dimensional structural materials (3D-SMs). These functional materials are normally zero-dimensional (0D) particles (*e.g.*, SiO_2[9] and Ag nanoparticles[10]), one-dimensional (1D) fibers or tubes (*e.g.*, carbon nanotube (CNT)[11] and metal nanowires[12]), and two-dimensional (2D) sheets or plates (*e.g.*, graphene[13-15] and boron nitride (BN)[16]).

Lightweight 3D-SMs with macroscopic appearances not only possess the intrinsic characteristics of individually functional materials from the components but also create new collective properties from the monoethnic architectures, such as high porosity, large specific surface area, unique conductive network, macroscopically mechanical properties, etc., widening the application possibilities of low-dimensional materials to functional composites.[17-19] However, how to assemble these small building blocks into 3D porous architectures over a desirable range remains a formidable challenge.[20] Freeze-casting is an alluring and well-tried tactic to produce porous materials,[21] effectively enabling the building blocks to be

assembled into a diversity of 3D monoliths by using growing ice crystals as templates.[22] Compared with the phenomenal chemical vapor deposition (CVD) and 3D printing, the straightforward freeze-casting is a comparatively low-cost and scalable assembly technique in the manufacture of 3D-SMs.

Freeze-casting, also known as ice-templating, is not a new technique, which can be traced back to 1926.[23, 24] However, this method did not attract much attention until the beginning of the new century when some epoch-making papers elaborating the freeze-casting technique to produce new and complex materials published.[20, 25-27] Alongside with traditional inorganic ceramics,[28-30] metals,[31-35] and emerging carbon materials,[36] the popularity of ice-templating strategy has risen to generate advanced functional polymer composites requiring unusual topology for improved practical efficiency. Freeze-casting is a facile yet powerful processing technique which can construct a myriad of microstructures and macroarchitectures,[37-41] such as isotropic porous structure,[42] honeycomb-like or cellular structure,[43, 44] fish-bone structure,[45] hierarchically interconnected structure,[46] nacre-mimetic or lamellar structure[47, 48] and radially aligned structure[49, 50] as well as complex structures[51] which are difficult to create through traditional processing routes for an broadening range of functionalities and applications, accompanying with the geometries of beads,[52] fibers,[53] films[54] and scaffolds[55]. Although tremendous progresses have been made in multifunctional polymer composites through the freeze-casting strategy over the past few decades, the majorities of the research results are far from practical applications.

Therefore, this review will put our emphasis on the processing–structure–performance correlations for polymer composites associated with freeze-casting technique and critically focus on highlighting representative examples of freeze-casting strategies

and their applications in the fabrication of multifunctional polymer composites. Based on the methodology and peculiarity of freeze-casting, 3D-SMs with customized structures have been developed to functionalize polymer composites in relation to different potential application scenarios, mainly including mechanically reinforced materials, shape memory materials, electrically conductive materials, electromagnetic interference (EMI) shielding materials, sensors, thermally conductive materials, thermally insulating materials, energy-related materials, and biomaterials. Finally, the major directions and challenges of multifunctional polymer composites associated with the ice-templating strategy are also discussed to provide some insights and guidance for the further improvement.

2. Methodology

2.1. Ice-templating principles

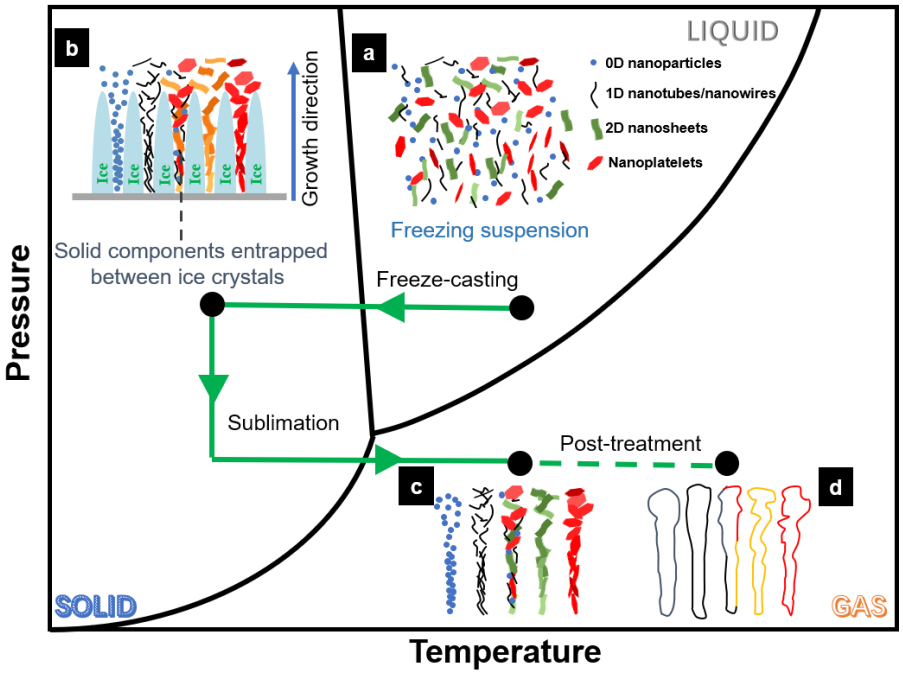

Figure 1. Phase diagram illustrating the ice-templating or freeze-casting principles with the four processing steps: (a) preparation of freezing suspension, (b) ice solidification, (c) sublimation and (d) post-treatment. The schematic diagram is inspired by references[56-61].

Ice-templating or freeze-casting, as a shaping technique, can yield porous parts with fine replicate of the growing ice crystals. Basically, the freeze-casting route contains three essential steps and one optional step.[56-61] i) A typical freezing suspension or slurry is a mixture of liquid freezing agents, solid functional components and additives (**Figure 1**a). Considering the feasibility, environmental friendliness and cost performance, water is usually applied as the freezing medium. However, this approach has fatal disadvantages, *i.e.*, the typically inferior water resistance and mechanical properties, which forces the use of organic solvents such as dimethyl sulfoxide (DMSO),[62-64] 1,4-dioxane,[65, 66] cyclohexane[67] and tert-butyl alcohol (TBA),[68] especially for water-insoluble polymers. On the other hand, it is wisdom to tailor the ice-templating processes by introducing additional operations, such as crosslinking[69] and emulsion lyophilization[70]. Solid component includes metals, ceramics, carbon materials and polymers as well as their hybrids in the form of 0D particles, 1D fibers or tubes, 2D plates or sheets, and coil chains. Accessional additives act as binders and dispersants (or plasticizers) to facilitate the processing. ii) The freezing step is essentially a process of shaping and structuring (**Figure 1**b), determining the final architectures and properties. During solidification, the solid components in the suspension are segregated from the moving solidification front and concentrated between the adjacent growing ice crystals. Homogeneous or directional solidification of freezing suspension is induced by isotropic or anisotropic cooling,[71] resulting in versatile structures, architectures and functionalities. A common freezing device presumably comprises four components: cold source inducing freezing, working stage connecting cold source with freezing suspension, mold holding the freezing suspension, heater or temperature control system tuning the freezing temperature or rate. A surge of alterations has been explored to achieve personalized

designs. One of the most attractive examples is the custom-made wedge system for long-range aligned lamellar structure. Such purposeful structure designs will be presented in this review. iii) After the mixture is fully frozen, the solidified ice is directly sublimated from a solid into a gas at a relatively low temperature and pressure to create porous scaffolds (**Figure 1**c), converting the ice crystals with specific shapes into porosity. The stability of the porous products depends heavily on the interactions of small building blocks or binders. iv) Partial porous scaffolds can be used directly, but some need to be further treated before being put into services (**Figure 1**d), such as sintering of organic additives, carbonization, densification, and infiltration of other constituents. Of note, although these post processing operations can endow the final composites with enhanced properties, the second freezing step is decisive and offers more potentialities and possibilities, which will be magnified in this review.

The morphologies and characteristics of the porous scaffolds fabricated by freeze-casting method are governed by several independent or interconnected parameters,[72] such as the nature of the solvent (single solvent or cosolvent), constituents (proportioning, concentration, and additives), geometry of solid components (dimensionality, size, and aspect ratio), freezing conditions (freezing surface, freezing temperature, freezing dimensionality, and assisting external fields). A morphology map has been proposed to intuitively reflect the relationship between influencing parameters and structural evolution, thus providing a guidance for the design of target structure.[73] Any slight modification of these parameters can lead to a direct effect on the structure of the 3D architectures and the performance of the final composites. Some critical and interesting subjects are well-advised to be highlighted in this review.

2.2. Freezing temperature

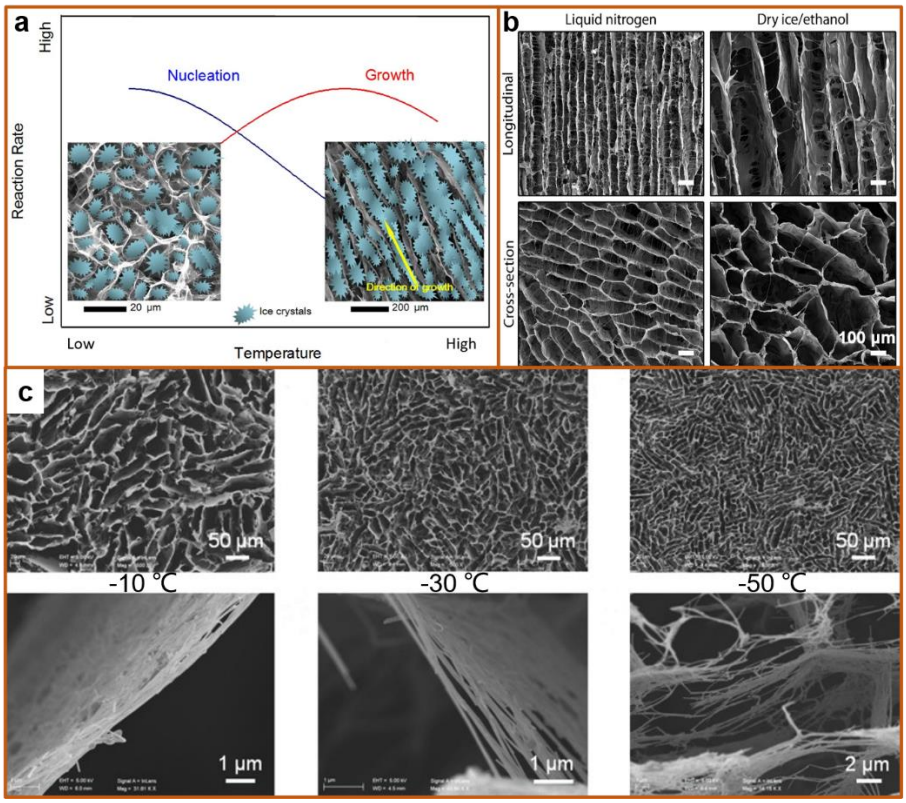

Figure 2. Effect of freezing temperature on the microstructures of 3D-SMs. (a) Qualitative schematic of the correlation between nucleation and growth of ice crystals as a function of freezing temperature.[74], Copyright 2013. Reproduced with permission from Springer Nature. (b) Longitudinal and cross-sectional scanning electron microscopy (SEM) images of aligned collagen porous scaffolds prepared by unidirectional freezing with liquid nitrogen and a dry ice/ethanol mixture.[75], Copyright 2015. Adopted with permission from the American Chemical Society. (c) Microstructures of 3D AgNW architectures fabricated by unidirectional freeze-casting method with various freezing temperatures (− 50, − 30, and − 10 °C) at a similar density.[76], Copyright 2014. Reproduced with permission from John Wiley & Sons Inc.

Ice solidification consists of two individual yet consecutive phases for ice crystals, namely nucleation and growth, and there is a competitive balance between these two phases, which is also common in polymer crystallization. **Figure 2**a shows that a large temperature gradient (or low freezing temperature) can induce the nucleation and improve ice solidification rate, whereas small temperature gradient (or high freezing temperature) tends to promote the growth and decrease ice solidification rate.

As a result, a low ice solidification rate yields large ice crystals, resulting in porous structures with large-sized pores. Meanwhile, solid components in the suspension are assembled between ice crystals during the growth of large ice crystals, leading to porous structures with thick walls. Conversely, a high ice solidification rate yields porous scaffold with small-sized pores and thin walls. Note that an overly slow ice solidification rate (excessively high freezing temperature) creates 3D architectures with extremely large-sized pores, which might give rise to structural defects, even block collapse.[74] These conclusions have been verified in many cases. For instance, aligned collagen (**Figure 2**b) and Ag nanowire (AgNW) (**Figure 2**c) porous architectures fabricated by unidirectional freeze-casting method with various freezing temperatures at a similar density possess various microstructures.[75, 76]

2.3. Viscosity of the freezing precursor suspensions

The properties of the freezing precursor suspensions, particularly the viscosity tuned by proportioning and concentration, affect the nucleation and growth kinetics of ice crystals during freeze-casting process, thus regulating the microstructures (pore size, pore shape, lamellae thickness, bridge, roughness) and macroarchitectures with collapse or not for 3D-SMs. In order to build free-standing 3D macroarchitectures, a sufficient quantity of building blocks is indispensable to form a percolation network, in which morphologies and chemical structures of the building blocks play a critical role. A discontinuous structural network could be obtained when the initial concentration of building blocks is relatively low, whereas 3D structural network becomes dense and perfect without significant defects as the concentration of suspension increases (**Figure 3**a).[76] For the case of lamellar structure shown in **Figure 3**b, the number of dendrite and bridge increases with the increase of the

suspension viscosity, which can be explained by the fact that the building blocks are more likely to be trapped to construct more dendrites and bridges during the growth of ice crystals when the viscosity of the freezing suspension is high.[47] Further tuning the concentration and formulation, the number of lamellae of stem-mimetic graphene aerogel increases at first and then decreases. The higher the suspension viscosity, the larger the nucleation density of ice crystals, further forming more lamellae. However, the initial nuclei of ice crystals could diminish or amalgamate when the concentration is excessive high,[77] leading to lower lamellae density. A phase diagram for the guidance of architectural control concerning viscosity of freezing precursor suspensions has been put forward.[78] Apart from the precursor solution concentration, the physicochemical structure of the materials, such as the geometry (dimensionality and size) and functional groups (liquid–particle and particle–particle interactions), will also affect the architectures and properties of the composites, and the specific details will be discussed in the following case studies.

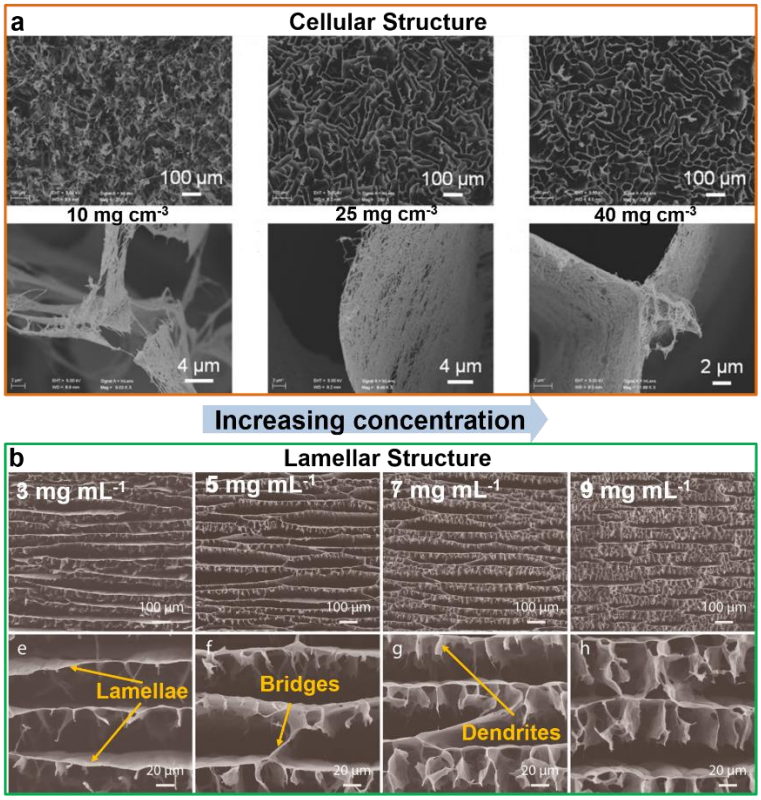

Figure 3. Effect of viscosity of the freezing precursor suspensions on the microstructures of 3D-SMs. (a) Cellular structure of 3D AgNW architectures fabricated by unidirectional freeze-casting method.[76], Copyright 2014. Reproduced with permission from John Wiley & Sons Inc. (b) Lamellar structure of nacre-mimetic graphene/polymer composite aerogels fabricated by bidirectional freeze-casting method with various freezing suspensions at the same freezing temperature.[47], Copyright 2017. Adopted with permission from the American Chemical Society.

2.4 Additives in the precursor suspensions

In addition to the freezing temperature and viscosity of precursor suspensions, the porous structure is also greatly affected by the incorporation of additives,[79, 80] such as salts, sugars, organic solvents, and hybrids. Munch et al.[81] have systematically investigated the effect of additives, including common antifreezers such as NaCl, sucrose, trehalose, glycerol and ethanol, gelatin and citric acid, on the ice-growth kinetics, the microstructures of ice crystals and the topologies of the ice-water interface. Through introducing additives influencing the interfacial energies, interparticle force, the viscosity of the freezing suspension and the solidification path, the overall architecture, micron and submicron structure can be modified. For example, the sample prepared with NaCl exhibits rougher wall than that prepared with sucrose and trehalose, and the samples prepared with trehalose and sucrose possess a high density of thin bridges and a low density of wide bridges, respectively. Also, ethanol[82] and tetrahydrofuran (THF)[83] can be utilized as the antifreezers to dramatically decrease the freezing rate and affect the crystallization behavior of the ice crystals through hydrogen bonding interactions, thus resulting in the construction of a large-scale aligned structure.

The effect of additions of polyethylene glycol (PEG) with various molecular weights (viscosity, **Figure 4**a), isopropanol alcohol (IPA) (freezing point from phase diagram,

Figure 4b) and NaOH/HCl (pH, **Figure 4**c) on the structures and consequent properties of porous TiO_2 scaffolds has been clarified.[84] Theoretically, since additives can alter the phase diagram of the freezing precursor suspensions, complex ice solidification behaviors and versatile architectures can be obtained by selecting the composition and solidification trajectory on the basis of the phase diagram, providing a promising guidance for the optimal design of complicated structures. However, there is rare study on this powerful approach. Therefore, a good understanding of the phase diagram for different studied systems is urgently needed.

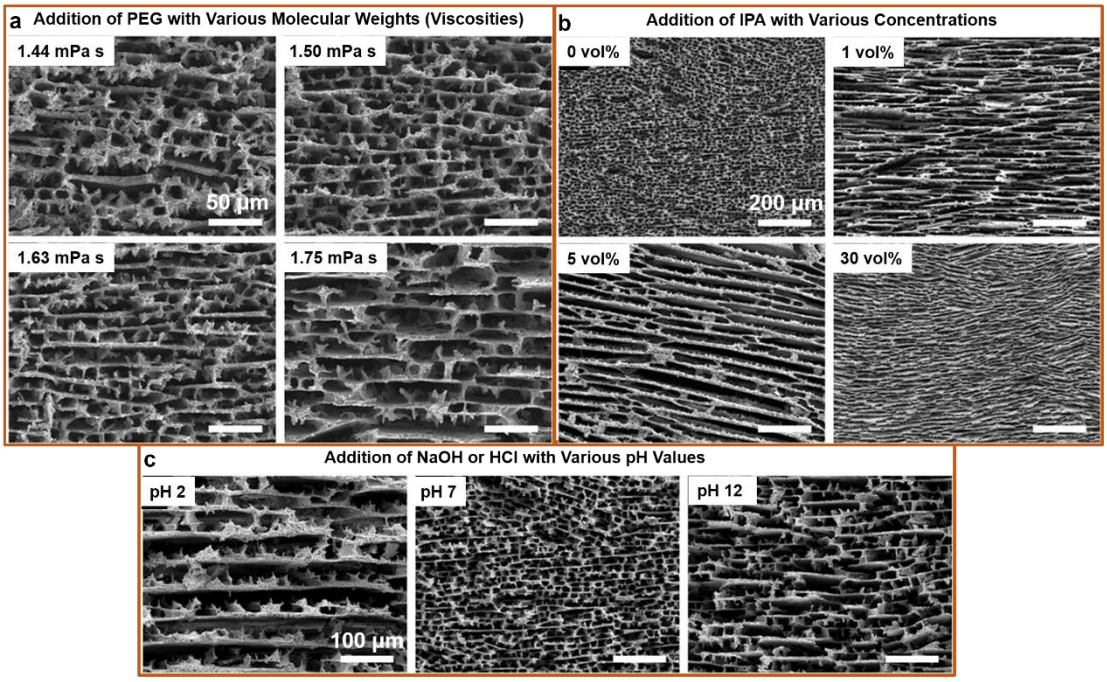

Figure 4. Effect of additives in the precursor suspensions on the microstructures of 3D-SMs: (a) 1 wt% PEG with various molecular weights (viscosity), (b) IPA with various concentrations and (c) NaOH or HCl with various pH values. Scalebars: 50 μm in a, 200 μm for in b and 100 μm in c. [84], Copyright 2014. Reproduced with permission from John Wiley & Sons Inc.

2.5. Dimensionality of freezing

The ice-templating strategy has been considered as a powerful technique to yield 3D-SMs with orderly porous architectures by controlling the nucleation and growth of ice

crystals. The microstructures of 3D architectures prepared by freeze-casting depend heavily on the patterns of the ice growth during ice solidification. According to the models of nucleation and ice-growth (*i.e.*, freezing direction), the ice-templating method can be broadly divided into four categories: nondirectional/random freezing,[42, 85] unidirectional freezing,[75, 76, 86-104] bidirectional freezing,[78, 105-109] and radial freezing (introverted type[49, 110-113] and extroverted type[114, 115]), constructing isotropic porous structure, honeycomb-like structure (cellular structure), long-range lamellar structure (nacre-mimetic structure), radially (graded) aligned structure respectively, as summarized in **Figure 5**.[116] It is noteworthy that a two-step freezing mode has been proposed.[117-119]

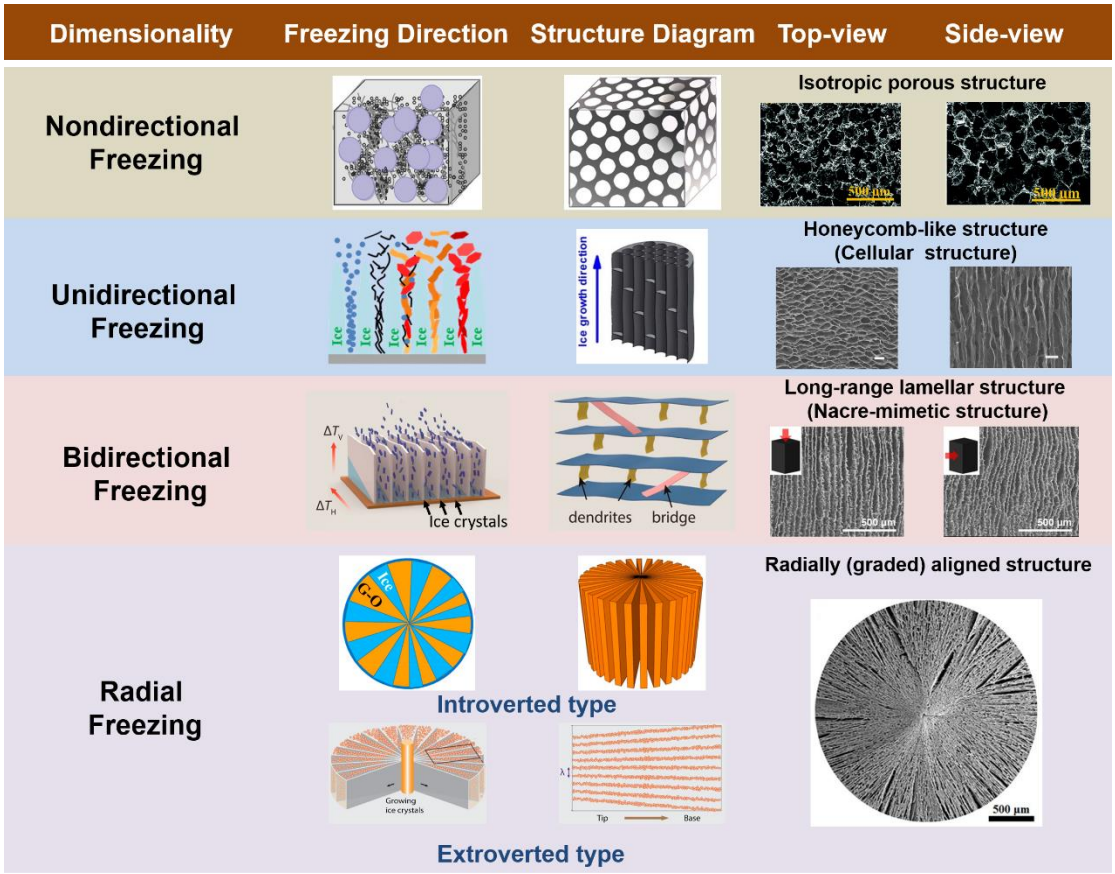

Figure 5. Multi-dimensionality and structural diversification of ice-templating strategy: nondirectional freezing for isotropic structure[42, 120] ([42], Copyright 2016. Adopted with permission from the Royal Society of Chemistry. [120], Copyright 2017. Adopted with permission

from John Wiley & Sons Inc.), unidirectional freezing for honeycomb-like structure or cellular structure.[87, 88] ([87], Copyright 2012. Adopted with permission from Springer Nature. [88], Copyright 2016. Adopted with permission from the American Chemical Society.), bidirectional freezing for long-range lamellar structure or nacre-mimetic structure[47, 107] ([47], Copyright 2017. Adopted with permission from the American Chemical Society. [107], Copyright 2018. Adopted with permission from the American Chemical Society.), radial freezing for radially (graded) aligned structure[49, 115] ([49], Copyright 2018. Adopted with permission from the American Chemical Society. [115], Copyright 2015. Adopted with permission from Elsevier Science Ltd.).

2.5.1. Nondirectional freezing

For simple nondirectional freezing, the dynamics of suspension freezing is random, that is to say, the probability of freezing in any direction is impartial, thus forming an isotropic structure. On the basis of this feature, the properties of the composites prepared in this way are also isotropic. Typically, the suspension is directly placed in a homothermic environment to freeze, such as refrigerators with different freezing temperatures, cryogenic thermostatic bath, and liquid nitrogen (− 196 °C). It should be noted that the homothermic environment does not always correspond to random/isotropic structure, and radial structure may emerge owing to a temperature gradient between the environment and the core of the freezing sample,[121] which is especially prominent in the preparation of beads or microspheres[52, 122, 123]. Compared with sugar- or salt-templating strategies associated with etching operation for producing 3D porous scaffolds,[124-127] ice-templating is a dynamic process,[128] driving solid components to assemble during ice growth. Therefore, ice-templating is also called ice-segregation-induced self-assembly technique.[129] In order to further improve the utilization efficiency of functional materials with

anisotropy, various modified ice-templating strategies (**Figure 6**) have been proposed to produce 3D orderly monoliths with highly aligned structures.

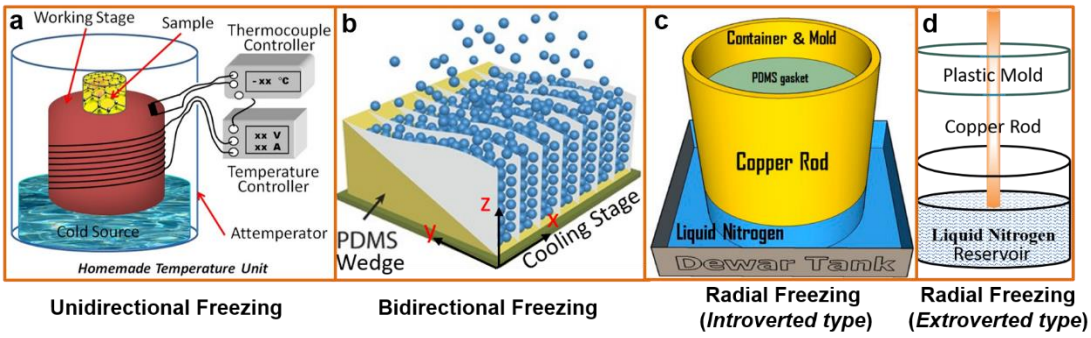

Figure 6. Sketches of the classic apparatuses of various directional freeze-casting methods: (a) unidirectional freezing ([74], Copyright 2013. Adopted with permission from Springer Nature.), (b) bidirectional freezing ([105], Copyright 2015. Adopted with permission from John Wiley & Sons Inc.), radial freezing with (c) introverted type ([49], Copyright 2018. Adopted with permission from the American Chemical Society.) and (d) extroverted type[115].

2.5.2. Unidirectional freezing

A typical apparatus of unidirectional freezing is illustrated in **Figure 6**a.[74] Briefly, a working stage or cold finger is immersed in the cold sources to create unidirectional temperature gradients in the vertical direction, in which the cold source and heating coil cooperate with each other to tune the temperature setting (above the rated temperature of cold source) of the working stage under the regulation of the control system (temperature controller and thermocouple controller). When the working stage reaches the setting temperature, a single vertical temperature gradient is generated, compelling the ice crystals to grow preferentially from the bottom to the top (**Figure 7**a).[76] Compared with the nucleation for nondirectional freezing in 3D, the nucleation for unidirectional freezing is in 2D because the nucleation of ice crystals occurs at the working stage surface. Upon freezing, solid components in freezing suspension are concentrated at the boundary of ice crystals and then repelled in

between the icicles, resulting in a highly aligned structure because of the squeezing effect from adjacent moving ice fronts. After sublimation of the ice crystals, a porous scaffold with a honeycomb-like structure is achieved. Liquid nitrogen, dry ice (−79 °C), freezing bath solvents and refrigerating fluids with different freezing temperatures can be effectively used as the cold sources.[130] Note that the 3D architectures tend to develop from honeycomb-like (cellular) structure to lamellar structure as the freezing temperature increases, which can be explained by the fact that the icicles can grow to contact with each other due to the longer freezing time at a relatively higher freezing temperature.

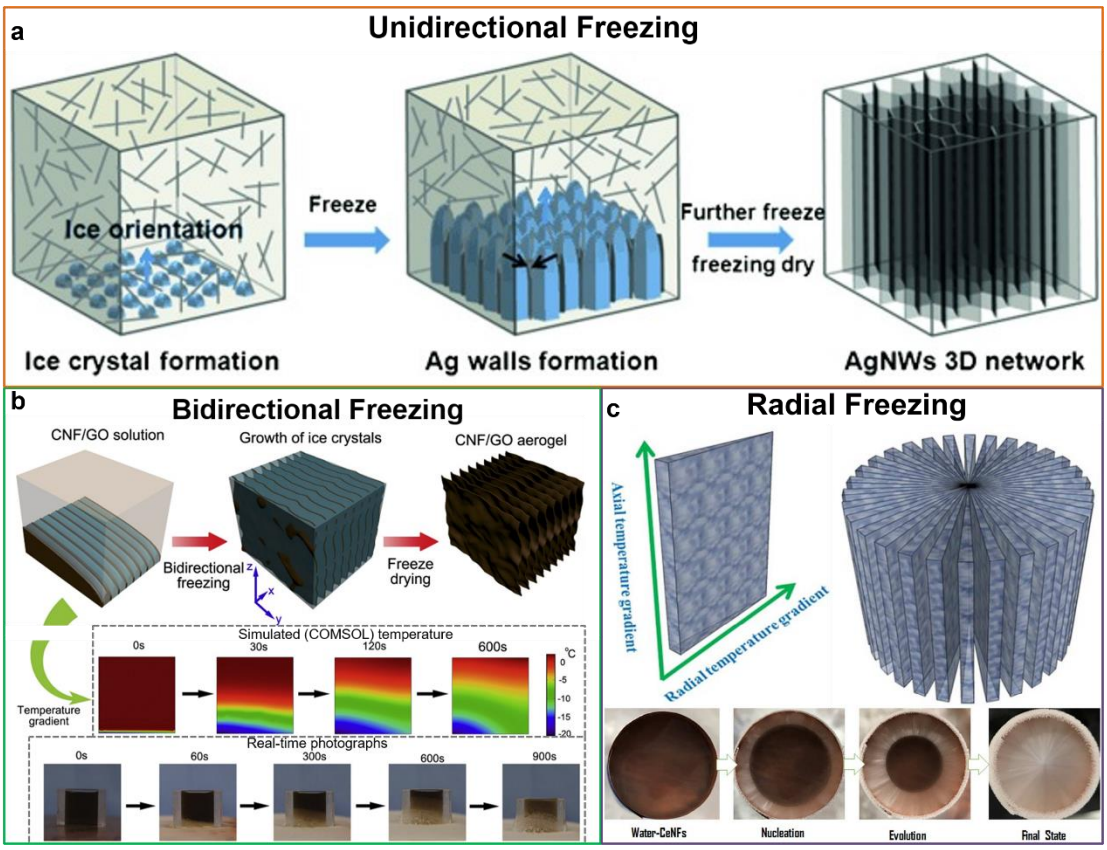

Figure 7. Evolution of directional freezing strategies: (a) unidirectional freezing, (b) bidirectional freezing and (c) radial freezing. (a) Schematic illustration of unidirectional freezing fabrication process for 3D cellular structure.[76], Copyright 2014. Adopted with permission from John Wiley & Sons Inc. (b) Schematic illustration of bidirectional freezing fabrication process with the simulated (COMSOL) temperature of the freezing solution and real-time photographs over time

for lamellar structure.[131], Copyright 2018. Adopted with permission from Elsevier Science Ltd. (c) Schematic illustration and photographs showing the growth of ice crystal platelet along both radial and axial directions and ice crystal arrays with radial and centrosymmetric structure.[49], Copyright 2018. Adopted with permission from the American Chemical Society.

2.5.3. Bidirectional freezing

Although the conventional unidirectional freezing and corresponding modified approaches have been proposed to further manipulate the alignment of the final 3D porous products, it turns out that only a limited scope in the lamellar structure is realized in some cases.[81, 132] Fortunately, a custom-made wedge system has been first developed to construct long-range alignment structure by Pot et al., which pushes the innovations of bidirectional freezing for long-range lamellar structure.[75] A classic apparatus with dual temperature gradients illustrated in **Figure 6**b has been designed to create driving forces for ice growth in both the horizontal direction along polydimethylsiloxane (PDMS) wedge and vertical direction away from the cold finger.[105] Upon freezing, the temperature of the bottom of PDMS wedge is lower than that of its top, generating the nucleation of ice crystals at the bottom end of the wedge, namely nucleation in 1D. A unique porous architecture with a long-range lamellar structure is obtained owing to the bidirectional temperature gradients, where solid components in suspension are expelled from the ice growth front to assemble between the ice crystals. Placing a PDMS wedge on a cooling stage is creative development in this case, and thus how does the slope angle of the wedge affect the structural alignment of 3D architectures? It has been proved that the alignment can be greatly improved and become uniform as the wedge angle increases from 0° to 20° at a relatively high cooling rate,[106] which is further confirmed by the following work from Chen et al.[133] Another homemade setup of bidirectional freezing is depicted

in **Figure 7**b. The simulated (COMSOL) temperature of the freezing solution and real-time photographs over time demonstrate that the freezing occurs at the lower left corner and the ice-growth speed in the *y* direction is faster than that in the *z* direction.[131]

2.5.4. Radial freezing

Radial freezing can be roughly divided into introverted type and extroverted type in the light of ice growth direction, and the corresponding apparatuses are sketched in **Figure 6**c and d, respectively. One major difference between these two types is the curvature of the ice front. Large concave ice front and small convex ice front are for introverted type and extroverted type, respectively. For introverted type (**Figure 6**c),[49] a cylindrical hole containing the freezing dispersion is made in the top of a copper rod with its bottom immersed in liquid nitrogen. The freezing dispersion has to be subjected to two temperature gradients, one in the axial direction and the other along the radial direction, compelling ice crystals to grow along planes radiating to the center of the mold (**Figure 7**c). Aqueous solution of cellulose nanofibers is utilized to intuitively observe the freezing process, and the freezing evolution and the radially orientated texture of the ice crystals can be clearly seen by the naked eye. Consequently, the width of pore channel decreases from the edge to the center. The as-prepared monoliths exhibit vertically and centrosymmetrically aligned lamellar structures.

For the case of extroverted type (**Figure 6**d),[115] a round plastic mold with a thin copper rod connected to a liquid nitrogen reservoir is designed. Compared with introverted type, lamellar ice crystals grow preferentially from the cooling copper rod outward to the plastic mold, creating a thickness gradient in the radial direction. The

obtained porous scaffold shows interconnected gradient channels mimicking the structure of natural bone. The further away from the central cooling rod, the larger the lamellar spacing.

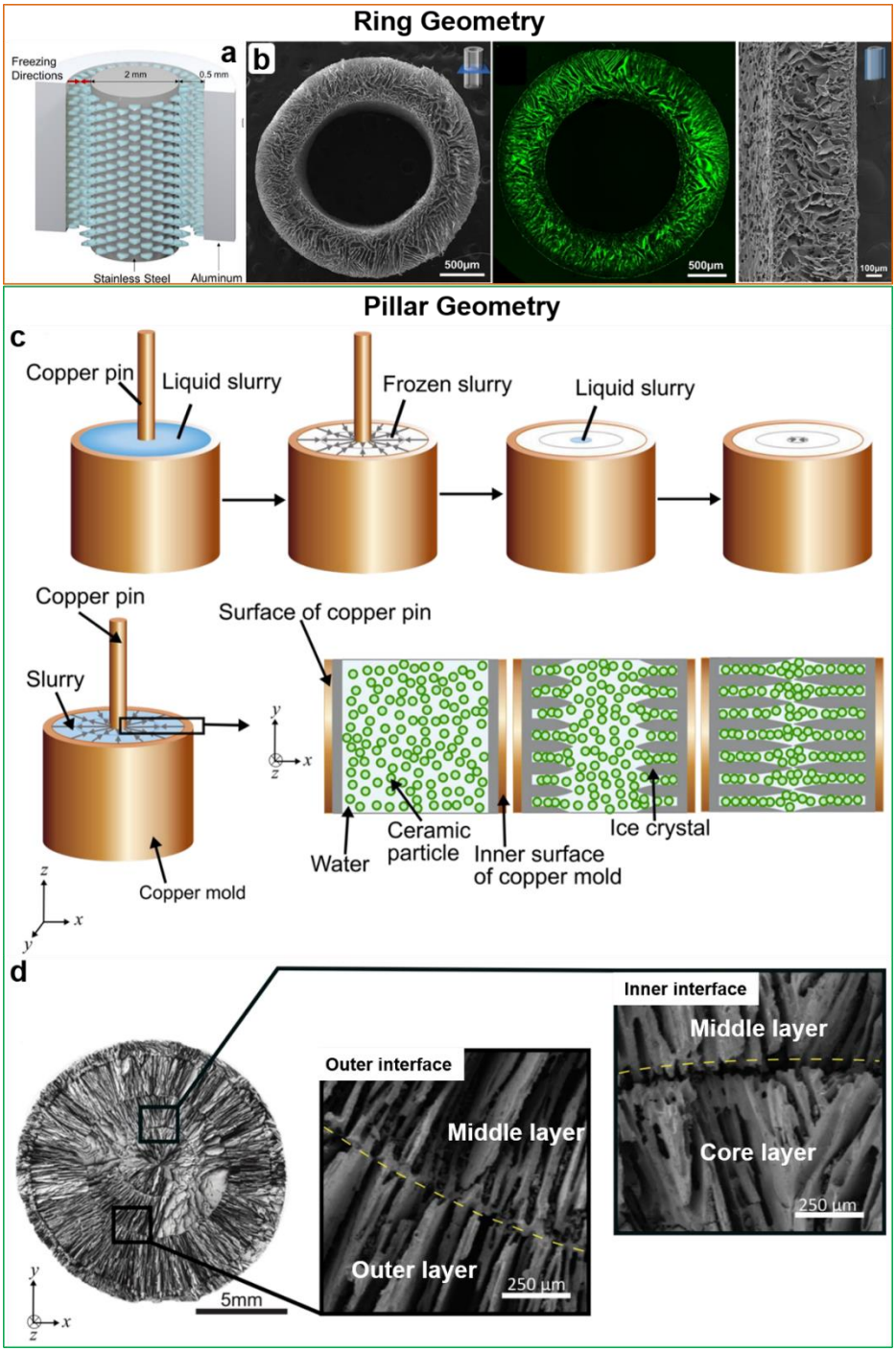

Figure 8. Modified radial freezing strategy named as radial-bidirectional or radial-concentric freezing for different geometries: (a-b) ring and (c-d) pillar. (a) Schematic illustration of radial-bidirectional freeze casting method. (b) Morphologies of porous stent obtained from radial-

bidirectional freeze casting method.[134], Copyright 2018. Adopted with permission from Elsevier Science Ltd. (c) Schematic illustrations of apparatus, evolution mechanism and technological steps of the radial-concentric freeze casting method. (d) Structural characterization of hierarchical porous scaffold obtained from the radial-concentric freeze casting method.[135], Copyright 2019. Reproduced with permission from MDPI.

Although the apparatuses and ice solidification process are different for these two radial freezing types, the porous products present a similar radial and centrosymmetric structure owing to that lamellar ice crystals grow preferentially from the center to the edge for the solid copper rod or from the edge to the center for the hollow copper mold. Furthermore, a radial-bidirectional (**Figure 8**a and b) or radial-concentric (**Figure 8**c and d) freezing strategy with a coupling of metal rod (pin) and metal (ceramic) mold has been put forward to manufacture concentrically hierarchical porous scaffolds with radially aligned structures/multidomain texture and various appearances (ring and pillar).[134, 135] For the case of the radial-concentric freezing strategy, the ice crystals grow inward from the outer copper mold and outward from the inner copper pin concurrently, generating outer layer and middle layer, and the core layer is created after removing the pin. Unquestionably, the above-mentioned three patterns of freezing are more popular than radial freezing, but its unique spontaneous capillary behavior generated from gradient channel structures provides a lot of possibilities for the designs of smart architectures with more sophisticated structures and functionalities.

2.6. External field assisted freeze-casting

Aside from above influencing factors, the coupling of assisting external fields such as electric field,[136-138] magnetic field,[62, 139-144] and acoustic field[145] influences the ice-growth direction, remotely controlling the microstructural patterns.

Given that the water molecule is a dipole, strong electric (up to 150 kV m^{-1}) and magnetic fields can alter the molecular structure and properties of water, resulting in the formation of various pore morphologies and orientations.[146] Note that applying relatively low electromagnetic fields (< 1 T) tends to dominate the behaviors of micro- or nano-particles in the freezing suspension.[147] Likewise, a strong acoustic field (> 900 kHz) can also promote the nucleation of ice crystals and subsequent crystallization growth.[145] Structural differences of porous scaffolds obtained from freeze-casting method with and without assisting external fields are presented in **Figure 9**,[145, 146, 148] indicating that external field assisted freeze-casting can create more orderly and changeable structures by tuning strength, direction and coupling mode of the assisting fields.[149] More details about external field assisted freeze casting can be tracked in the recent reviews.[150-152]

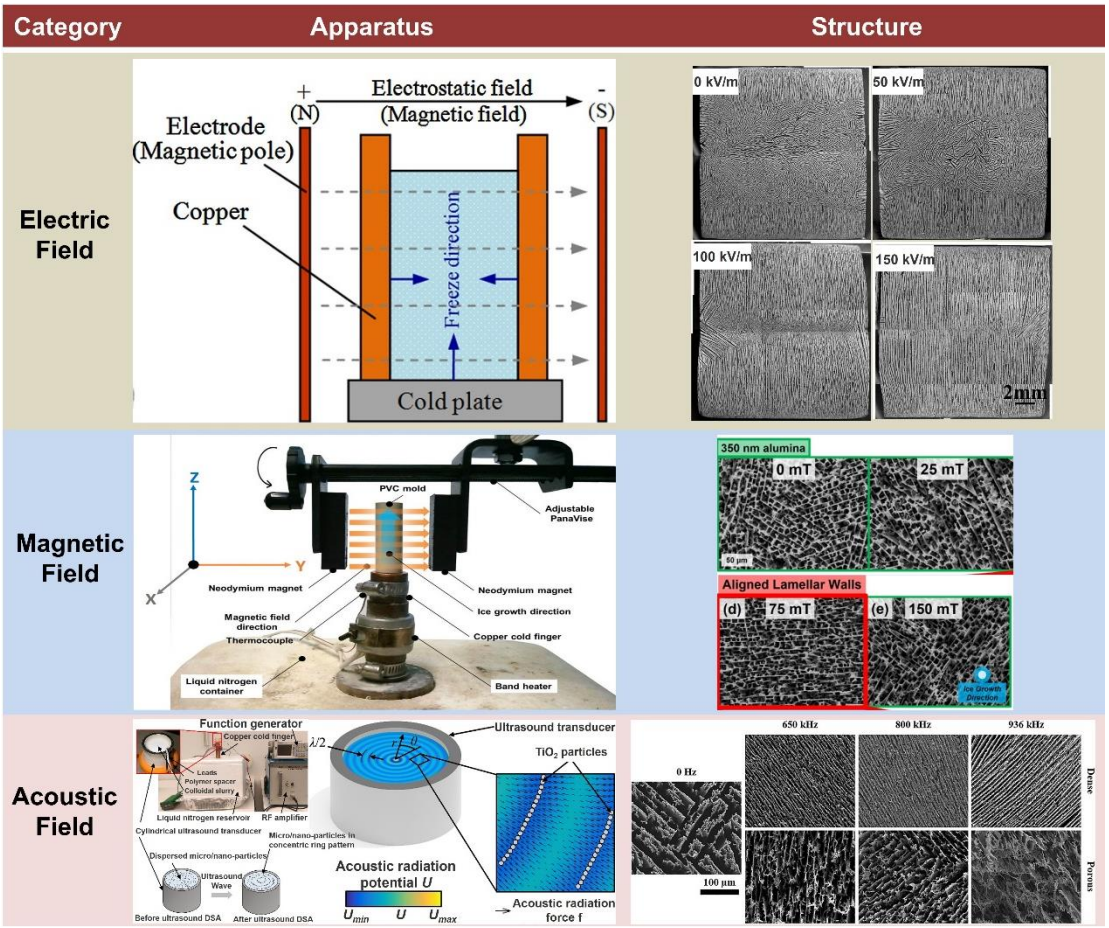

Figure 9. Apparatuses and structures of the external field assisted freezing with electric field ([146], Copyright 2016. Reproduced with permission from Elsevier Science Ltd.), magnetic field ([148], Copyright 2017. Reproduced with permission from Elsevier Science Ltd.) and acoustic field ([145], Copyright 2019. Reproduced with permission from Elsevier Science Ltd.).

Some unconventional operations are mostly used in inorganic materials, and there is plenty of room for the development of their practices in the polymer composites. All the above-mentioned influencing factors, technical parameters and implementing approaches can ideally be integrated, providing guidance for architectural control and functional optimization. For instance, the pore structure can be easily tuned by controlling the wettability of the freezing substrate,[153] and magnetic freeze-casting can be used to produce helix-reinforced structure[142]. Additionally, introducing freeze-casting into other processing techniques can generate novel structure and enhanced performance, just like the melt crystallization technique capable of *in situ* incorporation of pore structure and nanomaterials into polymer surfaces, the combination of freeze-casting and electrospraying, the integration of emulsification and directional freezing, the "interfacial directional freezing" strategy combining solution coating with directional freezing, unidirectional freezing in conjunction with vacuum-assisted self-assembly to construct long-scale aligned lamellar structure (**Figure 10**a), the novel additive manufacturing technique (**Figure 10**b) combining freeze-casting and extrusion-based 3D printing, and the creative "freeze-spinning" technique (**Figure 10**c) integrating solution spinning with directional freezing.[48, 53, 123, 154-159]

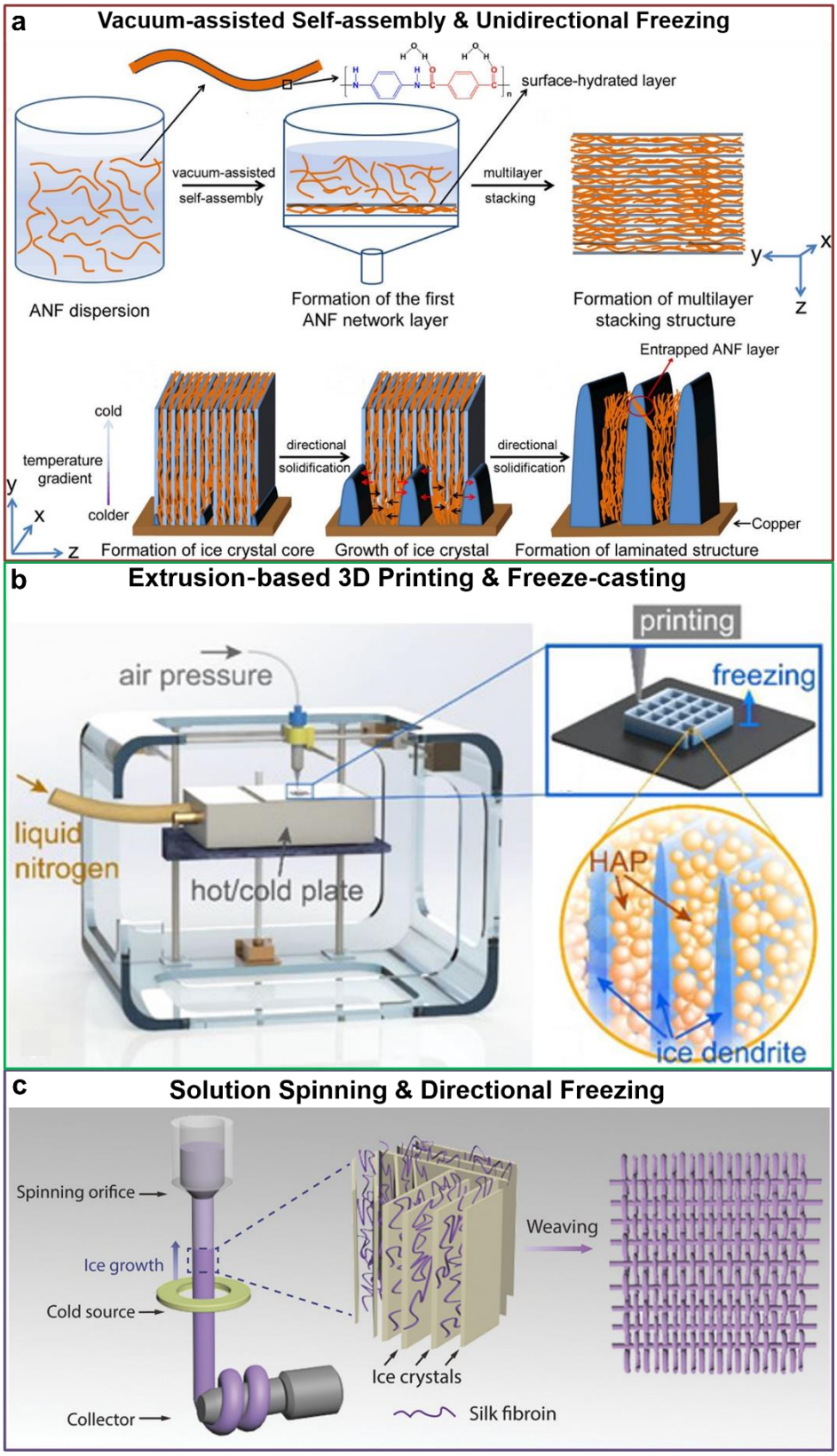

Figure 10. Integration of freeze-casting with other technologies. Schematic illustrations of (a) unidirectional freezing in conjunction with vacuum-assisted self-assembly to construct long-scale aligned lamellar structure ([48], Copyright 2019. Reproduced with permission from the American

Chemical Society.), (b) the novel additive manufacturing technique combining freeze-casting and extrusion-based 3D printing ([155], Copyright 2018. Adopted with permission from John Wiley & Sons Inc.) and (c) the "freeze-spinning" technique integrating solution spinning with directional freezing ([53], Copyright 2018. Adopted with permission from John Wiley & Sons Inc.).

3. Multifunctional polymer composites

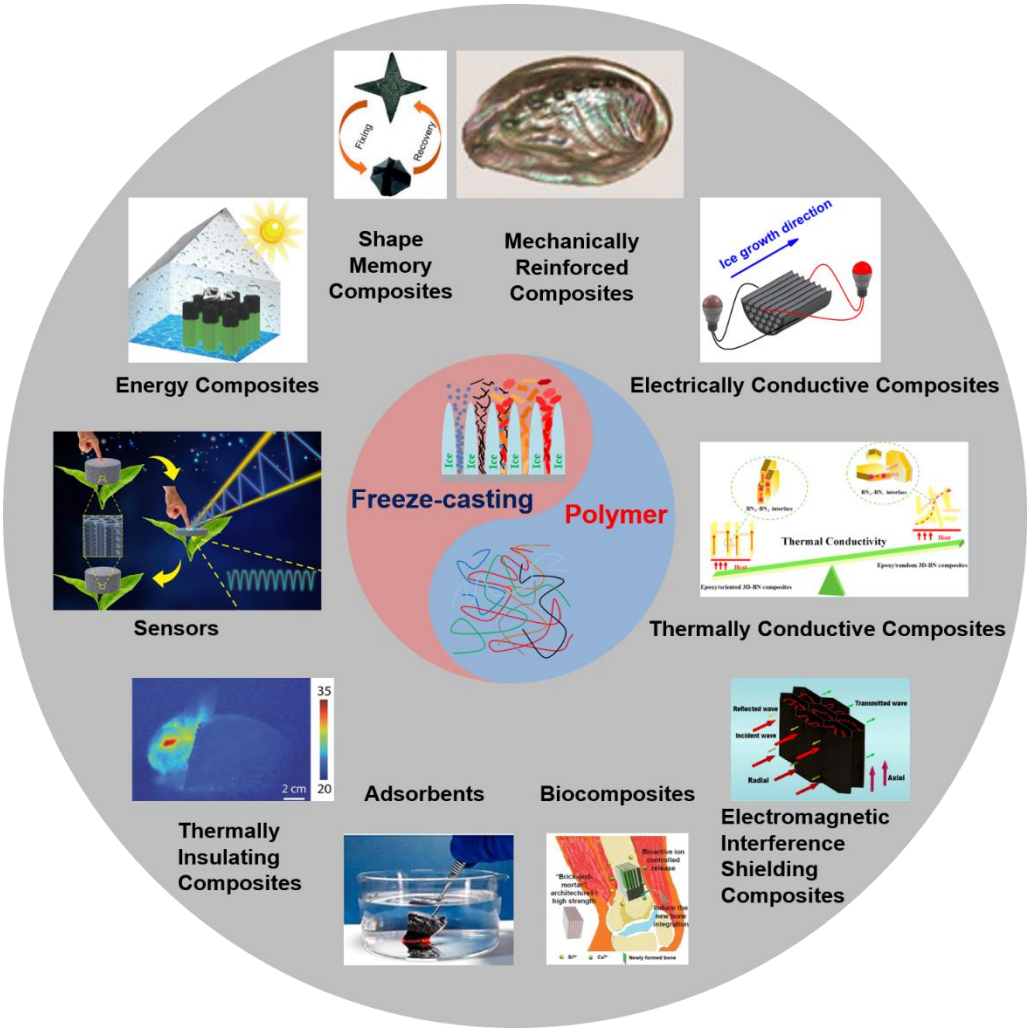

Figure 11. Freeze-casting technique has been applied to produce versatile polymer composites, including mechanically reinforced composites ([47], Copyright 2017. Adopted with permission from the American Chemical Society.), shape memory composites ([83], Copyright 2019. Adopted with permission from the Royal Society of Chemistry.), electrically conductive composites ([88], Copyright 2016. Adopted with permission from the American Chemical Society.), EMI shielding composites ([160], Copyright 2016. Reproduced with permission from

the American Chemical Society.), flexible sensors ([161], Copyright 2017. Reproduced with permission from the American Chemical Society.), thermally conductive composites ([162], Copyright 2017. Reproduced with permission from the American Chemical Society.), thermally insulating composites ([53], Copyright 2018. Adopted with permission from John Wiley & Sons Inc.), adsorbents ([163], Copyright 2017. Adopted with permission from Elsevier Science Ltd.), energy composites ([164], Copyright 2019. Reproduced with permission from the American Chemical Society.), biocomposites ([165], Copyright 2020. Adopted with permission from John Wiley & Sons Inc.).

Different from the traditional melting (*e.g.*, extrusion and injection) and solution (*e.g.*, coating and casting) blending processing technologies of polymer composites, the ice-templating technology used for inorganic ceramic materials in the early stage gradually enters the field of polymer processing, accelerating the development of functional polymer composites, which has been used in the fields of mechanically reinforced composites, shape memory composites, electrically conductive composites, EMI shielding composites, flexible sensors, thermally conductive composites, thermally insulating composites, adsorbents, energy composites, biocomposites, as summarized in **Figure 11**. Certainly, the freeze-casting method is simultaneously able to endow the composites with versatile or integrated functions. It is worth mentioning that combining the ice-templating method and other technologies (interface engineering, hybridization, pyroprocessing, etc.) can bring about a nice synergistic or reinforced effect because the structures constructed by freezing can only act as skeletons in some situations. Also, the ice-templating technique is constantly a complementary or cooperates with the traditional and emerging high-end polymer processing technologies, such as foaming for porous scaffolds,[166] 3D printing for sophisticated structure,[167] layer by layer assembly[168] or multilayer co-extrusion[169] for lamellar structure, etc.

3.1. Mechanically reinforced composites

One of research frontiers for the 21st century is the exploitation of lightweight but strong and tough structural materials as fundamental matrices to support advances in versatile and high-performance composites.[170] Natural structural materials, such as bone, teeth, seashells, silk, bamboo, and wood, display excellent properties with a unique integration of light weight, strength and toughness despite being made of weak constituents, which lies in the sophisticated but well-arranged hierarchical architectures comprising hard and soft phases and spanning from the nanoscale/microscale to the macroscale.[171-174] Inspired by biological structural materials with alternating layers of inorganic platelets and biopolymer at multiple length scales,[175] nacre-mimetic composites (artificial nacres) have been exploited *via* vacuum-assisted filtration processing,[176, 177] self-assembly strategy[178-181] and layer-by-layer technique,[171, 182, 183] which are usually limited to film products.[184] Alternatively, freeze-casting has been considered as a very promising technique to assemble small building blocks into large-sized (centimeter-scale) nacre-mimetic structure, followed by compression or infiltration to produce artificial nacres with typical "brick-and-mortar" architecture and superior mechanical properties.[185-189] Accompanying the progress report that Cheng et al.[190] systematically summarized the achievements in the freeze-casting technique for the preparation of lamellar scaffolds and corresponding bioinspired structural materials with excellent mechanical properties in 2017, relevant advances in mechanically reinforced polymer composites with a distinctive combination of strength and toughness (two contradictory elements) emerge one after another.

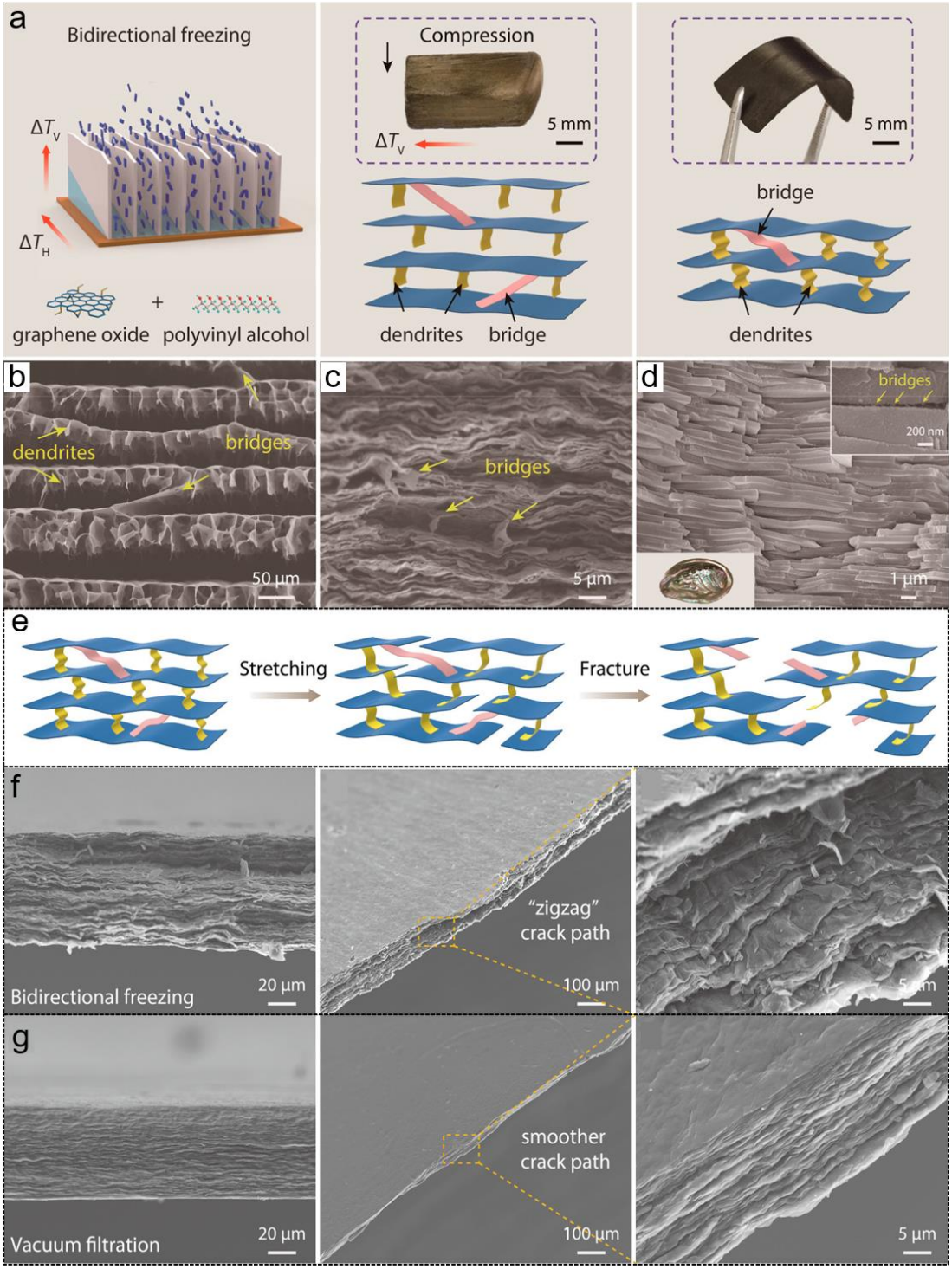

Figure 12. Comparison of nacre-mimetic film products prepared from freeze-casting and vacuum filtration. (a) Schematic illustration of the fabrication route of nacre-mimetic reduced graphene oxide (rGO)/PVA composite film after bidirectional freezing, hot-pressing and chemical reduction processes. Cross-sectional SEM images of (b) the as-prepared monolith, (c) film products, and (d) natural nacre. (e) Schematic illustration showing proposed fracture mechanism of nacre-mimetic film. SEM images of the fracture surfaces of films fabricated by (f) bidirectional freezing method

and (g) common vacuum filtration strategy.[47], Copyright 2017. Reproduced with permission from the American Chemical Society.

Similar to the vacuum-assisted filtration processing to produce nacre-mimetic composite film products, a bidirectional freezing method associated with follow-up uniaxial compression and chemical reduction has been proposed (**Figure 12**a). The as-prepared monolith (**Figure 12**b) and the final film products (**Figure 12**c) possess long-range lamellar structure with massive asperities and bridges, highly mimicking the "brick-and-mortar" structure with interlayer bridges from natural nacre (**Figure 12**d). The superstretchable composite film achieves a distinctive combination of strength and toughness. In contrast with the films obtained from common vacuum filtration, the graphene/poly(vinyl alcohol) (PVA) films exhibit higher tensile strength, fracture strain and toughness, but lower Young's modulus. From fracture models (**Figure 12**e) and fracture surface morphologies (**Figure 12**f and g), once the lamellae or bricks crack, the freeze-casting film does not rupture promptly because of the bridges connecting the adjacent lamellae, which is different from the straight crack propagation of the vacuum-filtration film during fracture. Meanwhile, the dendrites as asperities provide additional friction energy dissipation between adjacent lamellae. It is not until the bridges and dendrites are completely pulled out that the film fails, forming rough surface with "zigzag" crack paths. The lamellae, bridges and dendrites play momentous and interrelated roles in the mechanical performance improvement of nacre-mimetic composite films.[47]

Not only can freeze-casting produce thin films or micro-sized samples, but also it can create bulk nacre-mimetic composites with a series of polymers including poly(methyl methacrylate) (PMMA),[105, 191-194] cyanate ester (CE),[195] poly(vinylidene fluoride-trifluoroethylene) (P(VDF-TrFE)),[196] and epoxy[197-200].

In 2008, Munch et al.[191] prepared nacre-like Al_2O_3/PMMA composites with enhanced toughness through freeze-casting, cold-pressing, sintering and infiltration. The bridges created during cold-pressing and interfacial interactions after chemically grafting methacrylate groups onto the surface of ceramics can effectively limit sliding of the bricks and promote the formation of strong covalent bonding between the inorganic ceramic and organic PMMA phases, together providing additional improvement of mechanical properties. The additive alcohols (ethanol, *n*-propanol and *n*-butanol) can affect the solidification behavior of water, further optimizing the layered structure and ultimate mechanical properties of ZrO_2/epoxy composites.[201] Along this line, a bidirectional freezing route has been developed to conquer the bottleneck that it is difficult to create the lamellar structure over larger than centimeter domains using conventional freeze-casting.[105] The nacre-mimetic hydroxyapatite (HA)/PMMA composites with high flexural strength, elastic stiffness and work of fracture have been developed. Briefly, freezing and sintering operations creating porous HA scaffolds with long-range aligned lamellar structure, uniaxial compression making densified scaffolds, chemically grafting interface modification onto scaffolds, infiltrating monomers being in situ polymerized into PMMA into the grafted scaffolds were sequentially performed (**Figure 13**a). The chemically grafting interface modification on scaffolds can improve the interactions between lamellar scaffold and matrix. According to the crack-propagation behaviors tracked by SEM images (**Figure 13**b), the improvement of mechanical properties of the damage-tolerant structural materials is ascribed to the joint action of extensive crack deflection, polymer ligament bridges between the ceramic “bricks” and induced stable (subcritical) crack growth. A similar processing strategy has been also utilized to more ceramic/polymer systems, such as Al_2O_3/CE composites,[195] yttria-stabilized

tetragonal zirconia polycrystals (Y-TZP)/methacrylate resin composites[202] and silicon carbide/PMMA composites,[192] showing a certain degree of universality.

The content of inorganic materials in the aforementioned artificial nacres is much higher than that of polymers, which is comparable to the natural nacre composed of 95 vol% aragonite platelets (mineral calcium carbonate, hard phase) and 5 vol% organic layers (soft phase) containing proteins and polysaccharides.[203, 204] Very recently, inverse nacre-mimetic polymer-dominated composites have been created by Cheng's group using bidirectional freeze-casting method with tuning freezing rate (**Figure 13**c).[197] From mechanical tests, a stair-like decrease behavior for inverse artificial nacres emerges after the yield point at the end of the linear region, effectively restraining catastrophic failure. The enhancement of mechanical properties of the inverse nacre-mimetic composites is ascribed to the strong interface strength between the epoxy layer and the graphene skeleton. The thinner the polymer layers in the layered composites, the longer the crack propagation path, dissipating more local stresses and energy. The straight crack growth of neat epoxy leads to catastrophic failure, while the crack behaviors of the inverse artificial nacres are tortuous with branches and secondary cracks. The crack deflection, friction at the interface, crack branching, and crack bridging at different length scales synergistically improve their fracture toughness (**Figure 13**d).

Freezing rate and chemical structure of building block affect the lamellar structure and the performance of the final composites. With the increase of freezing rate, the lamellas, the spaces between lamellas, the surface of the lamellas and the corresponding organic polymer layers in composites become thin, narrow, coarse and narrow, respectively, due to an increase in the number of ice nuclei and dendrites. Chemical structure can influence the integration of the inorganic skeleton and organic

polymer. Also, the effect of initial suspension concentration (viscosity) on mechanical properties of inverse artificial nacres cannot be ignored. The fracture toughness of the layered nanocomposites increases as the concentration increases owing to a nacre-like lamellar structure without damages from volume shrinkage.[198]

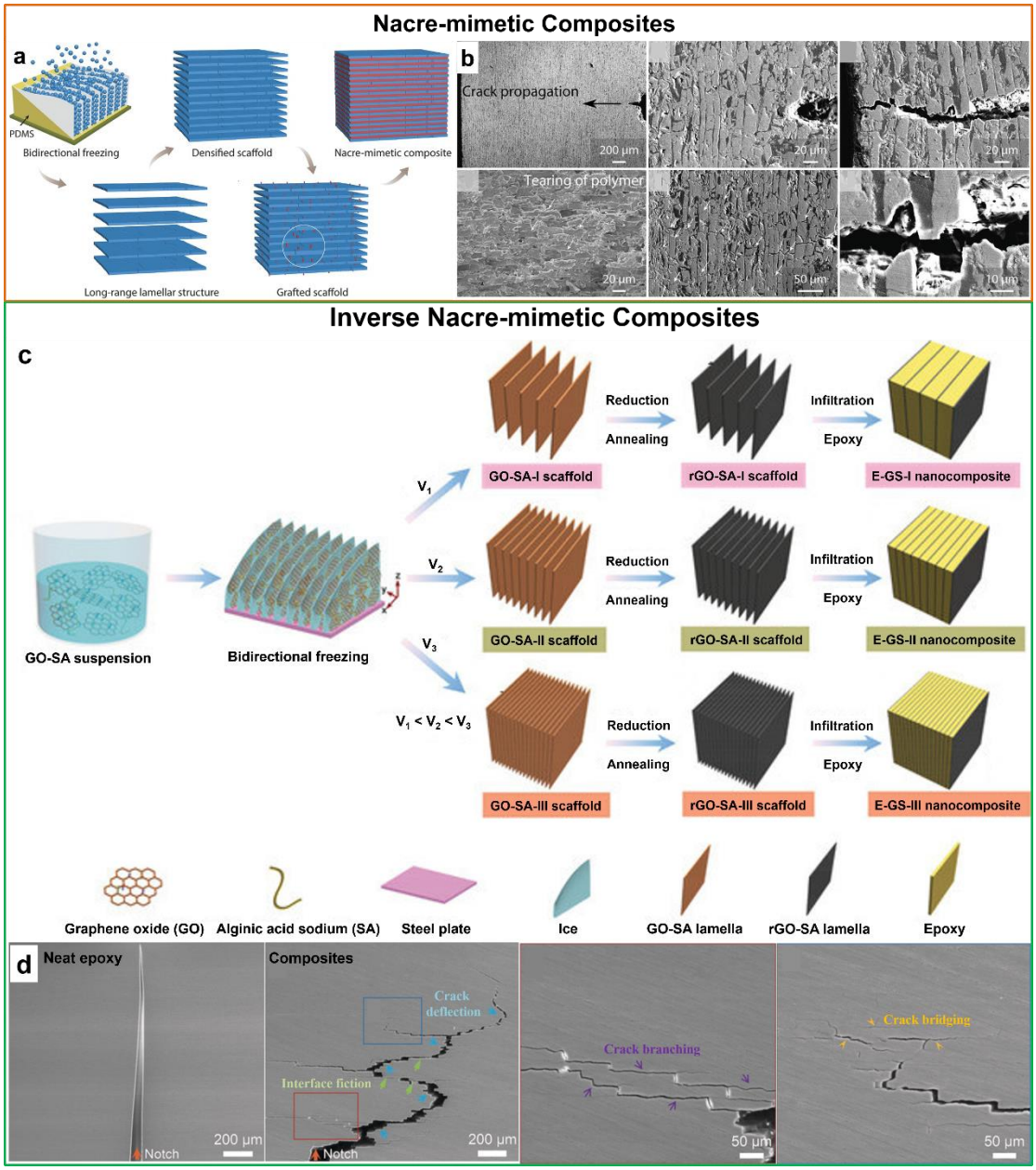

Figure 13. (a-b) Nacre-mimetic and (c-d) inverse nacre-mimetic bulk composites prepared from bidirectional freezing. (a) Schematic illustration of fabrication route of nacre-mimetic HA/PMMA composites using bidirectional freeze-casting technique. (b) SEM images indicating crack-propagation behavior of nacre-mimetic composites.[105], Copyright 2015. Reproduced with

permission from John Wiley & Sons Inc. (c) Schematic illustration of fabrication route of inverse nacre-mimetic epoxy/rGO-alginic acid sodium composites through bidirectional freeze-casting technique with different freezing rates. (d) SEM images showing crack propagation and fracture mechanism of neat epoxy and the composites.[197], Copyright 2019. Reproduced with permission from John Wiley & Sons Inc.

In conclusion, directional freezing, in particular bidirectional freezing, can be used as an effective technique to fabricate long-rang lamellar architectures and corresponding polymer composites with improved mechanical properties. Furthermore, the asperities and bridges (low freezing temperature or high initial GO concentration of freezing suspension) on the lamellar scaffolds, densification (compression or low freezing temperature) of layers, and interfacial interaction (chemical structure of scaffolds or grafting modification) between scaffold and matrix have a positive effect on the improvement of mechanical properties, in particular toughness.

Having said that, how will flexible nacre-mimetic or inverse nacre-mimetic bulk composites behave? Not limited rubber-based polymer composites, gel materials like hydrogels may be good candidates for the innovations of stretchable products capable of restraining crack growth to prevent material failure when a load is applied. It is envisaged that cellular or lamellar network is constructed in hydrogels via freeze-casting route to affect their mechanical behaviors, developing nacre-mimetic or inverse nacre-memetic composite hydrogels.

Apart from the mechanically reinforced solid polymer composites,[205] freeze-casting technique is suitable for the mechanical reinforcement of 3D monoliths and composites with high porosity. Compared with random structure, the highly aligned structures constructed by freeze-casting, in particular lamellar structure with multi-arch microstructure, can be designed to impart elasticity (elastic deformation with low energy loss and reversible energy storage) to 3D porous monoliths, which has been

achieved for porous carbon materials,[43, 78, 87, 206-208] ceramics,[209, 210] MXene,[211] polymer[48, 212] and polymer composites[89, 131, 213-216]. Based on cellular or lamellar structure, a crosslinking strategy can be used to further improve the mechanical properties of freeze-casting porous products, including polymers[133] and inorganic materials[217, 218]. Another feature is the use of fibrous materials such as cellulose and ceramic nanofiber as building blocks. The enhanced mechanical performance as the most basic function enables them to tolerate large geometric deformation yet prevent structural damage/collapse and to be available for post treatment (*e.g.*, densification, sintering, vacuum impregnation, modification, etc.) and a variety of functional application scenarios (*e.g.*, flexible porous materials for sensing systems, lightweight products for EMI shielding, compressive adsorbents for squeezing, compressive scaffolds for tissue engineering, etc.).

3.2. Shape memory composites

Shape memory polymers (mainly dual-shape polymers,[219] triple- or multiple-shape polymers,[220-222] and reversible shape memory polymers[223]),[224] as a unique class of smart materials, can be deformed or fixed into temporary shapes, and then recover to their permanent shapes upon exposure to certain stimuli, such as heat,[225, 226] light,[227] electricity,[228] moisture,[229] force,[230] pH,[231] CO_2,[232] solvent,[233] metal ions,[234] or magnetism[235].[236-238] Although shape memory polymers are a valuable platform for a broad scope of applications ranging from biomedical device to aerospace owing to their superiorities over metals and ceramics in terms of density, deformation capacity, biocompatibility and reliability,[239-243] they are still marred by many limitations and weaknesses, such as slow responsive speed, poor mechanical performance, etc.[244] Therefore, it is of significance and

value to develop shape-memory polymer composites by incorporating functional nanomaterials and specific structures, which involves several aspects: breakthrough in processing technology, consolidation of performance, innovation of driving mode and integration of multifunctionality.

Owing to the incorporation of a large number of rigid nanofillers and the weak interaction between fillers and matrices, it is desirable yet challenging to generate shape memory composites with the combination of mechanical properties and functionalities. Directional freezing cellular structure can construct efficient conductive network at a relatively low filler loading and impart elasticity to 3D-SMs. Shape memory polymers, semicrystalline *trans*-1,4-polyisoprene (TPI)[245] and epoxy[246, 247], have been introduced into the aligned conductive frameworks constructed by directional freezing processing to fabricate thermotropic and electro-induced shape memory composite foams and bulks. The interconnected cellular network with excellent electric/heat transfer characteristics in composites contributes to the fast response at a low actuating voltage.

As discussed earlier, the bidirectional freeze-casting can be adopted to develop the mechanically reinforced nacre-mimetic polymer composites, making it possible to obtain high-performance shape memory materials with anisotropic large-scale lamellar structure. Shape-memory epoxy based composites with an increased fracture toughness and thermally or electrically activated shape memory effect have been achieved (**Figure 14**a).[83] The composites inheriting the lamellar structure of freeze-casting porous scaffold (**Figure 14**b) can switch the appearances (circle, twist or fold) shown in **Figure 14**c back and forth under the heating or current stimuli owing to the perfect electrical conductivity originating from aligned graphene and 3D network structure. The recover behaviors follow the mechanism of a one-way dual-shape

memory effect (**Figure 14**d). Their glass transition temperature (T_g) related to the movement of the chain segment plays a primary role in the shape-memory performance. Once deformed by external force, the molecular chains can store entropic energy, being in high energy state. When exposed to heat or electrical stimulus, the molecular chains return to a low energy state, namely, the original configuration for the composites. The self-healing function of the shape-memory composites can be realized after a thermally reversible Diels–Alder network polymer substitutes for epoxy resin (**Figure 14**e).[248] The resultant nacreous composites (smart nacre) not only show extrinsic toughness and non-trivial self-healing capability because of the well-aligned ceramic layers and the dynamic covalent polymer network, but also acquire the abilities of shape re-configuration *via* plasticity (**Figure 14**f) and shape recovery behaviors (**Figure 14**g), even when a 50 g load is applied. These strategies concerning structural design open insightful avenues to devise multifunctional shape-memory composites which not merely possess mechanical and self-healing properties in the future. Additionally, intelligent shape-memory materials with delicate structure and function are the approaching development focus.

For biocompatible polymers, it has been proved that a shape-memory chitosan scaffold with aligned porous structure can be employed as a versatile host for self-assembly of a diverse range of nanoscale building blocks to create functional 3D macroarchitectures.[91] In a recent study, water-sensitive shape-memory chitosan/agarose porous composite hydrogels have been developed, in which ice-templating-induced orientated microfluidic channel play a leading role for the shape memory property.[249] The coupling of such straightforward processing method, multifunctionality and multi-staged biodegradation provides possibilities for the utilization in the tissue engineering. From the perspective of materials, poly(N-

isopropylacrylamide) (PNIPAm) is considered as one of the most potential polymers for the responsive functional applications including biomedicine and smart hydrogels owing to its appropriate performance at room temperature. A leaf-inspired intelligent solar steam generation system based on PNIPAm composites will be presented in the following separate section.

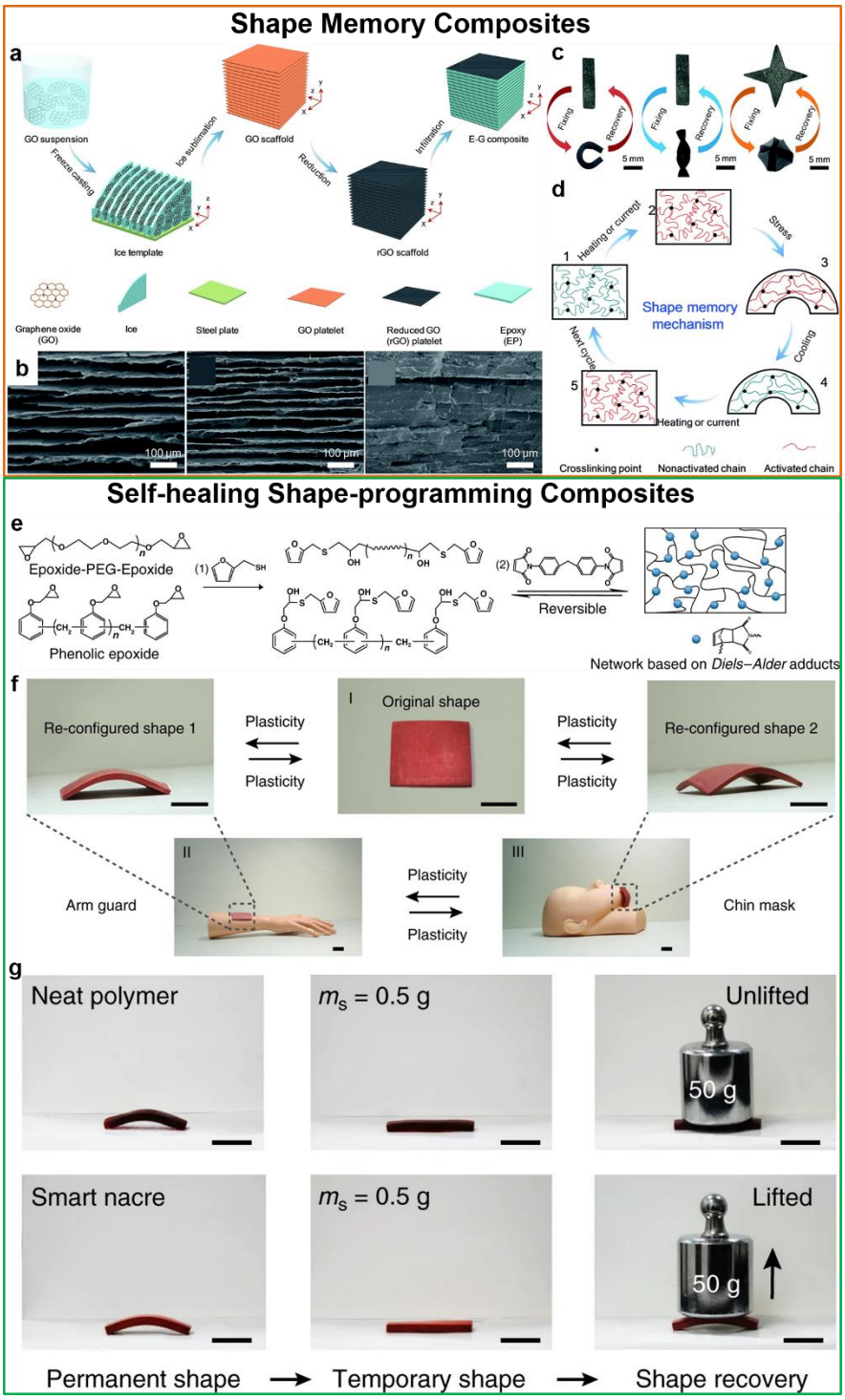

Figure 14. Bidirectional freezing strategy to construct long-rang lamellar structure for nacre-mimetic shape memory composites with enhanced mechanical properties. (a) Schematic illustration of the fabrication route of epoxy/rGO composites. (b) Cross-sectional SEM images of GO scaffolds, rGO scaffolds and the corresponding composites. (c) Shape-memory behaviors of the composites with various configurations (circle, twist and fold). (d) Schematic illustration of shape-memory mechanism of the nacre-mimetic composites.[83], Copyright 2019. Reproduced with permission from the Royal Society of Chemistry. (e) Synthetic process of the Diels–Alder network polymer. (f) Shape re-configuration *via* plasticity and (g) shape recovery behaviors of the smart nacre.[248], Copyright 2019. Adopted with permission from Springer Nature.

From the perspective of structures, 3D conductive pathways constructed by freeze-casting can facilitate electro/phonon transfer and water adsorption to develop shape memory composites with rapidly electrical and thermal response and water-sensitive shape memory composites, respectively. These ordered network structures are also conducive to the formation of ion or gas channels for high-performance ion- or gas-induced shape memory materials. Therefore, more other stimuli-induced shape-memory composites associated with freeze-casting are expected to develop.

3.3. Electrically conductive composites

Electrically conductive composites, a compound of host polymers and conductive fillers (metals,[250] CB,[251] carbon fiber (CF),[252] CNT,[253] graphene,[254] etc.), have been explored in broad applications (conductors,[255] antistatic materials,[256] EMI shielding materials,[257] sensors,[258] actuators,[259] thermoelectric materials,[260] etc.) and attracted a great deal of interest in academic and industrial circles in recent decades. When it comes to conductive polymer composites, two fairly important concepts have to be mentioned, *i.e.*, percolation threshold and tunneling effect, which play a significant role, even the decisive role in the conductive

mechanism and the application of conductive materials. When the conductive filler loading reaches a critical value, a jump (several orders of magnitude of rapid increase) reflecting an insulator-conductor transition in electrical conductivity emerges, thus forming an initial conductive network. This critical content is the so-called percolation threshold. Although the majorities of conductive filler in the composites are unable to contact with each other directly, the connectedness of conductive network throughout the whole sample is good. This is because electrons can transfer through an ultra-thin insulating barrier in the form of quantum mechanical tunneling between nearby conductive regions. Accordingly, a change in the local tunneling distance can bring about massive changes in the conductivity, realizing sensing performance and other functionalities.[261] Geometry, dispersion, interaction with polymer matrices and stacking mode of functional materials are important factors affecting the electrical conductivity of polymer composites, and more and more attention has been paid to the stacking mode in recent years. To the best of our knowledge, the construction of segregated structure is one of the most classical methods to prepare conductive polymer composites with low percolation threshold.[262] It is noteworthy that the low percolation threshold does not necessarily mean high electrical conductivity. Generally, conductive polymer composites with segregated structure exhibit poor mechanical properties,[263] especially composites with high filler loading, due to weak interface interaction between polymer and filler, which greatly limits the practical application of electrically conductive composites. Substantial efforts including modified segregated structure[264, 265] and ice-templated shaping network have been devoted to achieving high-performance composites with mechanical properties and functional characteristics. Preconstruction of a 3D conductive network of nanomaterials before

compounding with polymer matrices is an effective route for electron transfer to produce electrically conductive composites,[266] which exactly coincides with the technological characteristics of the freeze-casting.[267, 268]

A unidirectional ice-templating strategy has been adopted to directly assemble well-dispersed nanomaterials into freestanding macroscopic 3D architectures with cellular structure. To display the superiority of the 3D conductive architecture, PDMS is introduced into the compartmentalized monoliths to fabricate stretchable and foldable conductors with high electrical conductivity (up to 1250 S m^{-1} at an ultralow AgNW density) and good electromechanical stability.[76] With very large aspect ratio and wonderful electron mobility, CNT and graphene have been universally explored to prepare conductive polymer composites with exceptional electrical conductivity. GO can be employed as the precursor to construct graphene-based 3D architecture, but it is difficult for CNT without the assistance of additives. Thus, great efforts have been devoted to enhancing the electrical conductivity while lowering the percolation threshold of the composites by rationally assembling 2D graphene nanosheets into macroscopically 3D internal network. Noteworthily, a thermal reduction treatment is essential when GO is used as precursor to produce graphene aerogels. Benefiting from the interconnected and aligned graphene network structure of unidirectional graphene aerogel (UGA), epoxy based conductive composites exhibit anisotropically electrical properties and ultralow percolation threshold of 0.007 vol% (**Figure 15**a).[88]

On the basis of the highly aligned and interconnected network, the size and chemical structure of graphene have an important effect on the electrical conductivity of the polymer composites.[107, 269] The larger graphene nanosheets tend to form better orientation structure and less total intersheet resistance, and the high-quality graphene with less defect contributes to reducing phonon scattering. There are sizeable

interactions (*i.e.*, steric hindrance, hydrogen bond, π–π interaction and van der Waals forces) between neighboring ultralarge GO sheets to form highly aligned and interconnected network, while interactions for small GO sheets are so limited that the shrinkage and random orientation of 3D structure emerge after drying (**Figure 15**b). As a result, the composites with UGA obtained from ultralarge GO sheets outperform those prepared using large GO and small GO.[269] Considering a considerable decrease in transport and mechanical properties of GO or rGO nanosheets because of crystallographic defects primarily stemming from surface functional groups, the high-quality nonoxidized graphene flakes with high crystallinity and large lateral size have been utilized to fabricate highly aligned graphene aerogel *via* a bidirectional freeze-casting method (**Figure 15**c).[107] The final composites exhibit an exceptional electrical conductivity of 122.6 S m^{-1} in the ice-growth direction at a low graphene loading of 0.45 vol%, which is comparable to that of the epoxy-based composites embodying 3D interconnected graphene foam constructed by CVD.[270]

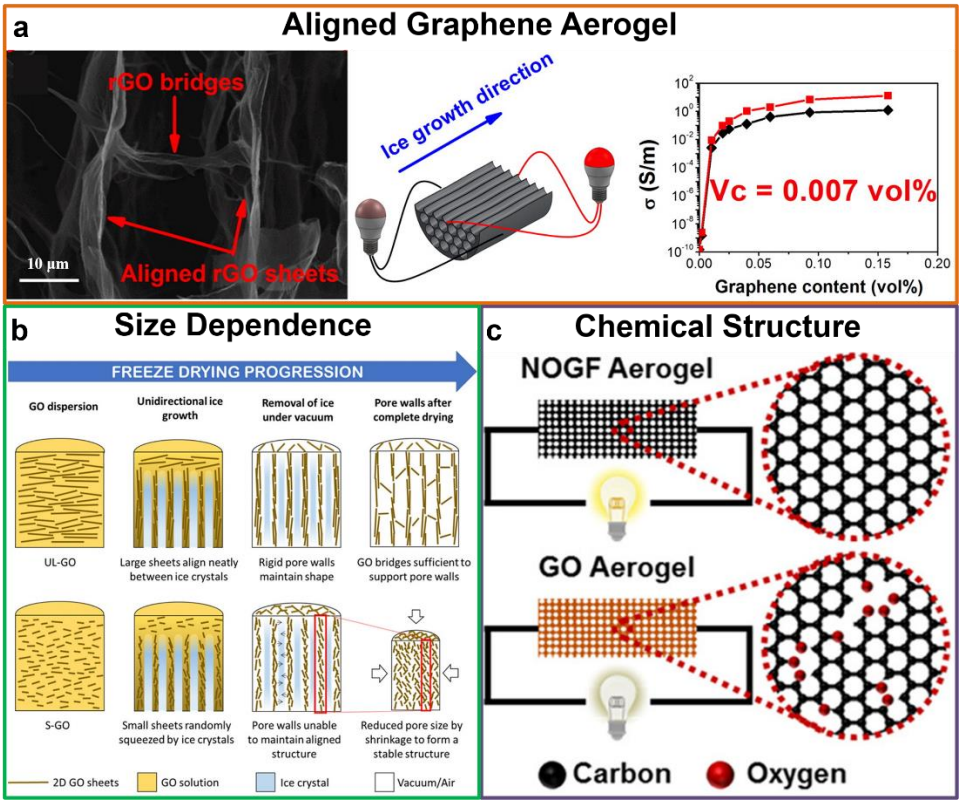

Figure 15. Electrically conductive epoxy based composites with 3D conductive structural graphene skeletons obtained from directional freeze-casting using different graphene precursors: (a) GO nanosheets, (b) ultralarge GO and (c) large nonoxidized graphene flakes with high crystallinity. (a) SEM showing unidirectionally aligned UGA with bridge structure and electrical conductivities of the composites in the parallel and perpendicular to ice-growth direction.[88], Copyright 2016. Reproduced with permission from the American Chemical Society. (b) Schematic illustration of the fabrication route of UGAs with varying sized GO sheets (ultralarge GO, large GO and small GO) at the same concentration (2.0 mg mL^{-3}).[269], Copyright 2018. Adopted with permission from the American Chemical Society. (c) Schematic illustration of nonoxidized or oxidized graphene aerogel based composites as conductors in a circuit.[107], Copyright 2018. Adopted with permission from the American Chemical Society.

3D-SMs assembled from large lateral graphene with high crystallinity are favorable for the fabrication of electrically conductive composites. The electrical conductivities parallel and transverse to the alignment direction for the polymer composites are highly anisotropic. This disparity arises from the anisotropic nature of the aligned structure constructed by directional freeze-casting and the possible displacement or breakage of the conductive bridges linking the walls during the liquid polymer infiltration process. Additionally, these graphene aerogels with the orderly structure endow the composites with enhanced fracture toughness, creating mechanically conductive polymer composites.

Relying on the ice-templating strategy, electrically conductive composites have been explored in diverse applications. Sequential/multiple freezing strategy can refine the structure of 3D-SMs, which provides a good solution to the contradiction of the improvement of dielectric constant usually accompanied by an increase in dielectric loss for the most of conductive polymer composites. For example, a two-step freezing method has been used to prepare electrically conductive graphene aerogel/PVA

composites with an extraordinary dielectric constant of more than 1000 and a notable dielectric loss of below 0.08.[271] After the first run of freezing (**Figure 16**a), the graphene aerogel/PVA composites present anisotropically aligned skeletons which are bridged by ribbon-like ligaments, forming a 3D continuous architecture (**Figure 16**b). A high dielectric constant has been achieved, which is mainly ascribed to two ameliorating features, *i.e.*, the uniform dispersion of graphene enlarging interfacial areas in the porous composites and the continuously aligned network structure serving as a slew of microscale capacitors. More intriguingly, PVA insulating barriers can be created on the originally conductive skeleton to replace the conductive ligaments during the 2nd run of freezing (**Figure 16**c), giving rise to the disconnection of tunneling current and the reduction of current leakage for the neighboring aligned conductive columns (**Figure 16**d) and achieving the high dielectric constant yet low loss for conductive polymer composites. In parenthesis, the freeze-casting strategy of constructing 3D ceramic network in dielectric polymer composites have been provided.[272-274] Besides, electrically conductive composites obtained from freeze-casting have been applied in the fields of the aforementioned electrically driven shape-memory composites, and EMI shielding composites and flexible sensors discussed later.

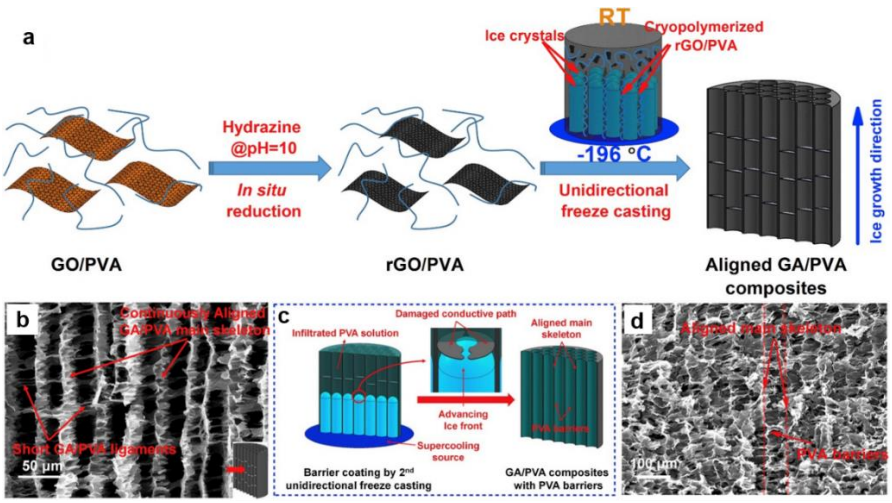

Figure 16. Graphene aerogel/PVA composites with high dielectric constant and low loss using two-step freezing method. (a) Schematic illustration of the fabrication route of highly aligned graphene aerogel and corresponding PVA based composites through unidirectional freezing. (b) Side-view SEM image of the composites. (c) Schematic illustration and (d) SEM image of the composites with PVA barriers after the 2nd run of unidirectional freezing.[271], Copyright 2017. Adopted with permission from Elsevier Science Ltd.

In the above cases, graphene is mainly used as conductive fillers. More highly conductive materials, such as low-cost 0D CB, 1D CNT and CF, need to be employed to produce electrically conductive composites. Meanwhile, the issue of their dispersion needs to be solved under the premise of ensuring the intrinsic conductivity as much as possible. Using the conducting surfactant such as poly(3,4-ethylenedioxythiophene)-polystyrene sulfonate (PEDOT:PSS) to disperse them instead of the insulating stabilizers is an available strategy. Emerging MXene which can be uniformly dispersed in aqueous solutions is another promising conductive material.[275] Aside from the alterations of physicochemical structure of building blocks, the microstructure of conductive network can be tailored by changing the freezing conditions to optimize conductivity and meet different application requirements. Also, stretchable conductors with low loading, low percolation threshold and high electrical conductivity are expected. Interfacial modification on the porous scaffolds can improve the interaction between porous scaffolds and matrices, further enhancing the mechanical properties and reducing electrical resistance.

An efficient transport channel constructed by a directional freezing method is not only conducive to the movement of electrons but also to the transport of ions. The liquid crystalline systems can be easily driven by the external forces provided from the ice-growth to shape the ordered structure. For example, PVA/halloysite nanotubes (HNTs)/ionic liquid (IL) ternary nanocomposite electrolytes with high ionic

conductivity have been successfully obtained after incorporating IL into PVA/HNTs scaffolds from their liquid crystalline dispersions.[276] Likewise, a 3D continuously pre-percolating graphene network in polymer composite electrolytes has been designed to improve proton conduction capability.[277] These hybrids with excellent ionic conductivity are expected to be employed as electrolytes of batteries, supercapacitor, piezoionic sensors, electrochemical actuators, etc. More details will be discussed in the following separate section.

3.4. Electromagnetic interference shielding composites

EMI shielding materials protecting a given target from electromagnetic waves are widely used in the fields of commercial and military electronics, aircraft, and medical systems. With the explosive development of telecommunications and electronic devices, electromagnetic pollution is becoming increasingly prominent, which not only affects the normal operation of the electronic systems, but also greatly threatens civic activities and health.[278, 279] Keeping pace with the rapid growth of nanomaterials and nanotechnologies, EMI shielding enclosures comprised of electrically-conductive or magnetic components have gradually evolved from conventional metal-based protective systems to lightweight nanocomposites. Recently, polymer composites with functional nanomaterials (mainly electrically conductive fillers) have been considered as competitive candidates for highly efficient EMI shielding materials.[280, 281] Fundamentally, EMI shielding capacity of a material is commonly evaluated by the shielding effectiveness (SE) with the unit of decibel (dB),[282] which is defined as the ratio of the incident energy or electric field or magnetic field to transmitted energy or electric field or magnetic field. Therefore, the SE (see **Eq. 1**) is determined by primary reflection loss (SE_R), absorption loss (SE_A)

and multiple reflection loss (SE_M). For SE_R, SE_A and SE_M, mobile charge carriers (electron and holes), electric or magnetic dipoles, and large surface area or interface play crucial roles, respectively. Also, how to balance the intrinsic characteristics such as permittivity, permeability and conductivity is of significance to achieve desired shielding performance.[283] Incidentally, hierarchically interconnected cellulose/MXene ($Ti_3C_2T_x$) aerogels and graphene@SiC aerogels without polymer produced by the freeze-casting approach have been achieved to act as lightweight and wide-bandwidth microwave absorbers.[284, 285] Directionally antagonistic GO-polyurethane (PU) foam sound absorbers with hierarchical cellular structure have been also developed through a directional freezing operation.[286]

$$SE\ (dB) = SE_R + SE_A + SE_M \tag{1}$$

Segregated yet continuous architecture is a classical structure providing high electrical conductivity and large interface for EMI shielding composites.[287-291] Ag platelets/GO foams with regular spherical hollow structures have been successfully copied to the epoxy based composites, forming an effective segregated network structure through freeze-casting (**Figure 17**a).[292] Exceptionally, the maximum EMI SE value of the resulting composites reaches as high as 58 dB at Ag platelets loading of 0.94 vol% and rGO loading of 0.44 vol% due to the increase of impedance mismatch between composites and air and multiple reflection inside the composites originating from the increase of electrical conductivity and the formed spherical hollow structures, respectively (**Figure 17**b).

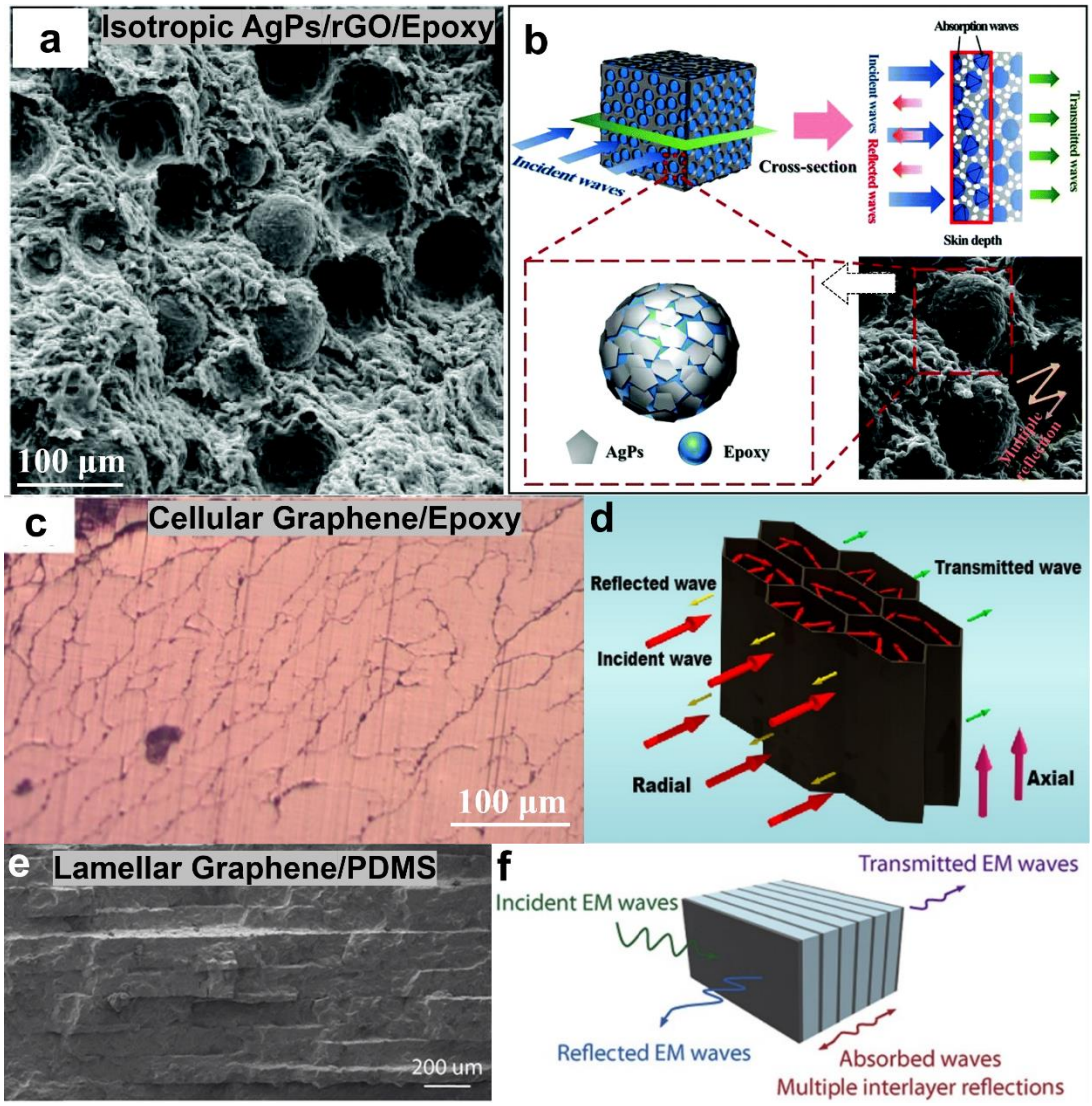

Figure 17. Ice-templating strategy to construct isotropic structure, anisotropic structure and lamellar structure for EMI shielding bulk composites. (a) Structure image and (b) schematic representation of EMI shielding mechanism of Ag platelets (AgPs)-rGO foam/epoxy composites with isotropic structure.[292], Copyright 2019. Adopted with permission from the Royal Society of Chemistry. (c) Structure image and (d) schematic representation of EMI shielding mechanism of graphene aerogel/epoxy composites with anisotropic structure.[160], Copyright 2016. Reproduced with permission from the American Chemical Society. (e) Structure image and (f) schematic representation of EMI shielding mechanism of graphene aerogel/PDMS composites with lamellar structure.[293], Copyright 2020. Adopted with permission from Elsevier Science Ltd.

When the 3D architecture prepared by an ice-templating method has evolved from isotropic segregated structure to anisotropic honeycomb-like and nacre-mimetic structures, numerous aligned polymer-conductive filler interfaces for the multireflection and decay of the incident electromagnetic waves can be formed, generating the composites with enhanced EMI shielding performance in a certain direction. Benefiting from the multiple interlayer reflection, highly aligned honeycomb-like (**Figure 17**c and d) and biaxially aligned lamellar (**Figure 17**e and f) graphene aerogels respectively prepared by unidirectional freezing and bidirectional freezing endow the polymer composites with intriguing EMI shielding performance along the orthogonal direction of ice growth, and EMI SE of the nacre-mimetic composites reaches ca. 65 dB at an extremely low graphene content (0.42 wt%).[160, 293] The lower freezing temperature the more lamellar interfaces, leading to more energy loss from electromagnetic waves and superior EMI shielding performance. These nanocomposites with superior EMI shielding performance can be potentially used to protect the target from suffering from electromagnetic radiation.

Currently, lightweight devices and systems are attracting growing interest. Thus, it is desirable to develop high EMI shielding composites with low density. It has been proved that both foaming[294, 295] and ice-templating technologies[296] can achieve this tough goal, and the latter can be employed to build a variety of structures. Aside from EMI SE value, specific SE (SSE, defined as SE divided by the density) and the surface SSE (defined as SSE divided by the thickness) are commonly used to simultaneously evaluate the shielding performance and the lightweight property. **Figure 18** summarizes recent researches on lightweight nanocomposites for highly effective EMI shielding, including compositions (water-borne polyurethane (WPU)/CNT 1$^{\#}$,[297] WPU/CNT 2$^{\#}$,[120] WPU/AgNW,[298] chitosan/CNT,[299]

and cellulose/CNT[300]), structures (aligned structure and interface structure), performance (EMI SE and the surface SSE) and mechanisms (multiple reflection at ameliorated cell wall or interface). With regard to three kinds of nanocellulose/AgNW aerogels with lamellar, honeycomb-like and random structures through adopting different freezing approaches, the lamellar structure endows the porous composite scaffolds with superior mechanical and EMI properties.[301] SE and the surface SSE of scaffolds respectively reach as high as 30.3 dB and 178235 dB cm^2 g^{-1} after optimizing lamellar porous structure. On the premise of the commercial shielding requirement (20 dB), the porous nanocomposites present higher value of the surface SSE than conventional dense shielding materials. Note that the porous nanocomposites can be easily tailored in a broad range of EMI SE and density owing to the controllable porous size, microstructure and compositions.

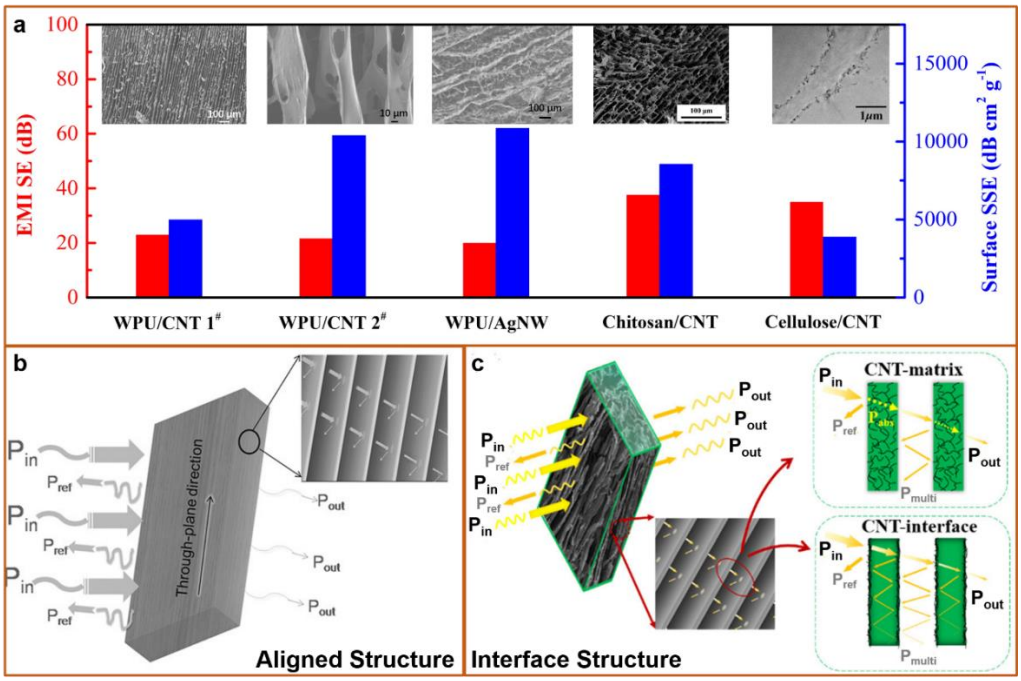

Figure 18. Structures (aligned and interface structures), performance (EMI SE and surface SSE) and working principles of lightweight porous EMI shielding composites. (a) Comparison of EMI SE and the surface SSE for composites with different systems and structures shown in upper SEM images: WPU/CNT 1# ([297], Copyright 2016. Adopted with permission from John Wiley & Sons

Inc.), WPU/CNT 2# ([120], Copyright 2017. Adopted with permission from John Wiley & Sons Inc.), WPU/AgNW ([298], Copyright 2017. Adopted with permission from the American Chemical Society.), chitosan/CNT ([299], Copyright 2018. Adopted with permission from Elsevier Science Ltd.), and cellulose/CNT ([300], Copyright 2018. Adopted with permission from the American Chemical Society.). Schematic representations of EMI shielding mechanisms for porous nanocomposites with (b) aligned structure ([297], Copyright 2016. Adopted with permission from John Wiley & Sons Inc.) and (c) interface structure ([300], Copyright 2018. Adopted with permission from the American Chemical Society.).

Compared with bulk materials, the mechanical properties of lightweight porous materials are relatively weak (*i.e.*, the compressive strength is basically lower than 1 MPa), especially for nanocomposites with extremely high surface SSE. Therefore, the exploitation of aforementioned EMI nanocomposites with a trade-off between high performance and enhanced mechanical properties is in urgent need. The lamellar structure in conjunction with interfacial design show great possibilities for the high-performance EMI shielding devices with low loading of functional fillers, which coincide with the features of structure constructed by bidirectional freezing and multiple freezing. It should be emphasized that MXene-based composites have been proved to outperform carbon-based composites and be as effective as metals in terms of EMI shielding.[302] Incorporating MXene into unique structure constructed by freeze-casting is a promising route to fabricate high-performance EMI shielding materials. Apart from existing bulk and porous EMI shielding composites, the membrane products need to be developed through freeze-casting approach, in particular bidirectional freezing, to expand their application scenarios. Besides, flexible and transparent electromagnetic interference shielding composites with desirable shielding performance while maintaining high light transmittances are another pursuit.

Although the majorities of the EMI shielding materials with high shielding performance are achieved by incorporating conductive fillers, a considerable sum of electromagnetic wave is reflected on the surface of the material, resulting in secondary pollution. Therefore, how to alleviate the contradiction between low or no reflection and high electromagnetic shielding performance to rationally devise absorption-dominated shielding materials is still desirable. Materials with high magnetic permeability can offer desirable electromagnetic wave absorption, but a high loading is required for a moderate EMI SE due to their low electrical conductivity. This can not only rely on functional materials, but also ought to go back to structure nature, namely, “structurally absorbing” ability. An example is the hierarchically porous architecture covering from micro or sub-micro to nanosized pores, exciting diffuse-reflection propagation mode.[303] Another example is the asymmetric conductive network with magnetically functional gradient (magnetic loss and impedance matching layer) and electrically functional gradient (conductive loss and reflection layer), forming absorption-reflection-absorption propagation mode.[304] Moreover, the influence of roughness of pore wall on electromagnetic wave propagation needs to be further clarified. These multiscale or asymmetric/gradient (including asymmetric distribution of functional materials and asymmetry of structure) architectures can be created and tuned by controlling the freezing parameters or coupling with other nanotechnologies.

3.5. Flexible sensors

Sensors are versatile devices that can transfer information into measurable signals. Flexible sensors have been developed owing to their broad and promising applications in wearable electronics, electronic skins (e-skins), personalized health-monitoring

devices, soft robotics, and so forth. Broadly, there are four kinds of transduction mechanisms for strain and pressure sensors based on the changes of resistivity, capacitance, piezoelectricity and triboelectricity of the systems when receiving external stimuli.[305] Commonly, flexible sensors have two important components: functional sensing elements and flexible supporting materials. Nanomaterials (AgNW, CNT, graphene, MXene, etc.) and conducting or semiconducting polymers (polyaniline (PANI), PEDOT:PSS, polypyrrole (PPy), etc.) with excellent electrical characteristics and mechanical durability are employed as active sensing materials while soft polymers (PU, PDMS, etc.) with remarkable flexibility and stretchability are utilized as supporting substrates.[306]

The working mechanisms of flexible and stretchable strain sensors such as resistive-type and capacitive-type sensors mainly involve tunneling effect, crack propagation, slippage and disconnection between sensing elements. Dimensional changes (geometrical effect) trigger the piezoresistive and piezocapacitance mechanisms of stretchable resistive-type and capacitive-type sensors according to the **Eq. 2** and **3**, respectively:

$$R = \frac{\rho L}{A} \tag{2}$$

$$C = \varepsilon_0 \varepsilon_r \frac{lw}{d} \tag{3}$$

where R represents the resistance, ρ represents the electrical resistivity, L and A respectively represent the length and the cross-sectional area of the conductor, C represents the capacitance, ε_0 and ε_r respectively represent the dielectric constant of vacuum and relative permittivity of dielectric media, l, w and d represent length, width, and thickness of the dielectric layer, respectively. Stretchability (operating range), sensitivity or Gauge Factor (GF, given by Eq. (4) for both resistive-type and

capacitive-type sensors), linearity in a wide strain range, response time especially for the viscoelastic polymers, hysteresis behavior under dynamic load, overshooting behavior originating from the stress relaxation of polymers, and dynamic durability (long-term service) are important parameters commonly used to evaluate the performance of flexible strain sensors.[306-308] Although great efforts have been made to improve the performance of flexible sensors, achieving a trade-off among aforementioned important parameters remains a great challenge.

$$GF = \frac{\Delta R/R_0}{\varepsilon} = \frac{\Delta C/C_0}{\varepsilon} \quad (4)$$

where ΔR and R_0 respectively represent the change in resistance (piezoresistivity) and initial resistance, ΔC and C_0 respectively represent the change in capacitance and initial capacitance, ε is the applied strain.

Microstructures of 3D-SMs in the composites play a critical role in strain sensing (the change of the electrical resistance). The sensing performance of freeze-casting composite sensors can be tuned by controlling architectures of 3D-SMs (isotropic, cellular and lamellar) and microstructures (pore size, wall thickness and bridge number). Isotropic, cellular and lamellar PDMS based composites have been developed by freeze-casting to produce high-performance strain sensors (**Figure 19**). The cell size and cell-wall thickness of the as-prepared 3D-SMs are correlated to the alterations in the sensitivities of the composite sensors. By increasing the graphene precursor concentration, the cell size of the graphene aerogel reduces, while its wall thickness increases, causing a decrease in sensitivity (the change in electrical resistance) for the final composite sensors. With the increase of freezing temperature, the cells enlarge and the number of the crosslinking sites (interconnections at the cell corners) for conductive path at a given volume reduce, bringing about a higher

sensitivity. On the other hand, the cell-wall thickness increases as the freezing temperature increases, resulting in a lower sensitivity owing to that the conductive overlap area remains almost unchanged. Consequently, the piezoresistive sensitivity (GF) of graphene aerogel/PDMS nanocomposite sensors reaches a maximum value at an intermediate freezing temperature (**Figure 19**a and b).[309]

Due to the anisotropic growth of ice crystals, freeze-casting is able to produce directional sensors with distinct anisotropic behaviors, including electrical conductivity, mechanical property and sensing performance. A directional strain sensor containing an anisotropic cellulose nanofiber/CNT aerogel with microhoneycomb channels possesses a 92% sensitivity difference between the aligned channel direction and its orthogonal direction.[310] The mechanical compression of the aligned structure into a porous film creates more contact area and more perfect conductive pathways (**Figure 19**c), simultaneously improving the stretchability (up to 122%), linear sensing region (0-110%), sensing sensitivity (*ca.* 7.2) and dynamic durability of the strain sensors when stretched along the transverse direction (**Figure 19**d), whereas the sensors show smaller sensing strain and higher strain sensitivity when stretched along the longitudinal direction. Moreover, the potential application in detection of human motions (finger and knee bending shown in **Figure 19**e) for the thin-film sensors is successfully shed light on.[311] Additionally, an advanced self-powered pressure and shear sensor consisting of PDMS and lead zirconate titanate (PZT) has been manufactured.[312] Typical lamellar piezoelectric architectures (**Figure 19**f and g) have been constructed in the composite sensors *via* freeze-casting route. The self-powered sensors are able to operate in pressure and shear sensing modes to detect light finger tapping and shearing (**Figure 19**h), enriching the application scenarios of the flexible sensor without external energy supply.

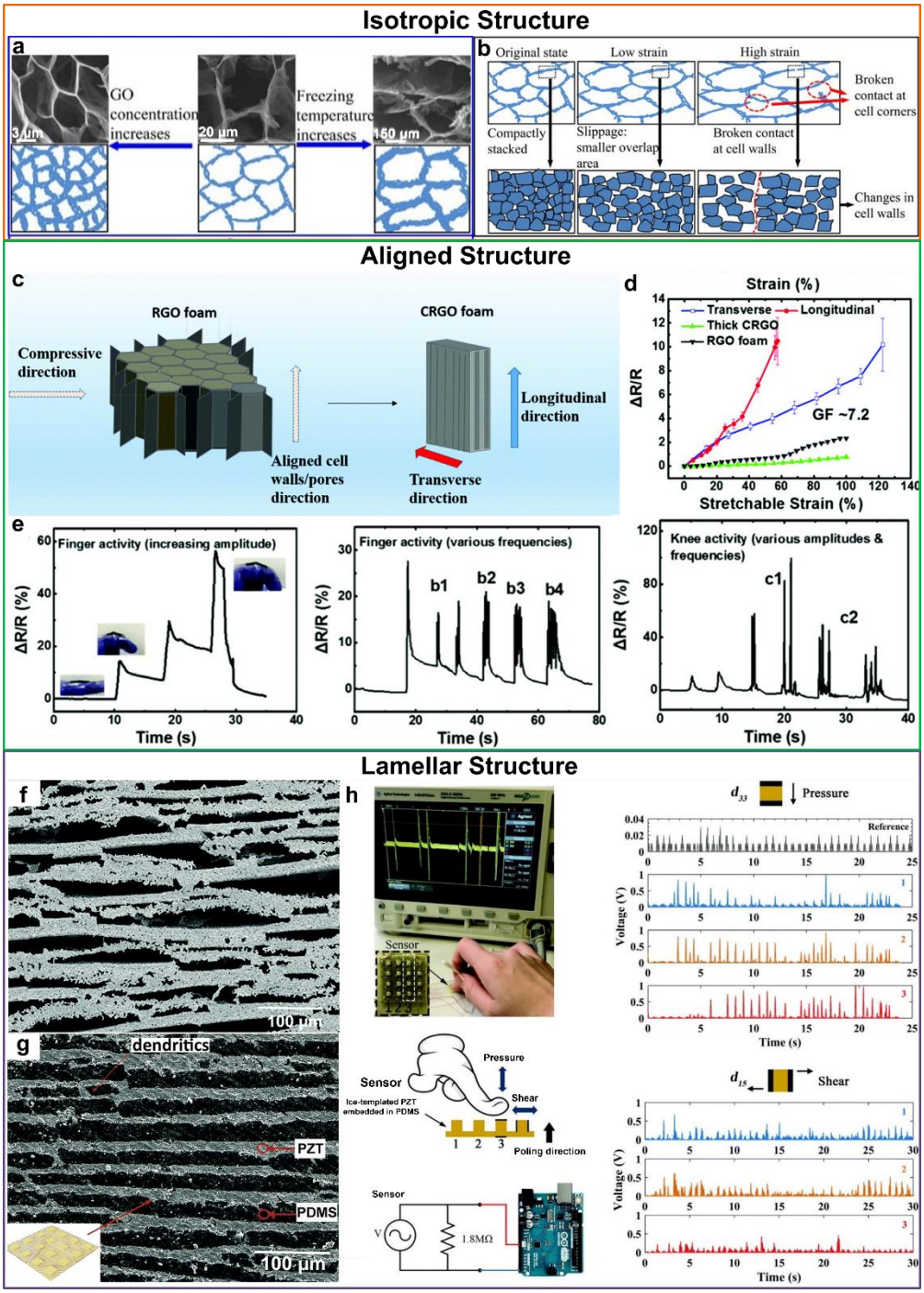

Figure 19. PDMS based composite sensors with (a-b) isotropic structure, (c-e) aligned structure and (f-h) lamellar structure constructed by freeze-casting. Schematic illustrations of (a) the microstructures of the graphene aerogels with different concentrations of GO and freezing temperatures and (b) piezoresistivity mechanisms in PDMS/graphene aerogel nanocomposite sensors.[309], Copyright 2016. Adopted with permission from the American Chemical Society. (c) Schematic illustrations of the preparation process of anisotropic compressed rGO foam. (d) Sensing performance of PDMS/anisotropic compressed rGO foam nanocomposite sensors: the

ratio of relative change in resistance *versus* strain curves of different strain sensors. (e) Monitoring of human motions: finger and knee bending activities with different amplitudes and frequencies.[311], Copyright 2017. Reproduced with permission from the Royal Society of Chemistry. SEM images showing lamellar structure of (f) porous PZT and (g) PDMS/PZT composites. (h) The measurement of sensor sensitivity of PDMS/PZT self-powered composite sensors through light finger tapping and shearing.[312], Copyright 2018. Reproduced with permission from the Royal Society of Chemistry.

Also, the directional ice-templating strategy has been adopted to fabricate lightweight pressure sensors in the form of aligned porous foams. Exactly as bulk composite sensors, the porous pressure sensors can be employed to detect the human motions, such as jump, walk, arm bending, standing on tiptoe and squat.[161] To tune the electromechanical properties, a third component epoxy has been introduced into CNT/thermoplastic polyurethane (TPU) foam.[121] Compared with the disordered foam, the aligned foams exhibit superior mechanical performance and piezoresistive reproducibility, maintaining the stability of porous sensors even under a large deformation, which is ascribed to the ladderlike and herringbone structures connecting the cell strut.

The 3D conductive network constructed by freeze-casting is generally good, and the resultant composite sensors are suitable for the scenarios with a relatively large deformation such as mechanical movement of human body. It is difficult for the freeze-casting sensors to detect a small strain like pulse. Imparting cracks and defects to the conductive network or reducing the number of bridges during or after ice solidification may be a solution. Some measures, such as defective nanomaterials and multistep freezing, may work for this target. Therefore, the parameters of ice-templating technology need to be adjusted according to the requirements of sensing performance for different application scenarios.

Rapidly increasing demands for human-machine interactions and artificially intelligent applications offer more opportunities for the development of smart sensors. However, ice-templating method has been adopted to prepare various porous aerogels or scaffolds for 3D sensing devices, which hampers their usefulness, such as e-skins and wearable applications. More attention needs to be paid on the fiber-based, film-based and gel-based sensors associated with freeze-casting. More importantly, there is an issue that the sensitivity is relatively low under a small strain when the majorities of 3D conductive composites act as strain sensors. Once a 3D conducting network is transformed into 2D conducting network, the strain sensor shows extremely high sensitivity under a small strain ($\varepsilon < 5\%$).[313] It is desirable to develop future sensors with 2D random or aligned conducting network through freeze-casting method.

3.6. Thermally conductive composites

Heat can be transferred in the form of radiation, convection or conduction. Generally speaking, heat conduction is the main mode of heat transfer in solid materials. Heat conduction is the result of collision and transfer of microscopic particles in matter, from a fundamental perspective. The carriers of heat conduction in matter mainly include electrons, photons and phonons. Overwhelming majorities of polymers rely mainly on phonons (energy quanta of atomic lattice vibrations) for their primary heat conduction. Thermal conductivity (k) in W m^{-1} K^{-1}, directly related to heat conduction, can be defined by **Eq. 5**:

$$k = \alpha C_p \rho \tag{5}$$

where C_p represents specific heat capacity in J kg^{-1} K^{-1}, α and ρ represent the thermal diffusivity in m^2 s^{-1} and the density in kg m^{-3}, respectively. Opposite to k, the thermal resistance (R, Kapitza resistance[314]) frequently stems from structural defects owing

to phonon scattering (phonon/phonon scattering, phonon/interface scattering and phonon/defect scattering). For polymer composites, there are many factors affecting their thermal conductivities,[315] mainly including intrinsic thermal conductivity of matrices (molecular chain structure, molecular chain orientation, crystallinity, etc.), geometric characteristics and aggregation or dispersion states of thermally conductive fillers, and the interfacial interactions between matrices and thermally conductive fillers.[316-318]

With the development of advanced electronic devices and energy conversion systems, the heat transport has become a critical issue for their applications.[319] It is of technological importance to develop novel polymer composites with high thermal conductivity. Unfortunately, bulk polymers commonly possess low thermal conductivity, about 0.2 W m^{-1} K^{-1} at room temperature.[320, 321] The thermally conductive fillers, including metals (*e.g.*, Cu[322] and Ag[323]), carbon materials (*e.g.*, CNT,[324] graphite,[325] graphene[326, 327]), and ceramic particles (*e.g.*, Al_2O_3,[328] BN,[329, 330] SiC[331]), are traditionally employed to enhance thermal conductivity of polymer composites. Additionally, it is remarkable that the low-dimensional nanomaterials show highly anisotropy. For instance, hexagonal BN, a typical two-dimensional layered material, exhibits anisotropic thermal conductivity, and the thermal conductivities along the in-plane and out-of-plane directions are about 600 and 30 W m^{-1} K^{-1}, respectively, as schematically illustrated in **Figure 20**a. The horizontally and vertically oriented BN platelets are responsible for the (002) and (100) peaks, respectively. Therefore, the degree of orientation of BN platelets can be estimated by X-ray diffraction (XRD) measurements.[332, 333] In order to make full use of the anisotropy of the low-dimensional nanomaterials and improve their utilization efficiency, plenty of researches focus on increasing their orientation to

enhance the thermal conductivity of composites. Two-roll mill,[334] casting,[335] vacuum-assisted filtration,[336, 337] and external fields (including magnetic field[338] and electric field[339]) have been applied to fabricate polymer composites with enhanced anisotropic thermal conductivity. In a sense, thermally conductive composite is the most successful case for the application of ice-templating strategy owing to the pre-construction of 3D continuous conductive network for phonon transfer in the composites. However, its implementation could be restricted by the polymer matrices, which is also an unavoidable issue for other functional composites.

Epoxy, a common thermoset, has been proved to be a good candidate for the fabrication of 3D-SMs based polymer composites. Graphene, BN, SiC and their derivatives have been used to construct 3D thermally conductive architectures with ordered structures for the epoxy based composites with enhanced through-plane thermal conductivity *via* the combination of ice-templating and self-assembly strategies, as listed in **Table 1**. Compared with random conductive structure, hierarchically ordered 3D networks, especially vertically aligned structure, are more conducive to the improvement of through-plane thermal conductivity.[162] Guided by this idea, GO liquid crystals have been employed as precursors to produce low-density vertically aligned and interconnected graphene frameworks for the preparation of epoxy composites with high thermal conductivity and thermal conductivity enhancement (TCE, calculated by **Eq. 6**).[340] In this line of interest, the conductive microstructures of these vertically aligned graphene aerogels have been tailored by changing the freezing rate (the relative location of mold, working stage and cold source) during the directional-freezing and freeze-drying processes to maximize phonon transfer (**Figure 20**b and c).[341]

It is worth mentioning that graphene is well-advised to be annealed at extremely high temperature for graphene-based thermal interface materials (TIMs) when GO is used as precursor to prepare graphitized graphene with high intrinsic thermal conductivity, otherwise it is difficult to repair its defects producing phonon scattering.[342, 343] Different from thermally conductive graphene/polymer composites with electrical conductivity, BN has been considered as a competitive candidate for the fabrication of thermally conductive yet electrically insulating composites. Unfortunately, exfoliating or functionalizing BN is troublesome, and thus it is difficult for bulk BN to construct macroscopically 3D network structure without the assistance of condiments, even for successfully exfoliated nanosheets. Graphene,[344, 345] cellulose,[329] water-soluble PVA[346] and chitosan[347, 348] are considered as common condiments for building 3D-BN functional architectures. Considering the small lattice mismatch (less than 2%), graphene is regarded as the most promising phonon-transferring substrate for BN, and thus a 3D BN-rGO skeleton with typical hierarchical microscale structure has been developed for the fabrication of thermally conductive yet electrically insulating polymer composites. BN plates are bridged by GO in the form of B−C and N−C bonds and then assembled into a vertically aligned phonon transport network through high energy ball milling treatment and directional ice-templating assembly, respectively (**Figure 20**d and e).[349] After the subsequent impregnation of liquid resin, the obtained epoxy/3D BN-rGO composites possess an ultrahigh through-plane thermal conductivity of 5.05 W m^{-1} K^{-1} at a low BN loading of 13.16 vol% (**Figure 20**f). In this case, the thermal conductivity of 3D framework is the most crucial factor affecting thermal conductivity of the resultant composites, rather than the interfacial thermal resistance of 3D skeleton-to-matrix and the intrinsic thermal conductivity of the matrix. Further to improve the utilization efficiency of BN, the exfoliated BN

nanosheets (BNNSs) have been used to prepare thermally conductive epoxy composites with long-range continuous conductive channels.[350, 351] Different from physical overlap between fillers, the covalently interconnected mode is more beneficial for the improvement of thermal conductivity owing to the reduction of phonon scattering at the joints. A vertically aligned SiC sheet scaffold for thermally conductive epoxy based composites has been prepared by a CVD method with ice-templating graphene skeleton as growth template.[352]

In addition to the typical 2D graphene, BN and SiC sheet, 1D SiC microwires (SiCMWs), SiC nanowires (SiCNWs), CFs and copper nanowires (CuNWs) as well as aluminum nitride (AlN) particles have been developed for the preparation of epoxy composites with enhanced through-plane thermal conductivity by means of ice-templating method.[353-357] For example, Yao et al.[354] has prepared a series of vertically aligned and interconnected SiCNW network structures by adjusting the proportion of components and infiltrated them with epoxy matrix. The final composites exhibit a high through-plane thermal conductivity up to 1.67 W m^{-1} K^{-1} at a relatively low filler loading (2.17 vol %). According to **Eq. 7**, TCE efficiency per unit volume loading (η) is 381%.

$$\mathrm{TCE} = \frac{k_c - k_m}{k_m} \tag{6}$$

$$\eta = \frac{TCE}{100V} = \frac{k_c - k_m}{100Vk_m} \tag{7}$$

Where k_c and k_m represent thermal conductivities of composites and matrix, respectively, and V represents the volume fraction of filler in composites.

Table 1. Comparison of through-plane thermal conductivity and η of the reported epoxy-based composites prepared by the combination of ice-templating and self-assembly strategies using laser flash measurement method.

Thermally Conductive Fillers	Loading (vol%)	Thermal Conductivity (W m^{-1} K^{-1})	TCE (%)	η (%)	Condiments	Ref.
Graphene	0.92	2.13	1231	1338	N/A	2016[340]
Graphene	0.75	6.57	3765	5020	N/A	2018[341]
BN	34.2	4.42	2226	65	Sodium carboxymethylcellulose	2017[162]
BN	13.16	5.05	2706	206	rGO	2018[349]
BNNSs	9.29	2.85	1681	181	PVA (carbonization)	2015[350]
BNNSs	4.4	1.56	734	167	Microcrystalline cellulose	2019[351]
SiC sheet	3.71	14.32	6126	1651	N/A	2020[352]
SiCMWs	1.32	0.62	288	218	Cellulose nanofiber	2019[353]
SiCNWs	2.17	1.67	828	381	Sodium carboxymethylcellulose	2018[354]
CFs	13.0	2.84	1395	107	Hydroxyethyl cellulose	2020[355]
CuNWs	1.12	0.79	365	326	Cellulose nanofiber	2020[356]
AlN	47.26	9.48	3411	72	N/A	2020[357]

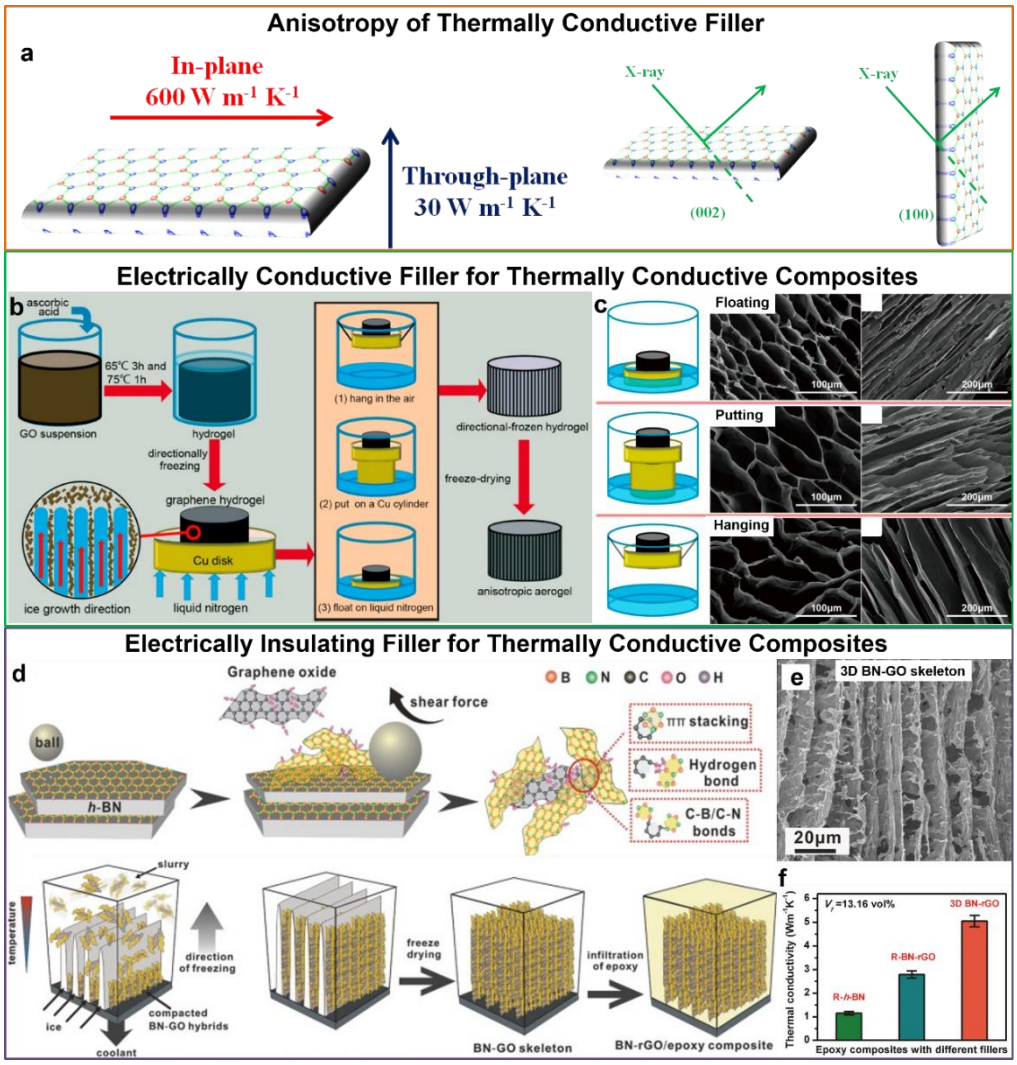

Figure 20. A unidirectional freezing strategy to fabricate representative epoxy based composites with high through-plane thermal conductivity using 2D electrically conductive graphene and electrically insulating BN. (a) Anisotropic thermal conductivity of hexagonal BN platelet: the thermal conductivities along the in-plane and out-of-plane directions are about 600 and 30 W m^{-1} K^{-1}, respectively. The illustration of the effect of the aligned BN on XRD pattern: the horizontally and vertically oriented BN are responsive for the (002) and (100) peaks, respectively.[332, 333] (b) Schematic illustration of the preparation route and (c) top-view and side-view SEM images of vertically aligned graphene aerogels with different microstructures by tailoring the freezing rates.[341], Copyright 2018. Reproduced with permission from Elsevier Science Ltd. (d) Schematic illustration of the synthesis of GO-BN hybrids *via* ball-milling method and the preparation of 3D BN-rGO and the corresponding epoxy composites. (e) Cross-sectional SEM image of 3D BN-GO framework. (f) The comparison of thermal conductivity for epoxy composites with three different types of fillers (randomly dispersed BN, randomly dispersed BN-rGO and 3D BN-rGO skeleton) at a similar loading.[349], Copyright 2018. Adopted with permission from John Wiley & Sons Inc.

Ice-templating method can be used not only to prepare the composites with high through-plane thermal conductivity as reported above, but also to prepare the polymer composites with high in-plane thermal conductivity. Currently, the composites with high in-plane thermal conductivity are usually thin film products,[336, 358, 359] and a directional freezing route has been adopted to produce thermally conductive polyimide (PI)/BNNS composites with the incorporation of AgNW as thermally conductive bridges.[360] More interestingly, a novel sequential bidirectional freezing strategy has been proposed to construct highly aligned micro-sandwiched structure with alternating conductive graphene and insulating BN layers for multifunctional PI nanocomposite film with high in-plane thermal conductivity, excellent dielectric performance, exceptional energy storage density and moderate breakdown strength (**Figure 21**a).[361] The distinctively separated BNNS and graphene layers (**Figure 21**

b) impart higher thermal conductivity to the composites compared with those consisting of mixed fillers, which can be explained by the fact that the phonon transport at the interfaces between two identical species with the same phonon vibrational characteristics is superior than that at graphene/BNNS hetero interfaces (**Figure 21**c). Likewise, the bulk composites with enhanced in-plane thermal conductivity are also badly needed. Nacre-mimetic polymer-based TIMs with a much high in-plane thermal conductivity up to 6.07 W m^{-1} K^{-1} at a low BNNS loading of 15 vol% have been yielded owing to the construction of prolonged phonon pathways from long-range organized conductive lamellar structure (**Figure 21**d-f).[362] The polymer-based composites as TIMs (**Figure 21**g) and thermal protection materials (**Figure 21**h) exhibit improved performance and potential application in thermal management of electronic packaging devices.

The composites with nacre-mimetic lamellar network exhibit superior thermal conductivity and faster thermal response rate than those with randomly distributed and uniaxially aligned networks, and the moderate layer density and thickness are the preferred selection for improving thermal conductivity of the composites. Similar to vacuum-assisted filtration, bidirectional freezing can construct nacre-mimetic lamellar structure and shows superiorities in the preparation of in-plane conductive composites. Note that in-plane thermal conductivity of the composites increases with an increase in the measured temperature owing to that conductive network can be stacked closely under the thermal expansion of the resin to form an enhanced phonon pathway, whereas through-plane thermal conductivity hardly changes.

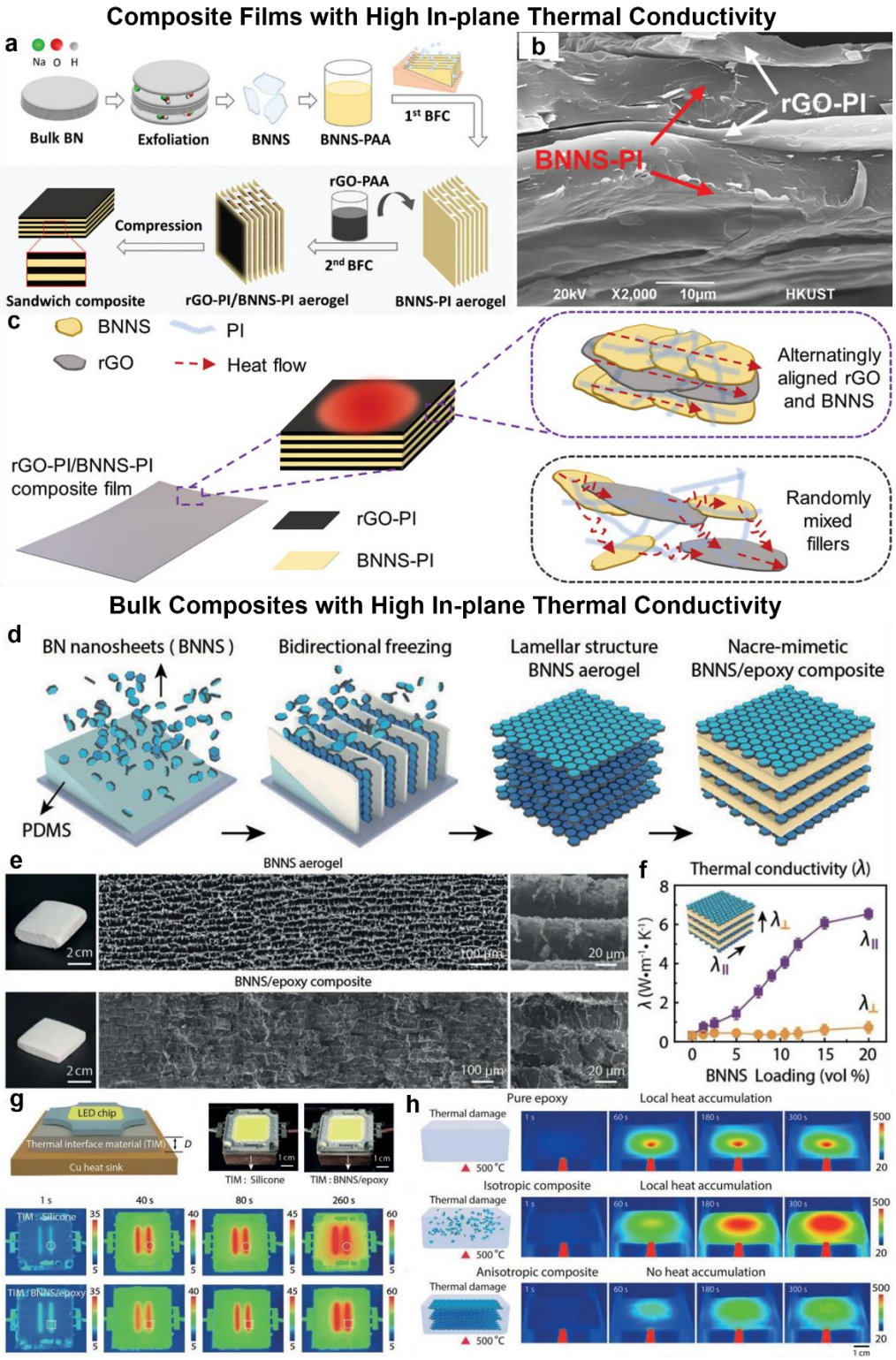

Figure 21. Bidirectional freezing strategy to fabricate (a-c) polymer composite films and (d-h) bulk composites with high in-plane thermal conductivity. (a) Schematic illustration of the fabrication route of graphene-PI/BNNS-PI composites by sequential bidirectional freezing. (b) SEM image showing alternately layered structure of graphene-PI/BNNS-PI composites. (c) Schematic illustration of mechanisms for heat conduction in graphene-PI/BNNS-PI

composites.[361], Copyright 2020. Reproduced with permission from John Wiley & Sons Inc. (d) Schematic illustration of the fabrication route of BNNS aerogels with long-range aligned lamellar structure and the epoxy based composites using a bidirectional freezing technique. (e) Optical and SEM images of BNNS aerogels and epoxy-based composites. (f) In-plane thermal conductivity ($\lambda_{\parallel}$) and through-plane thermal conductivity ($\lambda_{\perp}$) of epoxy/BNNS composites. Potential applications of epoxy/BNNS composites as (g) TIMs and (h) thermal protection materials.[362], Copyright 2019. Adopted with permission from John Wiley & Sons Inc.

Apart from robust polymer composites, rubber-based polymers can also be employed to produce flexible conductive composites using 1D CF,[363] 2D BN or BNNS,[364, 365] 2D MXene,[366] 1D SiCNW/2D graphene hybrids[367] (**Figure 22**). These vertically aligned and interconnected conductive network structures endow PDMS based composites with high through-plane thermal conductivity and TCE. The difference in thermal conductivity predominantly originates form the intrinsic thermal conductivity of fillers, the aspect ratio of fillers, the topological structure of conductive network, the coupling between fillers and the interaction between filler and matrix. In the case of hybrid fillers, apart from aligned conductive structure, there is a synergistic effect from hybrid fillers with different geometries on the improvement of thermal conductivity. To further improve the interfacial interaction and the wettability between the functional filler network and silicone rubber matrix, PDMS can be grafted with hydrophilic PEG before infiltrating vertically aligned SiCNW/rGO/cellulose nanofiber scaffolds. Consequently, thermal conductivity of the silicone rubber composites is up to 2.74 W m^{-1} K^{-1} at 1.84 vol% hybrid filler network.[367] As expected, these flexible products exhibit stable heat dissipation capacity with a wide working temperature range and can be utilized as a thermal management component of electronics such as CPU core.

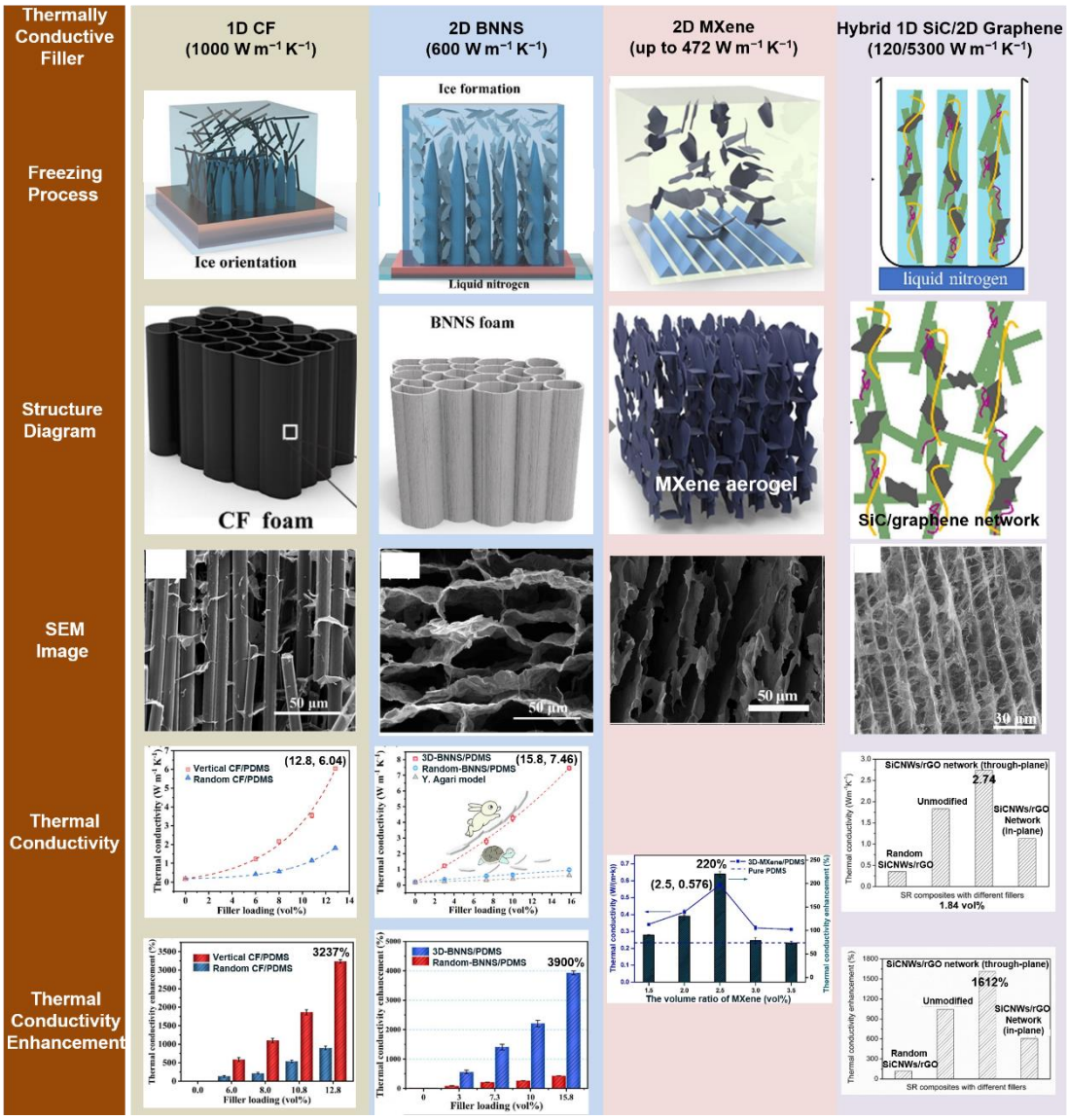

Figure 22. Directional freezing strategy to fabricate flexible PDMS based composites with high through-plane thermal conductivity using 1D CF ([363], Copyright 2019. Adopted with permission from Elsevier Science Ltd.), 2D BNNS ([365], Copyright 2019. Adopted with permission from the American Chemical Society.), 2D MXene ([366], Copyright 2019. Adopted with permission from Elsevier Science Ltd.), and 1D SiCNW/2D graphene hybrids ([367], Copyright 2020. Reproduced with permission from Elsevier Science Ltd.).

Also, a breakthrough has been achieved in nature rubber based composites used as heat dissipation component.[368, 369] Bonding modes and assembly morphologies of fillers play a significant role in thermal conductivity improvement of the composites. Namely, the covalent bonding and the construction of ordered 3D network of

functional fillers are instrumental in reducing the interfacial thermal resistance of fillers-to-fillers and fillers-to-matrix, respectively. The ingenious combination of surface modification of filler or grafting modification of matrix and highly ordered architecture constructed by ice-templating method will greatly enhance thermal conductivity of composites, achieving the effect of "1 + 1 > 2". Considering that they can fit with devices well to squeeze out the air at the interfaces, the flexible materials show great application potential in the preparation of thermally conductive composites with low thermal contact resistance (R_c) obtained from **Eq. 8** and **9** and are expected to be a hotspot in the next stage.[370]

$$R_{TIM} = \frac{BLT}{k_{TIM}} + R_{C1} + R_{C2} \tag{8}$$

$$\frac{1}{R_c} = \frac{5k_1k_2}{2(k_1+k_2)}\left(\frac{m}{\sqrt{\sigma_1+\sigma_2}}\right)\left(\frac{P}{H}\right)^{0.95} \tag{9}$$

Where R_{TIM}, BLT and k_{TIM} respectively represent the thermal resistance of TIMs, the thickness of interface and the thermal conductivity of TIMs, R_{C1} and R_{C2} are the thermal contact resistances at the two bounding interfaces, k_1 and k_2 are thermal conductivity of the two contact surfaces, P is the contact pressure, H is the surface microhardness of the softer one of the two contacting surfaces, and σ_1 and σ_2 are the surface roughness of the two contacting surfaces, m is the mean asperity slope.[371, 372]

With the assistance of the ice-templating strategy, Yang et al.[42, 46, 373] successfully constructed the typical porous GO/BN porous scaffolds with isotropic and aligned network structures, giving rise to the formation of thermally conductive pathways in PEG based composite phase change materials (PCMs). In the case of isotropic structure (**Figure 23**a), BN platelets are driven and self-assembled into the

effective heat transport pathways akin to the segregated/sacrificial salt templating structures by the ice-growth.[374, 375] Similar results have been further verified in subsequent study when chitosan substitutes for GO as the support material.[376] More interestingly, the aligned porous scaffolds with variable microstructures have been obtained by changing the freezing temperature, and thermal conductivity of the porous scaffolds and the composite PCMs reaches a maximum value at − 50 °C (**Figure 23**b). As the freezing temperature increase, the reduction of the thermally conductive interface and the higher degree of orientation of fillers contribute to the improvement of thermal conductivity. Further increasing freezing temperature, the well-formed conductive network for aligned structure with bridges is destroyed due to the growth of the large-size ice crystals, resulting in the phonon scattering at the defect. Likewise, the microcrystalline cellulose/graphene nanoplatelets aerogels with highly aligned network structure have been constructed by pre-refrigeration and freeze-drying processes to improve thermal conductivity of PEG.[377] Radial freezing method has been also applied to prepare hierarchical AgNW aerogel with axially and radially aligned structure for high-efficiency thermal energy storage composites.[378] These composite PCMs with high thermal conductivity greatly improve the working efficiency of the latent heat energy conversion and storage systems.

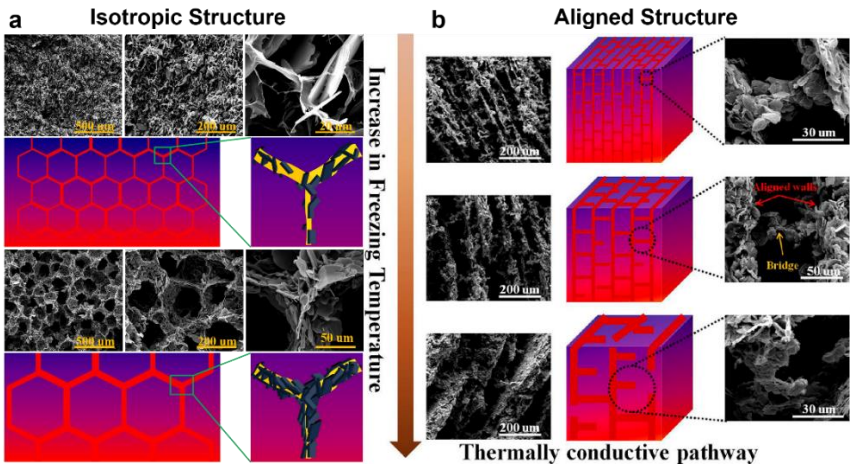

Figure 23. Ice-templating strategy to fabricate PEG based composite PCMs with high thermal conductivity and the effect of freezing temperature and stacking mode of conductive fillers on their thermal conductivities. SEM images and schematic diagrams of variable microstructures and thermally conductive pathways in the composite PCMs with (a) isotropic GO/BN hybrid porous scaffolds ([42], Copyright 2016. Reproduced with permission from the Royal Society of Chemistry.) and (b) aligned GO/BN hybrid porous scaffolds ([373], Copyright 2018. Reproduced with permission from the American Chemical Society.).

The aforementioned cases reveal the effect of the thermally conductive pathways ingeniously constructed by the ice-templating method on thermal conductivity improvement of polymer composites. The combination of ice-templating assembly and interfacial modification can endow the composites with better performance owing to that the latter can further reduce the thermal resistance inside the as-formed conductive network or between the conductive network and the matrix. From the perspective of functional fillers, the hybrid fillers with different categories and geometries can cooperate with each other to build synergistic conductive pathway. On the other hand, thermal conductivity of the composites is far below the inherent properties (up to 5300 W m^{-1} K^{-1}) of graphene due to the presence of defects in the sophisticated operations and limited reduction of GO precursor.[379] Therefore, highly crystalline functional materials with large aspect ratio, such as nonoxidized graphene[380] and graphite sheets,[381] are expected to be put in a dominant position in the preparation of thermally conductive composites. Additionally, flexible and thermostable (*e.g.*, PI and aramid nanofiber) polymer matrices are good candidates for the production of thermal management materials conforming to curved/rough surfaces and high-temperature conditions.

The correlation of the thermal conductivity of as-prepared scaffold and the thermal conductivity of final composites as well as the specific role of the bridge between

adjacent layers needs to be clarified. For different stacking modes (isotropic structure, aligned cellular structure and aligned lamellar structure), the freezing temperature seems to play different roles in the construction of conductive network. A closer inspection shows that a relatively high freezing temperature (slow freezing rate) is conducive to the construction of heat conduction network in the composites, but it weakens their mechanical properties. In other words, it is difficult for the structure with thick wall and large pore size to simultaneously enhance thermal conductivity and mechanical properties of the polymer composites. CVD technique has been proved to be able to construct hierarchical structure to improve the shape-stability of organic PCMs, creating high-performance composite PCMs with enhanced thermally conductivity and shape-stability.[382, 383] It may be an effective way to construct secondary structure on the basis of large-size porous structure using the freeze-casting technique, but it needs to be further confirmed.

According to **Eq. 8**, aside from thermal conductivity, the thermal management ability of TIMs is dependent on the thickness of interface. At present, freeze-casting strategy is mainly adopted to fabricate bulk composites with high through-plane thermal conductivity and composite films with high in-plane thermal conductivity. Therefore, it is meaningful and challenging to develop composite films with high through-plane thermal conductivity. In the most of practical application scenarios, high through-/out-of-plane thermal conductivity of TIMs can promote heat transfer (**Figure 24**a). However, the recent studies reveal that in-plane oriented composites exhibit superior performance when applied to the scenarios where heat is generated from small localized regions (*i.e.*, spot heat source), which can meet the requirements of the integration and miniaturization for electronics (**Figure 24**b).[384, 385] Therefore, it is of significance to customize conductive structures according to various application

scenarios. If a device works as radiant or pillar heat source shown in **Figure 24**c, it is unclear whether through-plane composites are applicable. The deformation difference in the inner and outer regions and additional adhesive operation for through-plane composites should be taken into account. The radial monoliths seem to be capable of evading them well. Freeze-casting strategy can be used to construct isotropic structure, cellular structure, lamellar structure and radial structure and fabricate the corresponding composites. Will the radial-plane composites be available for radiant or pillar heat source?

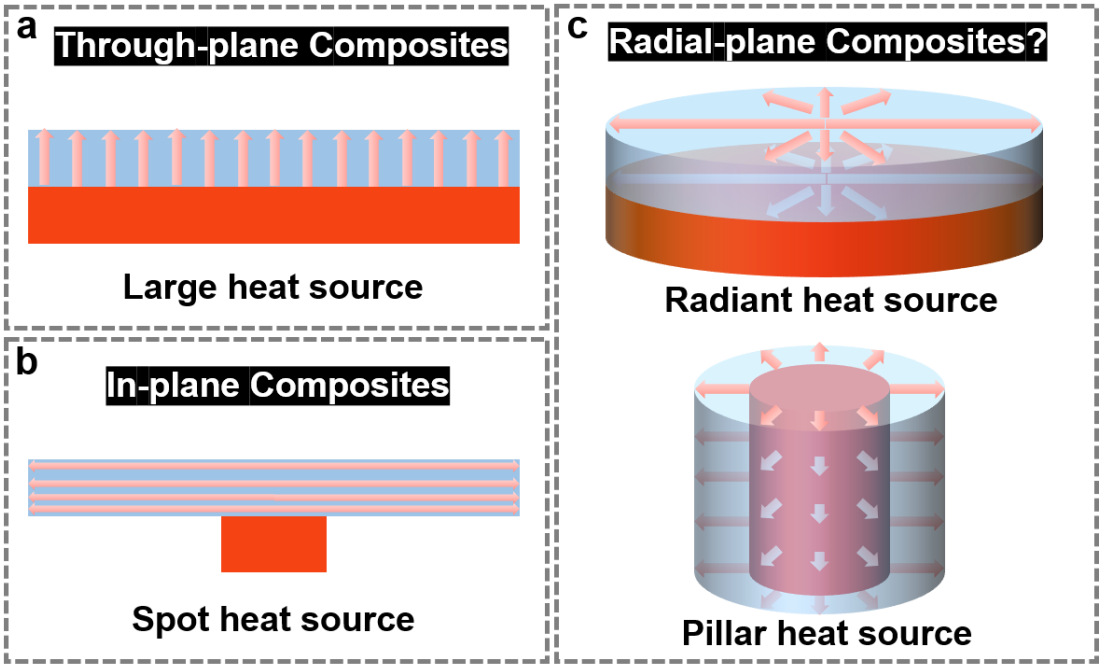

Figure 24. Thermally conductive composites for different application scenarios: (a) through-plane composites for large heat resource, (b) in-plane composites for spot heat source and (c) radial-plane composites for radiant or pillar heat source.

3.7. Thermally insulating composites

Opposite to the thermally conductive materials, thermally insulating materials possess extremely low thermal conductivity, showing broad application prospects in buildings,[386] aerospace,[387] fabrics,[388] etc.[389] Although strenuous efforts

have been devoted to substantially reducing thermal conductivity value,[390-392] it is still challenging for high-performance thermally insulating materials to achieve satisfaction value below the most common superinsulating criterion (25 mW m^{-1} K^{-1}, synonymous with thermal conductivity of air).[393, 394] Inorganic insulating materials with nanostructures such as silica aerogel exhibit exceptionally thermal insulation performance below 20 mW m^{-1} K^{-1}, but they are mechanically brittle and their cost-effective mass production is difficult to realize.[395] To improve the mechanical strength of the inorganic insulating materials, the construction of organic-inorganic hybrids[396, 397] and cross-linking with elastic network[218] have been regarded as effective strategies. Interestingly, the ice-templating method has been launched in the preparation of superinsulators.

Polymer building blocks can be directly assembled into superinsulators by nondirectional freezing, but the aerogel products show relatively poor mechanical performance.[398] Toward highly effective and mechanically enhanced thermal insulating polymer composites, aligned porous structures have be designed (**Table 2**). Additionally, the nanosized components, microstructures of the pore wall and few interlamellar connection or “bridge” can work as phonon barrier to substantially reduce solid heat conduction. Nanomaterials have been assembled into anisotropic tubular pore structures by unidirectional freezing to produce fire-retardant cellulose nanofibres/GO/sepiolite nanorod insulators[399] and artificial polymeric woods based on chitosan and phenol-formaldehyde resin or melamine-formaldehyde resin[400]. The artificial composites containing GO exhibit enhanced comprehensive performance, comparable mechanical properties of natural wood, preferable thermal insulation (ca. 21 mW m^{-1} K^{-1}), prominent inherent corrosion resistance to humidity and acid and fire retardancy.[400] Similar to nanomaterials, hollow GO microspheres

have been designed to fabricate thermally insulating PI/rGO composites with thermal conductivity of 9 mW m^{-1} K^{-1} due to the increase of phonon scattering at the cellular walls.[401, 402] Owing to a decrease in solid heat conduction, the lamellar aerogels with fewer bridges connecting the cell walls exhibit the superior thermal insulating performance than those with isotropic pore structure and honeycomb-like structure along the direction of lamella, which is nearly half of thermal conductivity in the orthogonal direction.[403]

Table 2. Freeze-casting strategy to produce polymer based superinsulators.

Material System	Density (mg cm^{-3})	Radial Thermal Conductivity (mW m^{-1} K^{-1})	Freezing Mode	Ref.
Esterified cellulose nanocrystals/Chitosan/Agar	3.3	21	Random	2019[398]
Cellulose nanofibres/GO/Sepiolite	7.5	15	Unidirectional	2015[399]
Chitosan/Phenol-formaldehyde resin/GO	<85	21	Unidirectional	2018[400]
PI/rGO	~8	12	Unidirectional	2019[401]
PI/rGO	9.2	9	Unidirectional	2017[402]
PI/Bacterial cellulose	46	23	Bidirectional	2019[403]

Enlightened by the hollow structure of polar bear hair, a “freeze-spinning” method (**Figure 10**c) has been proposed to achieve continuous production of axially aligned porous fibers using silkworm cocoons (precursor of silk fibroin) and chitosan as raw materials.[53] The aligned porous structure shown in **Figure 25**a-c is more beneficial to the improvement of mechanical properties of fibers than the random porous structure, which is consistent with the previous conclusion. The smaller the pore size of fiber becomes, the better the thermal insulating performance is, which can be explained by the fact that the small pore size creates numerous solid-air interfaces for tortuous photon conduction and multiple scattering. The biomimetic textiles woven from porous fibers inherit superior thermal insulating performance than commercial

textiles (**Figure 25**d), offering great potential in the development of thermal stealth clothing with a wide range of working temperature from −10 to 40 °C (**Figure 25**e). The "freeze-spinning" technique proposed here shows untapped potential in the manufacture of smart fibers or textiles for more wearable systems, such as flexible electronics,[404] temperature regulating clothing,[405] energy harvesting devices,[406] fabric sensors,[407] etc.

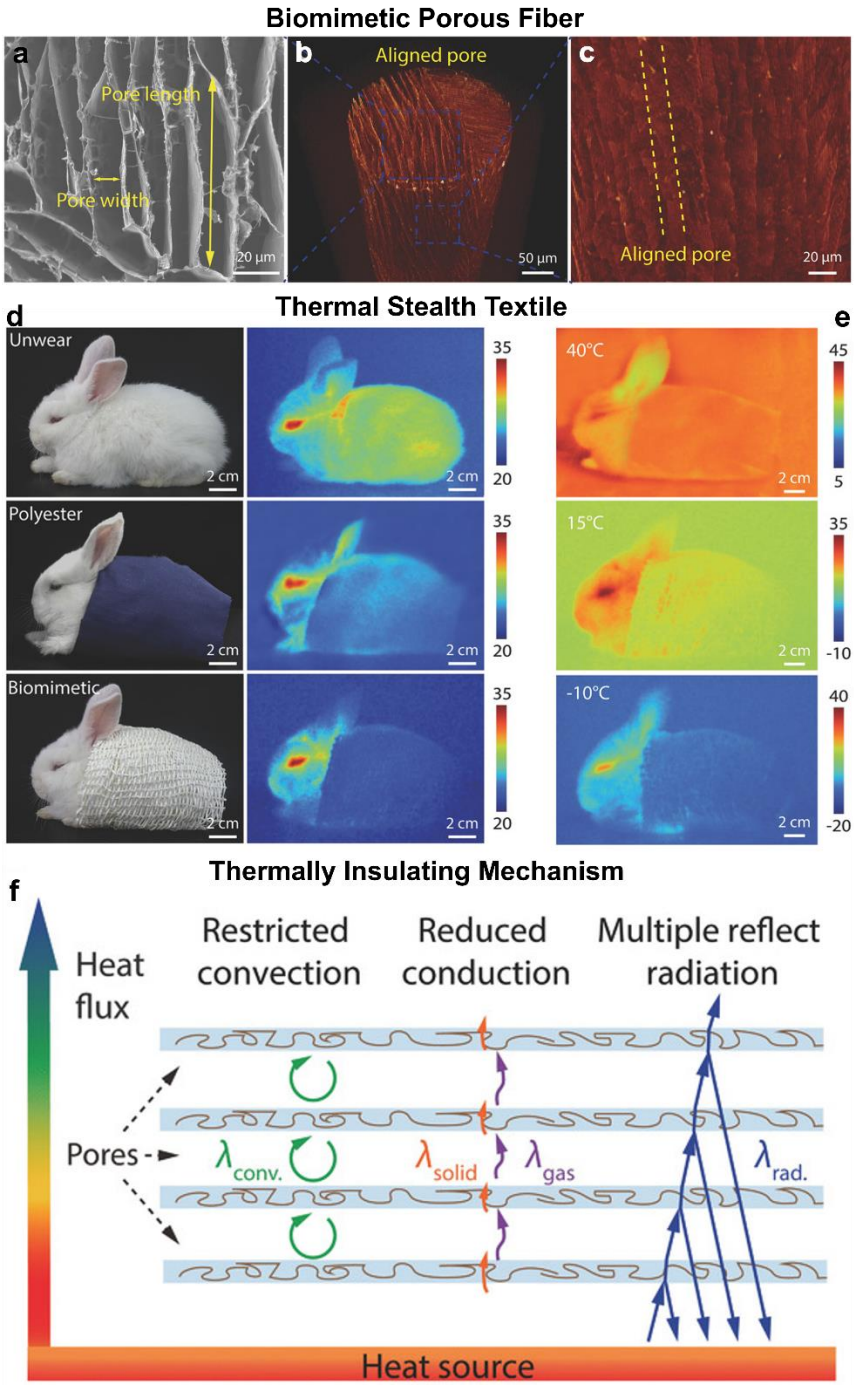

Figure 25. A thermally insulating textile prepared by "freeze-spinning" technique. (a) Radial cross-sectional SEM and (b, c) X-ray computed microtomography images of a biomimetic porous fiber. (d) Optical and infrared thermal images of a rabbit before and after wearing the commercial polyester textile and the textile woven with biomimetic porous fibers. (e) Infrared thermal images of a rabbit wearing the textile woven with biomimetic porous fibers at different background temperatures. (f) Schematic illustration of heat transfer mechanism of the composites with aligned pores.[53], Copyright 2018. Adopted with permission from John Wiley & Sons Inc.

Integrated with the above examples, thermal conductivity of thermally insulating composites can be determined by the sum of thermal convection, thermal radiation, solid and gas thermal conduction, and several features for the design of superinsulators can be extracted (**Figure 25**f). First, the anisotropic porous structure restricts the thermal convection, conduction and radiation in the radial direction, originating from low thermal conductivity of gas, numerous solid–air interfaces and multiple reflective effect, especially for small pore size. Second, the sub-microstructures of the pore walls further impede thermal conduction because the pore size is smaller than the mean free path of the gas molecules within the channel. Thirdly, the nanomaterials provide additional interfacial thermal resistance of solid skeleton, resulting in the decrease of solid thermal conduction. Last but not least, the reduction of bridges between neighboring walls generates phonon scattering, further reducing the solid thermal conduction. These characteristics provide guidance for the structural design and preparation of superinsulators.

Compared with fossil-fuel-based foams, insulating performance of biopolymer-based thermal insulators such as wood chips is weaker (40–50 mW m^{-1} K^{-1}). Other nonnegligible issues for biopolymer-based materials are inflammability and poor corrosion resistance. Fortunately, the emergence of the nanoscale engineering represented by nanocellulose and functional nanomaterials provides possibilities for

the fabrication of superinsulators with enhanced comprehensive performance, widening their potential applications from personal protection to space system. The flexible utilization of nanostructured materials such as carbon materials requires us to think more. Carbon materials can create nanostructures and interface to improve the thermal insulation, mechanical performance and flame retardancy of the composites, whereas their high intrinsic thermal conductivity is beneficial for heat conduction. In addition, carbon materials can act as efficient infrared absorbers to weaken the radiative contribution in insulating materials. Another contradiction is that reducing density improves thermal insulation but weakens mechanical properties, which push the innovations of structural materials with anisotropy and wrinkle.

In addition to the originally protective function, modern clothing is aesthetically pleasing, durable and suitable for specific purposes. Comfort related with temperature is also a significant function of clothing. One promising application of thermal insulation composites is to produce smart clothing for the personal thermal management. The porous aerogel fibers demonstrate great application potentials in the production of thermal management textiles.[408-410] The innovative processing technologies include the foregoing one-step freeze-spinning route and two-step route in which hollow fibers are formed through coaxial wet spinning, followed by embedding porous structure through freeze-casting.

3.8. Adsorbents

Over the past few decades, the growing water contaminants (*i.e.*, heavy metal ions, dyes and organics) arising from emission of industrial or agricultural wastewater, spill of toxic organic solvents, and leakage of crude oil or oily products have been posing serious danger to human health and ecological balance.[411, 412] To date, various

techniques have been proposed for the treatment of contaminated waters, including ion exchange,[413] bioremediation,[414] reverse osmosis,[415] photodecomposition,[416] absorption,[417] etc. Among these methods, absorption is considered as the most competitive one due to its appreciable cost performance ratio.[418] Although conventional adsorbents, such as polymer resin,[419] zeolites,[420] and activated carbon,[421] have been broadly investigated owing to their unique microporous structure, they possess fatal shortcomings, including low efficiency, sophisticated separation operation, and inevitable secondary pollution. Therefore, it is of significance to develop cost-effective and durable adsorbents with prominent absorption selectivity and capacity to efficiently treat the contaminated waters. Fortunately, the lightweight 3D porous materials (sponge,[422, 423] foam[424] and aerogel[425]) with low density and high porosity have been proved to be ideal candidates for the treatment of contaminated waters, and freeze-casting technique is regarded as one of the best masters to prepare these 3D adsorbents, in particular graphene based adsorbents.[426-433] Coincidentally, a unidirectional freezing assembly has been adopted to produce diffusion-dominated aerogel filters for the capture of ultrafine airborne particulates.[434]

Up to now, latex,[435] chitosan,[119, 436, 437] cellulose,[131, 163, 438] TPU[439] and PVA[440] have been employed to prepare 3D hybrid porous products as compressible adsorbents for removal of heavy metal ions, dye adsorption, adsorption of organic solvents and oil-water separation through directional freezing approach (**Figure 26**). The microstructures of porous adsorbents can be tuned by controlling the freezing conditions to match with static and flowing scenarios for wastewater treatment. Freeze-casting method has been adopted to fabricate HA/chitosan porous scaffolds with various topological structures, in which chitosan can act as a binder to

construct 3D framework and another adsorbent to remove heavy metal ions (**Figure 26**a).[436] Apart from the removal of heavy metal ions, the chitosan based composites can be used to adsorb methyl orange dye.[437] Interestingly, inorganic–organic heterobeads consisting of GO core encapsulated by chitosan shell have been developed by a two-step freezing method. Compared with bare chitosan beads, the core–shell beads show enhanced adsorption capacity of methyl orange at 318 K (353 mg g^{-1}) because more adsorption sites are provided.[119]

Chemical modifications are conducted to impart hydrophilicity and hydrophobicity to freeze-casting porous scaffold. Polydopamine (PDA) deposition and silanization reaction are common hydrophilic and hydrophobic modification strategies, respectively, endowing adsorbents with improved adsorption performance and selectivity. Cellulose acetate nanofiber/GO aerogels with interconnected porous network exhibit high selective adsorption capacity (q_e) towards cationic dyes, including neutral red (NR, > 800 mg g^{-1}), crystal violet (CV), methylene green (MG), methylene blue (MB) and rhodamine B (RB), but they possess poor decolorization effect on anionic dye indigo carmine (IC) (**Figure 26**b).[163] After chemical modification *via* vapor deposition operation, the modified aerogel@hexadecyltrimethoxysilane with superhydrophobicity is able to adsorb oils and organic solvents with a commendable saturated adsorption capacity (Q_w), especially for phenixin up to 734 g g^{-1}. To improve the mechanical durability of porous materials, thermosetting epoxy can be employed to tailor their microstructure and properties. TPU/CNT/epoxy ternary composite foams with herringbone-like structure have been prepared for rapid and selective adsorption of oils and organic solvents (**Figure 26**c).[439]

A dopamine decorated graphene/PVA Janus aerogel with hierarchical architecture presents double-deck opposite superwettability (one side is hydrophobic and the other side is superhydrophilic), achieving a switchable separation performance for various oil/water emulsions or mixtures.[440] Bidirectional freeze-shaping technique can been applied to fabricate lamellar porous materials with excellent mechanical properties. Highly compressible anisotropic cellulose/graphene aerogels with laminated structure have been developed by bidirectional freezing method. After grafting long carbon chains through a silanization reaction, the superhydrophobic aerogels, as promising super adsorbents, are able to selectively adsorb oils in water with a striking absorption capacity up to 197 times its weight and retrieve ca. 85% oil after simple squeezing.[131] The super-elasticity and hydrophobicity or superoleophilicity can be imparted to the lamellar sodium alginate/cellulose hybrid aerogels through chemical crosslinking and silane modification, and the obtained products can be reused for the continuous separation of oil/water mixture (**Figure 26**d).[438] The bidirectional-freezing lamellar porous materials with enhanced mechanical performance and adsorption ability are promising super adsorbents for water treatment.

Generally, the adsorbents can be well recycled by simple mechanical squeezing after absorbing organic solvents or oil, but the bare carbon-based absorbers are unable to withstand being compressed owing to their brittleness. The addition of the second component such as fibrous or organic materials can effectively improve their mechanical strength capable of enduring the frequent squeezing operation and endow them with excellent recyclability, which can definitely prolong their service life. Based on the above cases, the mechanical properties of 3D network can be further improved by using directional freeze-casting processing technique, especially

bidirectional freezing for lamellar structure discussed in the first part. 3D compressible structural materials with radial or gradient structure may be a next-generation advanced adsorbent owing to their unique capillary behaviors, but their mechanical properties remain to be studied.

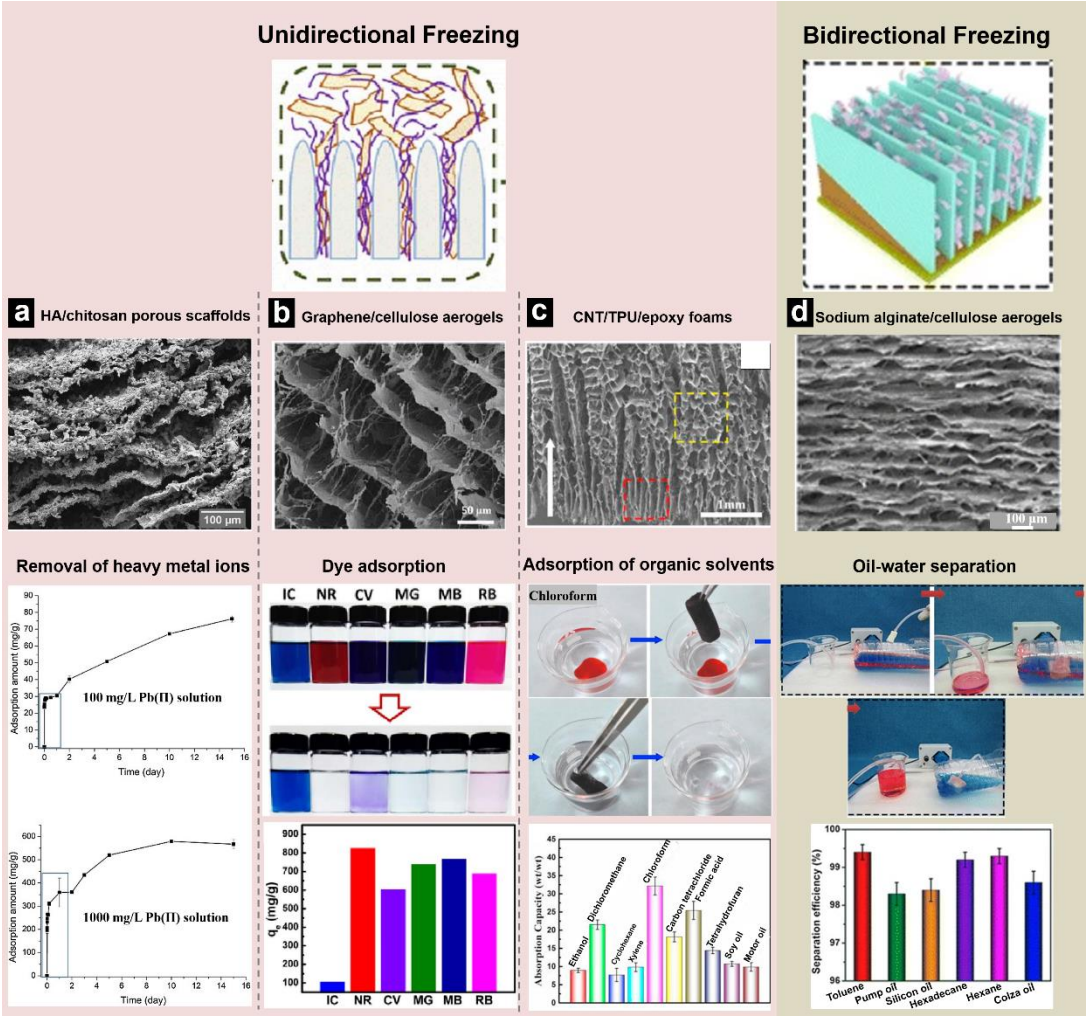

Figure 26. Directional freezing approaches to fabricate adsorbents for different applications: (a) removal of heavy metal ions, (b) dye adsorption, (c) adsorption of organic solvents and (d) oil-water separation. (a) HA/chitosan porous scaffolds for removal of heavy metal Pb(Π) ions.[436], Copyright 2019. Adopted with permission from Elsevier Science Ltd. (b) Cellulose acetate nanofiber/GO aerogels for dye adsorption.[163], Copyright 2017. Adopted with permission from Elsevier Science Ltd. (c) CNT/TPU/epoxy foams for adsorption of organic solvents.[439], Copyright 2018. Adopted with permission from Elsevier Science Ltd. (d) Sodium

alginate/cellulose aerogels for oil-water separation.[438], Copyright 2018. Adopted with permission from Springer Nature.

The large majorities of the aforementioned adsorbents prepared by ice-templating strategy contain graphene, which is an expensive technology in terms of materials and processing. In the light of the cost and work efficiency, polymers and their composites with conventional adsorption materials (*e.g.*, polymer/clay (montmorillonite) composites, polymer/diatomite composites, polymer/zeolite composites, polymer/active carbon composites, etc.) are likely to be employed to fabricate high-efficiency adsorbents with various geometries (beads, films and scaffolds) through ice-templating optimized design.[441] Besides, green and biodegradable adsorbents such as cellulosic porous composites are decent candidates.

3.9. Energy composites

With the rapid growth of population and the acceleration of industrialization, the problems of environmental pollution and energy shortage have become increasingly prominent, pushing the explosive development of green renewable energy resources (solar energy, tidal energy, wind energy, geothermal energy, hydrothermal energy and bioenergy) and all kinds of energy conversion and storage systems (perovskite solar cells,[442] lithium-ion batteries,[443] supercapacitors,[444] piezoelectric nanogenerators,[445] triboelectric nanogenerators,[446] thermoelectric generators,[447, 448] solar steam generation,[449] catalysts,[450] etc.). Freeze-casting associated with polymer composites is penetrating into relevant fields through constructing aligned channel structure with low tortuosity, facilitating water transport, electron transfer and ion diffusion (**Figure 27**).

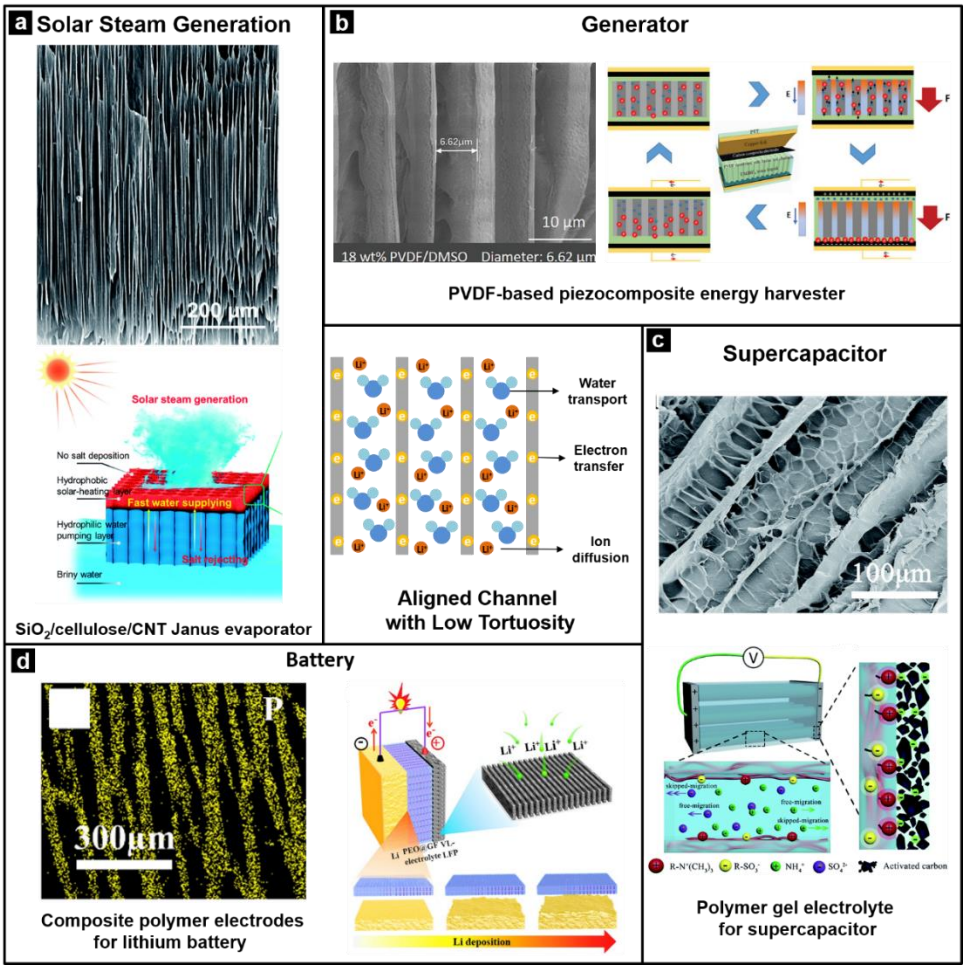

Figure 27. Ice-templating strategy to construct aligned structure with low tortuosity facilitating water transport, electron transfer and ion diffusion for high-performance solar steam generation systems, generators, supercapacitors and batteries. (a) A SiO_2/cellulose nanofiber/CNT Janus evaporator with aligned channel structures for seawater desalination.[451], Copyright 2019. Adopted with permission from the Royal Society of Chemistry. (b) A PVDF-based piezocomposite energy harvester with bionic ion channels.[452], Copyright 2020. Reproduced with permission from John Wiley & Sons Inc. (c) Aligned polymer gel electrolytes for supercapacitors using the "hot ice" templating method.[453], Copyright 2018. Reproduced with permission from the Royal Society of Chemistry. (d) A design of ion-transporting channels in composite polymer electrodes for all-solid-state lithium batteries.[454], Copyright 2019. Adopted with permission from Elsevier Science Ltd.

Solar steam (vapor) generation, a system capable of harvesting solar energy and converting it to heat for water evaporation, is considered as one of the most promising

techniques to relieve freshwater shortage scarcity and realize water purification.[455] Efficient photothermal absorbers and water absorptive/transporting architectures play a pivotal role in the work efficiency of solar steam generation systems, and the latter can be achieved by ice-templating strategy to construct aligned channel structure with low tortuosity. Nanostructured carbon materials have been considered as efficiently photothermal absorbers for solar steam generation systems.[456] Spray-freezing carbon spheres[457] and unidirectional freezing graphene membrane[82] and aerogel[458] have been assembled for solar-driven steam generation system. For the cases of polymer composites, SiO_2/cellulose nanofiber/CNT Janus evaporator with low-tortuosity channels exhibits stable steam generation for long-term solar desalination through reducing the salt accumulation (**Figure 27**a).[451] Along this line, a bilayer aerogel structure consisting of thin light-absorbing CNT layer and porous water-supply cellulose nanofibril layer has been designed by the combination of ice templating and coating, in which porous structure and heat localization are favorable to reduce the heat loss.[459] Carbon materials act as photothermal absorbers and vertically aligned channels promote the water pumping, giving rise to a superb solar thermal conversion efficiency under on sun illumination.

Biomimetic structures have been designed by ice-templating strategy to achieve high-efficiency and intelligent solar steam generation systems (**Figure 28**). Enlightened by tree with high-efficiency water extraction, an effective water-cycling system composed of bilayer-structured porous architecture with CNT heat collector on the top of a polymer aerogel has been manufactured successively through radial freezing, *in situ* cryo-polymerization, freeze drying and coating of a CNT layer (**Figure 28**a).[164] The radially aligned channels with micron pores and molecular meshes (**Figure 28**b) and CNT layer coated on the top of the hierarchical polyacrylamide

(PAAm) aerogel can respectively work as antigravity water transport vessels and solar absorbers to strengthen its long-distance transport ability and evaporation efficiency. A solar steam generation system associated with the bilayer-structured polymer aerogel arrays has been artificially designed to perform water transpiration and collection (**Figure 28**c), manifesting that the water evaporation rate and the energy conversion efficiency are up to 2.0 kg m^{-2} h^{-1} and 85.7% under one solar irradiation, respectively. Likewise, a leaf-inspired intelligent solar water evaporation system based on microstructured graphene/PNIPAm composite membrane has been developed using a laboratory-made directional freeze-casting apparatus (**Figure 28**d and e).[460] The obtained graphene/PNIPAm membrane presents a typical microporous structure and a well-organized layer-by-layer structure from top-view and cross-sectional SEM images, respectively (**Figure 28**f and g). The self-adaptive membrane possesses tunable water evaporation through the reversible transformation of microstructures akin to stomatal opening/closing features of leaves in compliance with the change of solar intensity. These biomimetic designs with the superiority of water transport and evaporation offer guidance for the design of smart solar steam generation systems.

With freeze-casting processing, existing polymer composites, as solar steam generation devices, are composed of aligned porous polymer architectures for water adsorption/transport and photothermal nano-absorbers. Apart from carbon-based absorbers, conducting polypyrrole (PPy),[461] melanin-like PDA[462] and emerging MXene[463, 464] exhibit great potential in the fabrication of solar steam generation systems with high photothermal conversion efficiency owing to the low cost, the strong affinity capable of coating on a large number of substrates under mild conditions and 100% internal light-to-heat conversion efficiency, respectively.[465]

More importantly, they can facilely couple with freeze-casting 3D skeletons. Hybrid devices with increased power and ability of all-weather-available continuous steam generation are another trend.

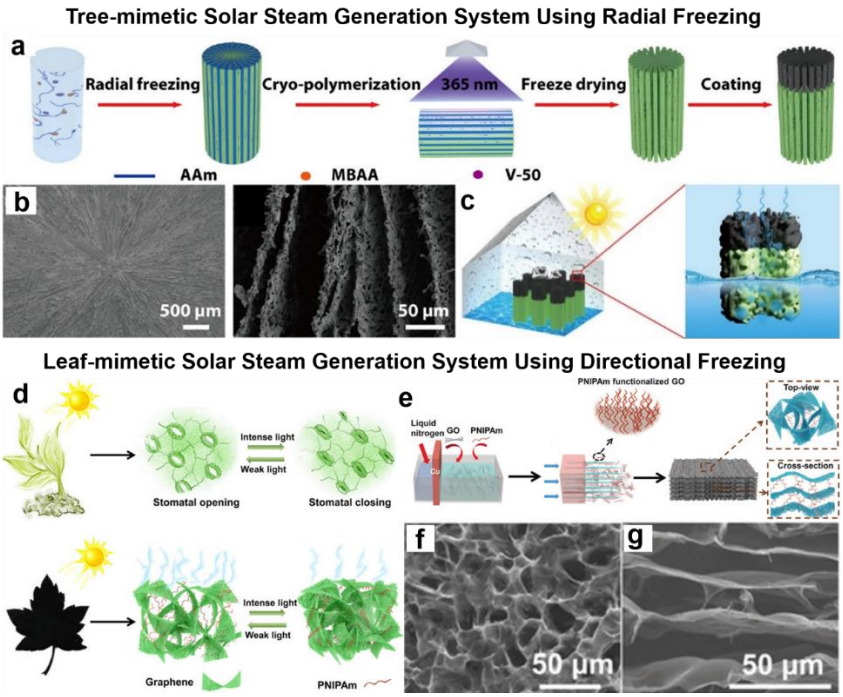

Figure 28. Ice-templating strategy to construct biomimetic structure for solar steam generation systems: (a-c) tree-mimetic and (d-g) leaf-mimetic composites. (a) Schematic illustration of fabrication route of PAAm-radial aerogel coated with CNT layer. (b) SEM images of the aerogel with radially aligned channels. (c) Schematic illustration of solar vapor generation setup based on the bilayer PAAm-radial aerogel arrays. Reproduced with permission.[164], Copyright 2019. Adopted with permission from the American Chemical Society. Schematic illustrations of (d) working mechanism of a leaf-like intelligent solar water evaporation and (e) fabrication route of microstructured graphene/PNIPAm membrane. (f) The top-view and (g) cross-sectional SEM images of the self-adaptive membrane. Reproduced with permission.[460], Copyright 2018. Reproduced with permission from John Wiley & Sons Inc.

Electricity harvest from water, heat and mechanical motion is an ongoing pursuit. Advanced generators, including piezoelectric nanogenerators, triboelectric nanogenerators, thermoelectric generators and hydroelectric generators, have received

a lot of attention in recent decades.[466-468] A unidirectional freezing method has been applied to assemble biomacromolecule nanofibrils into aligned-channel aerogels as biological generators producing a streaming potential when exposing them to moist air flow.[469] The highly aligned channels are not only beneficial to water transport, but also can accelerate ion diffusion. A polyvinylidene fluoride (PVDF)-based piezocomposite energy harvester has been obtained by implanting ions and constructing bionic ion channels through a freeze-casting strategy (**Figure 27**b).[452] Apart from a considerable short-circuit current at low-frequency pressure, an open-circuit voltage of the piezo-devices can accumulate step by step owing to that the voltage originating from the capacitive performance of ion carriers cannot decay completely in each operation cycle. Accompanying the energy harvesting device from graphene[470] and PZT ceramics[471, 472], few ice-templating polymer composite generators emerge. Therefore, there is still plenty of room for the growth of energy harvesters with water-/ion-/electron-transporting channel and large contact interface using freeze-casting technique.

Charge transfer not only affects the function of the generator, but also plays an important role in the performance of the electrochemical energy storage devices. There is a massive interest in high-performance supercapacitors owing to their high power density.[473] Pseudo-polymer-coated graphene aerogel bead with radial channels and biomass carbon framework with unique pore morphologies have been prepared by freeze-casting method for supercapacitor application.[52, 474] Porous graphene aerogel/PANI composites have been synthesized through *in-situ* polymerization of PANI on the as-fabricated graphene aerogel scaffold using a unidirectional freezing. The long-range aligned graphene scaffold can facilitate ion diffusion in the electrolyte, leading to the improvement of electrochemical

performance for PANI supercapacitor.[475] Apart from polymer composites, other electrodes, graphene films,[476] MXene architectures,[477] graphene/Ag nanocomposites[478] and MXene/CNT films[479] with cellular or lamella structures for high-performance supercapacitors, 3D MXene/graphene hybrid aerogels for self-healing microsupercapacitors[480] and hierarchical graphene network for low-temperature pseudocapacitors[481], have been developed based on freeze-casting method.

Considering the possible leakage of harmful liquid electrolytes and the undesired dislocation of electrodes, solid-state supercapacitors based on gel electrolytes with excellent electrochemical properties and mechanical integrity are favored. Ice-templating strategy has been employed to develop a series of polymer-based aligned ionogel electrolytes for solid-state supercapacitors in Wang's group (**Figure 27**c).[453, 482, 483] In comparison to the nonaligned gel, the electrolytes with anisotropic structure exhibit superior ionic conductivity and specific capacitance. This is because the vertically aligned liquid ionic channels pose as "highways" to reduce the internal resistance and accelerate ion transfer.[276] Note that a "hot ice" ($NaAc \cdot 3H_2O$ crystal) template has been proposed to fabricate a polymer gel electrolyte with oriented micrometer-sized porous structures.[453]

Stretchable supercapacitors enduring large and complex deformations are desirable for portable and wearable electronic applications. Hydrogels assembled from conducting polymers facilitate a promising integration of high conductivity from conductive component and good stretchability from hydrogel architecture. Vapor-phase deposition has been adopted to embed the electroactive component, PPy, into unidirectionally aligned PAAm aerogel, creating a wood-inspired all-solid-state hydrogel supercapacitor.[484] More interestingly, the pore size of aerogel can be

tuned from 47 to 12 μm by integrating hydrophilic PVA in the precursor solution, further giving rise to superior electrochemical performance owing to a larger specific area and anisotropic channels for ions transfer. Uniquely, a creative cryopolymerization strategy integrating unidirectional freezing with polymerization, has been proposed to prepare anisotropic PVA/PANI hydrogel with diverse shapes and superelasticity for high-performance all-solid-state supercapacitor. Benefiting from its excellent mechanical properties and aligned bi-continuous phase structure containing ionic conductive PVA scaffold and electrochemically active PANI nanofibrous network, the obtained supercapacitor exhibits an excellent specific capacitance, high energy density and remarkable stability under stretching, compressing, and bending operations. Highly interconnected microchannel structure with a 3D active network promotes rapid ion and electron transfer in the electrode.[485]

Compared with supercapacitors, rechargeable batteries, as another advanced electrochemical energy storage device, possess a higher energy density but suffer from a lower power density.[486] Ice-templating strategy has been extended to produce high-performance lithium batteries, involving lithium-ion batteries, lithium-metal batteries and lithium-sulfur batteries.[68, 487-490] For example, this shaping technique has been used to produce highly aligned and low-tortuosity porous structures for lithium ion battery anodes[63, 491-493] and cathodes[494-496]. These designs shorten Li^+ transport distance and facilitate Li^+ transfer. For polymer composites, lamellar composite polymer electrodes have been designed for high-performance lithium batteries with high loading of active materials (**Figure 27**d).[454, 497] It is popular that polymer based composite electrolytes with aligned channel microstructure are developed to eliminate the unacceptable safety hazards concerning

the flammable organic-liquid electrolytes in lithium batteries, launching thermally stable solid-state battery products. Flexible solid composite electrolytes can be fabricated by introducing vertically aligned ceramic films into poly(ethylene oxide) (PEO) matrix to maximize the ionic conduction for rechargeable batteries.[498-500]

Besides, an ice-templating strategy has been reported to prepare highly aligned polymer/carbon composite electrodes for environmentally benign organic batteries.[501] The ice-templating method offers great opportunities in manipulating and optimizing the performance of organic batteries. A GO/CF/poly(amic acid) aerogel precursor for sodium ion battery with remarkable specific capacity and cycling stability has been fabricated by directional freezing strategy.[502] After carbonization, conductive CF interpenetrated graphene architecture with vertically aligned channels is obtained, leading to rapid electrolyte penetration and Na^+ transfer. In such a design, abundant CFs are perpendicularly placed across the adjacent carbon layers to prevent the restacking of graphene sheets and improve mechanical integrity and electrical conductivity. Hierarchically porous chitosan/graphene bioanodes for high-performance microbial fuel cell have been developed, in which the large specific surface area and aligned architecture induced by freeze-casting accelerates electron transfer.[503]

Although ice-templating strategy to fabricate energy-related polymer composites remains in infancy, its instinct for the construction of unique structures provides possibilities for high-performance energy conversion and storage devices. Freeze-casting channel microstructures for carrier mobility and 3D architectures for supporting effect offer potentials in the production of next-generation electrochemical energy storage devices, such as energy systems capable of working under extreme environments (*e.g.*, ultralow temperature), all-solid-state energy devices and thick-

electrode batteries with high-content active materials.[504, 505] As the positive effects of aligned porous channel with low tortuosity on ion diffusion, electron transportation, active material accumulation and Li-deposition behaviors are disclosed,[54, 506-508] the influencing factors at smaller scale (*e.g.*, pore size, layer thickness, wall roughness, bridge number, etc.) are well-advised to be further explored, and these microstructures can be easily tuned by freezing conditions. Conducting polymers, such as PANI, PPy and PEDOT, are promising candidates for the fabrication of electrochemical composite electrodes and electrolytes when adopting freeze-casting processing.

3.10. Biocomposites

Freeze-casting has gained popularity as a manufacturing technique for biomaterials. Given that the ice solidification is physical process, the processing route is straightforward and environmentally-friendly, in particular when biocompatible water is used as liquid carriers. Raw materials are so abundant that the compositions can be easily adjusted in line with the targeted applications. The porosity and pore geometry of scaffolds are controllable above 40 % and to the range usually suitable for tissue engineering, respectively. Despite their high overall porosity, the porous scaffolds possess desirable mechanical property (usually the compressive strength) for bone tissue engineering. The products can be functionalized and personalized during the whole freezing process, for instance by tuning their cell-wall or interface properties such as the roughness and chemistry. These structural features of the porous architectures made from freeze-casting route provide opportunities for bioengineering applications.[57, 509] Natural or biocompatible polymers and their composites, such as collagen,[110] chondroitin sulphate,[510] silk fibroin,[511] chitosan,[512-515]

PVA,[516-518] polycaprolactone (PCL),[519] poly(lactic-co-glycolic acid) (PLGA),[520, 521] and PEDOT:PSS[522] have been diversely employed to construct 3D-SMs *via* freeze-casting method. Herein, we focus briefly on the latest representative polymer-based biocomposites with directional structures.

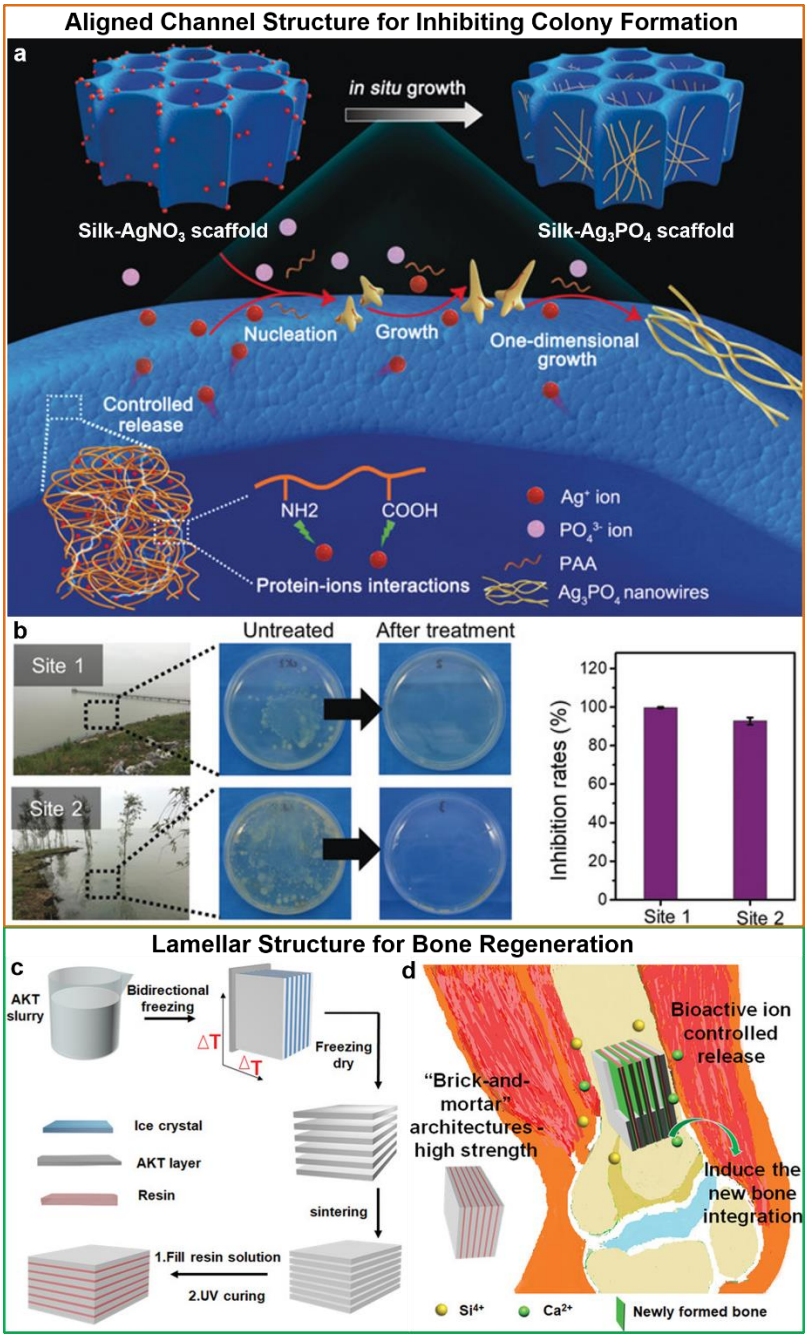

Figure 29. Directional freezing strategy to construct (a-b) aligned channel structure for inhibiting colony formation and (c-d) lamellar structure for bone regeneration. (a) Schematic illustration of the preparation of silk fibroin/Ag_3PO_4 nanowire composite scaffolds using unidirectional freezing

and interface-mediated growth methods. (b) Photographs of colony formation and disinfection efficiency at the two natural water sites before and after the treatment using the composite scaffolds.[523], Copyright 2019. Adopted with permission from John Wiley & Sons Inc. Schematic illustrations of (c) the preparation route and (d) the bone regeneration application of the bioceramic/resin composites.[165], Copyright 2020. Reproduced with permission from John Wiley & Sons Inc.

The unidirectional open channels constructed by freeze-casting can accelerate the transportation of precursors and provide abundant nucleation sites. A dense Ag_3PO_4 nanowires is *in situ* grown on the as-assembled robust silk scaffolds as microreactors, producing silk/Ag_3PO_4 composite scaffolds in the addition of polyacrylic acid (PAA) (**Figure 29**a).[523] The composite scaffolds can effectively inhibit colony formation, achieving the sterilization of natural water (**Figure 29**b). It remains desirable yet challenging for the current biomaterials to simultaneously possess satisfactory mechanical properties and excellent bioactivity. A bidirectional freezing technique can construct nacre-mimetic structure with excellent mechanical performance and high porosity for porous bio-scaffolds. Silicate-based composites with alternately layered bioceramics (AKT) and biomedical resin interlayers (**Figure 29**c) have been fabricated by the bidirectional freezing for the potential in bone regeneration (**Figure 29**d).[165] The lamellar structure in nacre-mimetic composites is more beneficial to induce the growth of new bone along the direction of the open channels to implement the bone integration in comparison to the blank and the composites containing disordered porous bioceramics.

3D biocompatible polymer composite scaffolds with oriented microstructure, high mechanical strength and desirable porosity can be regarded as promising materials for tissue engineering. Considering the one-step casting strategy to produce seamless large porous bio-scaffolds mimicking the shape of the whole organs, future freeze-

casting is promising for a wider application in complex structures at multiple scales for precise porous composite bio-scaffolds. For example, a mimicking seamless hollow collagen bladder scaffold with appendices has been constructed by freeze-casting process (**Figure 30**).[524] The porous exterior with unidirectional channel along the thickness and the closed luminal surface can facilitate the cell infiltration *in vivo* and the formation of a urothelial lining, respectively. To obtain a scaffold with an estimated thickness, the collagen suspension is frozen at higher freezing temperature for longer time, resulting in larger pores which is advantageous to cell infiltration depth. This casting method is flexible with respect to scaffold geometry, pore size and wall thickness which can be adapted by altering mold shape and freezing protocol. Another example is the newly-developed porous chitosan ureteral stents with enhanced drainage for potential as medical devices.[134]

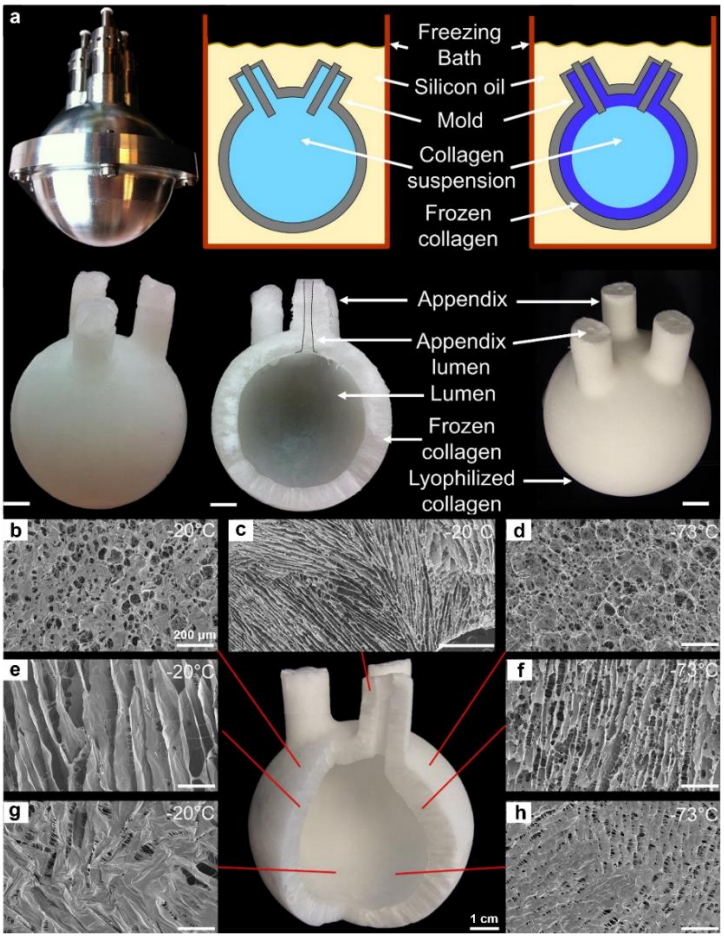

Figure 30. Construction of complex structures for bio-scaffolds through freeze-casting. (a) Setup and photographs of a whole bladder scaffold with appendices. (b-h) SEM images of the bladder scaffold at different locations (lumen, cross-sectional wall, exterior, cross-sectional appendix) and two freezing temperatures (− 20 °C and − 73 °C). The scalebars in SEM images and photograph represent 200 μm and 1 cm, respectively.[524], Copyright 2016. Reproduced with permission from Elsevier Science Ltd.

4. Conclusions and perspectives

This review summarized the recent progresses in the coupling between ice-templating strategy and advanced porous or bulk composites associated with a diverse range of polymers, described the ice-templating methodology, and put our emphasis on the correlations among processing characteristics, microstructures, macroarchitectures and performance. The soul of freeze-casting can be expressed as “transport” (electron transport, ion transport, phonon transport, mass transport) and “interface” (interface interaction, interface resistance, interface reflection) when it comes to the production of high-performance functional composites. It is hoped that this review can provide some inspirations for readers who focus on the utilization of ice-templating processing technique, the construction of 3D architectures from low-dimensional nanomaterials and the fabrication of high-performance modern composites, such as which polymers (epoxy, PDMS, PU, cellulose, etc.) or functional nanomaterials (graphene, CNT, AgNW, MXene, etc.) are completive candidates for ice-templating strategy, lamellar structure to improve mechanical properties, orderly aligned structure to improve conductivity, interfacial structure to improve electromagnetic shielding performance, among others. The recent achievements and breakthroughs of ice-templating technique have laid a solid foundation of multifunctional polymer composites. Although great progresses have been witnessed over the past decades, so

far there has been some technical challenges in the realistic applications of 3D architectures and multifunctional polymer composites fabricated by the ice-templating processing method. The desired improvements involve the following aspects, enlightening future research directions.

i) The structure can be reasonably designed through facile ice-templating strategy for the controllable fabrication of multifunctional (all-in-one) polymer composites rather than traditional single-functional composites. The freezing process is more about physical behaviors, and more chemical interactions, such as directly introducing monomers or precursors rather than ready-made polymers, crosslinking treatment and chemical modification, are expected in the future. Applying freeze-casting is to construct nature-inspired structures and architectures, just like nacre-mimetic structure for mechanically enhanced materials, wood-inspired structure for supercapacitors, leaf-enlightened structure for self-adaptive solar water evaporation systems, etc. Additionally, more processing devices, analysis systems and application scenarios matching with freeze-casting are exploited to facilitate the manufacturing of 3D-SMs with versatile structures.

ii) The freeze-casting technique can serve as a powerful tool to construct orderly structures for advanced functional composites, referring to what is mentioned and not mentioned in this review. There is a many-to-one or one-to-many mapping relationship between the structure and function collection (**Figure 31**). For example, high-performance conductive composites can be prepared by constructing 3D isotropic porous structure, honeycomb-like structure and hierarchically interconnected structure, and the nacre-mimetic structure is a competitive candidate for the preparation of mechanically reinforced composites, shape memory composites and

electromagnetic interference shielding composites. Undoubtedly, this network will be more abundant, providing guidance for customized composites.

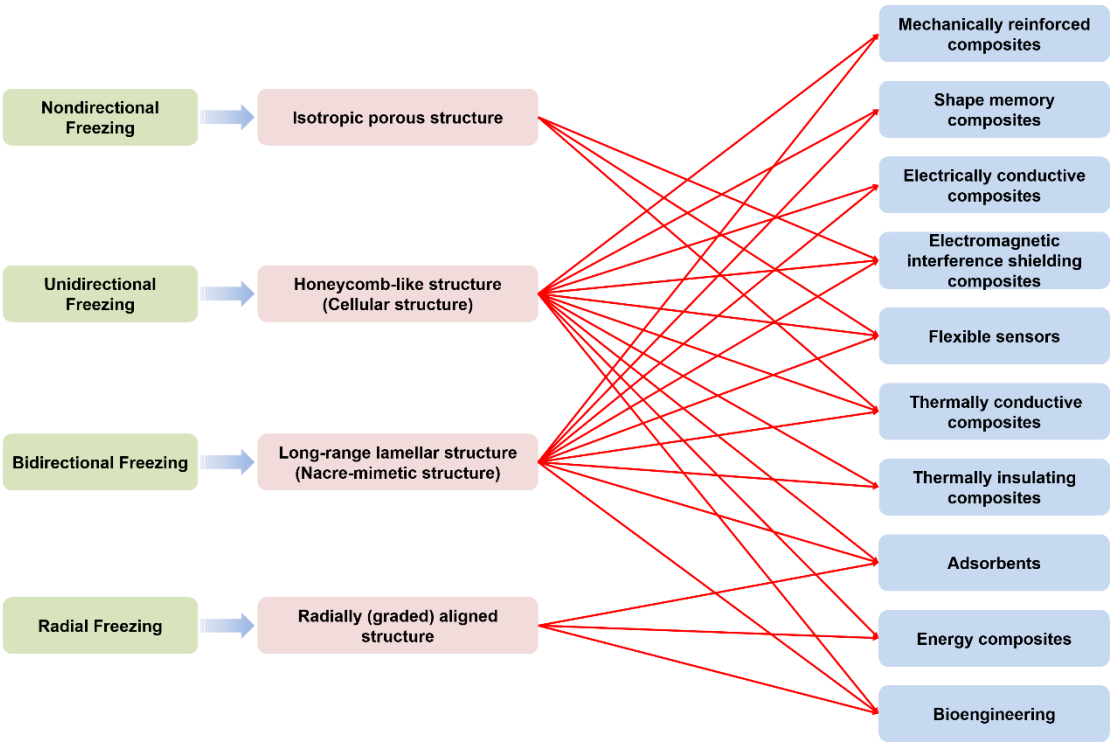

Figure 31. Mapping relationship among techniques, structures and functionalities.

iii) Freeze-casting is not only limited to the production of 3D-SMs with high porosity, but also to the network construction of solid materials without the sublimation operation, such as hydrogels, another major branch of material science, which in turn reduces the processing cycle time. Thermoresponsive PNIPAm/clay platelets composite hydrogels with hierarchical structure (highly aligned macroporous structure at micrometer scale and nacre-mimetic lamellar structure at nanoscale)[525] and PVA/PANI hydrogel with bi-continuous phase structure as electrodes for all-solid-state supercapacitor[485] have been developed by using ice-templating assembly. A novel ice-templating photo-patterning technique has been proposed based on a hydrogel enabling photo-induced a rearrangement of dynamic covalent polymer network.[526] A rapid preparation of a cellulose hydrogel can be achieved by using

UV-induced thiol-ene click chemistry.[527] If we can combine the freeze-casting with thiol-ene click crosslinking chemistry, the hydrogels with unique conductive network for ion/electron/phonon transportation would be facilely and rapidly fabricated, which may be a time-saving and low-budget package. These hydrogels show great potential applications in energy-related systems, sensing devices, bioelectronics, etc. It is most likely that freeze-casting and hydrogels will become the next generation of golden partners.

iv) The integration of freeze-casting with other technologies, especially containing solvent technologies, is another big trend. For instance, the “freeze-spinning” approach has been used to produce fiber products, which shows great potential in the flexible and wearable applications.[528, 529] The “freeze tape casting” is an effective route to fabricate electrochemical electrode with ion-transporting channel.[530, 531] Combining the freeze-casting method with the external fields enriches the microstructures of 3D architectures, so as to further heighten the existing properties of composites. The bidirectional freezing and the external field assisted freezing can be combined to construct highly aligned structure at the macro and micron levels for conductive composites.

v) Sequential/multiple freezing strategy has been proposed to refine the structure of 3D-SMs, especially for functional materials with interrelated and inter-restricted properties, such as dielectric constant and loss,[271] electrical conductivity and thermal insulation[361]. More structures (**Figure 32**), bridge structure, alternately layered structure, asymmetric structure, interfacial structure, hierarchical structure and hybrid structure, can be constructed by this strategy to investigate the effect of structure on performance and get the trade-off of multifunctionalities. For example, what is the effect of bridge on conductive properties of as-prepared scaffolds and final

composites? Interfacial design is expected to reduce the loading of functional materials and enhance the properties (*e.g.*, mechanical performance, EMI performance, conductive performance, etc.) in the whole system. Hierarchical structure commonly obtained from modified CVD method[382, 532] can be used to create lager specific surface area and simultaneously improve the thermal conductivity and shape-stability for PCMs.

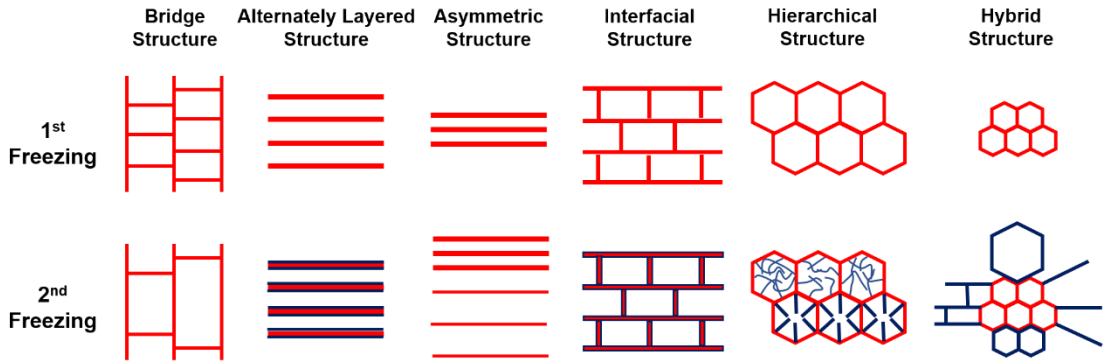

Figure 32. Structures constructing by sequential/multiple freezing strategy: bridge structure, alternately layered structure, asymmetric structure, interfacial structure, hierarchical structure and hybrid structure.

vi) Of equal importance is fundamental studies on ice-templating physical phenomena and mechanisms which will provide scientific guidance for its exploration and innovation, instead of blindly pursuing structure and performance. With the development of nanomaterials and nanotechnologies, relevant theories are expected to be enriched, such as the effect of nanomaterials with different geometries on the ice nucleation and growth, the understanding of phase diagram of multiple freezing suspensions and distribution of temperature field for different freezing modes. Nanomaterials like GO have been introduced into liquid water to investigate its crystallization behaviors.[533] The growth and recrystallization of ice crystals are greatly suppressed by GO owing to that the curved surface lowers the freezing temperature stemming from the preferred adsorption of GO on the surface of ice

crystals. In addition, more hydrogen bonds are created between liquid water and GO with abundant oxygen-containing functional groups on the basal plane, generating a molecular-level effect on ice growth and shape. Aside from the growth of ice crystals, it is universally acknowledged that ice nucleation also plays a crucial role in water freezing, and the theory of a critical ice nucleus has been put forward for nearly a century. At the end of 2019, this century theory was perfectly verified by experimental data with the assistance of multiscale GO nanosheets, instantaneously arousing extensive attention in the academic community. On these grounds, the formation of ice crystals with specific morphologies can be controlled or even induced, aiming at more diverse applications.[534] A small number of additives like salt and alcohol can significantly alter the crystallization behavior of the freezing medium. The understanding of phase diagram of these freezing suspensions needs to be further deepened, then adopting matching freezing conditions to control the structure more precisely.

vii) The structures of 3D-SMs constructed by freeze-casting are relatively orderly, which is conducive to the combination of structural design and computational simulation, thus sequencing the influencing factors according to their importance and elucidating the working mechanisms of functional composites. Following the trend, a database would be established based on ice-templating method to provide optimal reference for the preparation of target composites and avoid frequent restarts (trial-and-error). That is, given that the improvement effect on individual performance for each factor is not the same, the weight proportion should be taken into consideration when preparing multifunctional composites, in turn selecting the most appropriate material, structure and processing route.

viii) Currently, the preparation of high-performance polymer composites using ice-templating strategy is still in the laboratory stage, and how to realize the leap from laboratory to factory is an urgently technical challenge. One of the drawbacks is the removal of the solvent. It is a time-consuming and energy-consuming process when water is used as freezing medium, while the use of organic solvents for insoluble polymers will cause environmental problems. Another issue is that the products containing water-soluble polymers exhibit inferior water resistance. These factors hinder commercial implementation of freeze-casting technique. Crosslinking and emulsion lyophilization strategies have been adopted to conquer this difficulty.[69, 70] The above-mentioned UV-crosslinking route for hydrogels may be another option. Of note, an economic irradiation-crosslinking method without chemical additives may be a competitive candidate for the production of polymer based composite aerogels or foams.[535, 536] There is a long way to go for the mass production of polymer composites through freeze-casting technique. Nevertheless, the versatile microstructures and architectures constructed by freeze-casting have positive significance for the study of the structure-performance correlation for functional composites.

Acknowledgements

The authors would like to thank the project 2018YFC2000900 supported by National Key R&D Program of China, the project 21975214 supported by National Natural Science Foundation of China, and the project BE1H supported by Start-up Fund of The Hong Kong Polytechnic University.

References

[1] Tjong SC. Structural and mechanical properties of polymer nanocomposites. Mater Sci Eng R 2006;53:73-197.

[2] Jancar J, Douglas JF, Starr FW, Kumar SK, Cassagnau P, Lesser AJ, Sternstein SS, Buehler MJ. Current issues in research on structure–property relationships in polymer nanocomposites. Polymer 2010;51:3321-43.

[3] Salzano de Luna M, Wang Y, Zhai T, Verdolotti L, Buonocore GG, Lavorgna M, Xia H. Nanocomposite polymeric materials with 3D graphene-based architectures: from design strategies to tailored properties and potential applications. Prog Polym Sci 2019;89:213-49.

[4] Balazs AC, Emrick T, Russell TP. Nanoparticle polymer composites: where two small worlds meet. Science 2006;314:1107-10.

[5] Kumar SK, Benicewicz BC, Vaia RA, Winey KI. 50th anniversary perspective: are polymer nanocomposites practical for applications? Macromolecules 2017;50:714-31.

[6] Gao F. Clay/polymer composites: the story. Mater Today 2004;7:50-5.

[7] Huang J-C. Carbon black filled conducting polymers and polymer blends. Adv Polym Technol 2002;21:299-313.

[8] Balberg I. A comprehensive picture of the electrical phenomena in carbon black–polymer composites. Carbon 2002;40:139-43.

[9] Lee DW, Yoo BR. Advanced silica/polymer composites: materials and applications. J Ind Eng Chem 2016;38:1-12.

[10] Wang F, Zeng X, Yao Y, Sun R, Xu J, Wong CP. Silver nanoparticle-deposited boron nitride nanosheets as fillers for polymeric composites with high thermal conductivity. Sci Rep 2016;6:19394/1-9.

[11] Spitalsky Z, Tasis D, Papagelis K, Galiotis C. Carbon nanotube–polymer composites: chemistry, processing, mechanical and electrical properties. Prog Polym Sci 2010;35:357-401.

[12] Ma J, Zhan M, Wang K. Ultralightweight silver nanowires hybrid polyimide composite foams for high-performance electromagnetic interference shielding. ACS Appl Mater Interfaces 2015;7:563-76.

[13] Kim H, Abdala AA, Macosko CW. Graphene/polymer nanocomposites. Macromolecules 2010;43:6515-30.

[14] Hu K, Kulkarni DD, Choi I, Tsukruk VV. Graphene-polymer nanocomposites for structural and functional applications. Prog Polym Sci 2014;39:1934-72.

[15] Shi G, Araby S, Gibson CT, Meng Q, Zhu S, Ma J. Graphene platelets and their polymer composites: fabrication, structure, properties, and applications. Adv Funct Mater 2018;28:1706705/1-44.

[16] Yu C, Zhang J, Tian W, Fan X, Yao Y. Polymer composites based on hexagonal boron nitride and their application in thermally conductive composites. RSC Adv 2018;8:21948-67.

[17] Wu Y, Zhu J, Huang L. A review of three-dimensional graphene-based materials: synthesis and applications to energy conversion/storage and environment. Carbon 2019;143:610-40.

[18] Yang J, Tang L-S, Bai L, Bao R-Y, Liu Z-Y, Xie B-H, Yang M-B, Yang W. High-performance composite phase change materials for energy conversion based on macroscopically three-dimensional structural materials. Mater Horiz 2019;6:250-73.

[19] Guan L-Z, Zhao L, Wan Y-J, Tang L-C. Three-dimensional graphene-based polymer nanocomposites: preparation, properties and applications. Nanoscale 2018;10:14788-811.

[20] Zhang H, Hussain I, Brust M, Butler MF, Rannard SP, Cooper AI. Aligned two- and three-dimensional structures by directional freezing of polymers and nanoparticles. Nat Mater 2005;4:787-93.

[21] Deville S. The lure of ice-templating: recent trends and opportunities for porous materials. Scr Mater 2018;147:119-24.

[22] Scotti KL, Dunand DC. Freeze casting–a review of processing, microstructure and properties via the open data repository, FreezeCasting.net. Prog Mater Sci 2018;94:243-305.

[23] Moran T. The freezing of gelatin gel. Proc R Soc Lond A 1926;112:30-46.

[24] Hardy WB. A microscopic study of the freezing of gel. Proc R Soc Lond A 1926;112:47-61.

[25] Deville S, Saiz E, Nalla RK, Tomsia AP. Freezing as a path to build complex composites. Science 2006;311:515-8.

[26] Fukasawa T, Deng ZY, Ando M, Ohji T, Goto Y. Pore structure of porous ceramics synthesized from water-based slurry by freeze-dry process. J Mater Sci 2001;36:2523-7.

[27] Bandi S, Bell M, Schiraldi DA. Temperature-responsive clay aerogel−polymer composites. Macromolecules 2005;38:9216-20.

[28] White MA, Conrad J, Chen R, Romao C, Pereira A, Hill I. Applications of ice-templated ceramics. Int J Appl Ceram Technol 2018;15:1075-83.

[29] Zhang Y, Roscow J, Xie M, Bowen C. High piezoelectric sensitivity and hydrostatic figures of merit in unidirectional porous ferroelectric ceramics fabricated by freeze casting. J Eur Ceram Soc 2018;38:4203-11.

[30] He F, Zhou L, Zhang X, Li W, Yang L, Zhao H, He X. Synthesis and anisotropic properties of alumina-silica aerogels constructed by silica sols infiltrated into unidirectional frozen alumina templates. Ceram Int 2019;45:11963-70.

[31] Fukushima M, Yoshizawa Y-i. Fabrication of highly porous nickel with oriented micrometer-sized cylindrical pores by gelation freezing method. Mater Lett 2015;153:99-101.

[32] Park H, Noh Y, Choi H, Hong K, Kwon K, Choe H. Processing, microstructure, and oxidation behavior of iron foams. Metall Mater Trans A 2016;47:4760-6.

[33] Jo H, Kim MJ, Choi H, Sung Y-E, Choe H, Dunand DC. Morphological study of directionally freeze-cast nickel foams. Metall Mater Trans E 2016;3:46-54.

[34] Röthlisberger A, Häberli S, Spolenak R, Dunand DC. Synthesis, structure and mechanical properties of ice-templated tungsten foams. J Mater Res 2016;31:753-64.

[35] Huang J, Wang H, Liang B, Etim UJ, Liu Y, Li Y, Yan Z. Oriented freeze-casting fabrication of resilient copper nanowire-based aerogel as robust piezoresistive sensor. Chem Eng J 2019;364:28-36.

[36] Luo S, Samad YA, Chan V, Liao K. Cellular graphene: fabrication, mechanical properties, and strain-sensing applications. Matter 2019;1:1148-202.

[37] Deville S. Freezing colloids: observations, principles, control, and use: applications in materials science, life science, earth science, food science, and engineering. Cham: Springer, 2017. 598 pp.

[38] Li WL, Lu K, Walz JY. Freeze casting of porous materials: review of critical factors in microstructure evolution. Int Mater Rev 2013;57:37-60.

[39] Klotz M, Amirouche I, Guizard C, Viazzi C, Deville S. Ice templating-an alternative technology to produce micromonoliths. Adv Eng Mater 2012;14:1123-7.

[40] Chau M, De France KJ, Kopera B, Machado VR, Rosenfeldt S, Reyes L, Chan KJW, Förster S, Cranston ED, Hoare T, Kumacheva E. Composite hydrogels with tunable anisotropic morphologies and mechanical properties. Chem Mater 2016;28:3406-15.

[41] Zhang H. Ice templating and freeze-drying for porous materials and their applications. Weinheim: John Wiley & Sons, 2018. 363 pp.

[42] Yang J, Tang L-S, Bao R-Y, Bai L, Liu Z-Y, Yang W, Xie B-H, Yang M-B. An ice-templated assembly strategy to construct graphene oxide/boron nitride hybrid porous scaffolds in phase change materials with enhanced thermal conductivity and shape stability for light–thermal–electric energy conversion. J Mater Chem A 2016;4:18841-51.

[43] Si Y, Wang X, Yan C, Yang L, Yu J, Ding B. Ultralight biomass-derived carbonaceous nanofibrous aerogels with superelasticity and high pressure-sensitivity. Adv Mater 2016;28:9512-8.

[44] Abarrategi A, Gutierrez MC, Moreno-Vicente C, Hortiguela MJ, Ramos V, Lopez-Lacomba JL, Ferrer ML, del Monte F. Multiwall carbon nanotube scaffolds for tissue engineering purposes. Biomaterials 2008;29:94-102.

[45] Schroeder WF, Williams RJJ, Hoppe CE, Romeo HE. Unidirectional freezing as a tool for tailoring air permeability in macroporous poly(ethylene glycol)-based cross-linked networks. J Mater Sci 2017;52:13669-80.

[46] Yang J, Yu P, Tang LS, Bao RY, Liu ZY, Yang MB, Yang W. Hierarchically interconnected porous scaffolds for phase change materials with improved thermal conductivity and efficient solar-to-electric energy conversion. Nanoscale 2017;9:17704-9.

[47] Zhao N, Yang M, Zhao Q, Gao W, Xie T, Bai H. Superstretchable nacre-mimetic graphene/poly(vinyl alcohol) composite film based on interfacial architectural engineering. ACS Nano 2017;11:4777-84.

[48] Xie C, He L, Shi Y, Guo ZX, Qiu T, Tuo X. From monomers to a lasagna-like aerogel monolith: an assembling strategy for aramid nanofibers. ACS Nano 2019;13:7811-24.

[49] Wang C, Chen X, Wang B, Huang M, Wang B, Jiang Y, Ruoff RS. Freeze-casting produces a graphene oxide aerogel with a radial and centrosymmetric structure. ACS Nano 2018;12:5816-25.

[50] Yao Y, Li Y, Zeng X, Sun N, Sun R, Xu J-B, Wong C-P. Liquid nitrogen driven assembly of nanomaterials into spongy millispheres for various applications. J Mater Chem A 2018;6:5984-92.

[51] Gutiérrez MC, Ferrer ML, del Monte F. Ice-templated materials: sophisticated structures exhibiting enhanced functionalities obtained after unidirectional freezing and ice-segregation-induced self-assembly. Chem Mater 2008;20:634-48.

[52] Ouyang A, Cao A, Hu S, Li Y, Xu R, Wei J, Zhu H, Wu D. Polymer-coated graphene aerogel beads and supercapacitor application. ACS Appl Mater Interfaces 2016;8:11179-87.

[53] Cui Y, Gong H, Wang Y, Li D, Bai H. A thermally insulating textile inspired by polar bear hair. Adv Mater 2018;30:1706807/1-8.

[54] Xue P, Liu S, Shi X, Sun C, Lai C, Zhou Y, Sui D, Chen Y, Liang J. A hierarchical silver-nanowire-graphene host enabling ultrahigh rates and superior long-term cycling of lithium-metal composite anodes. Adv Mater 2018;30:1804165/1-10.

[55] Serrano MC, Patiño J, García-Rama C, Ferrer ML, Fierro JLG, Tamayo A, Collazos-Castro JE, del Monte F, Gutiérrez MC. 3D free-standing porous scaffolds made of graphene oxide as substrates for neural cell growth. J Mater Chem B 2014;2:5698-706.

[56] Deville S. Freeze-casting of porous ceramics: a review of current achievements and issues. Adv Eng Mater 2008;10:155-69.

[57] Wegst UG, Schecter M, Donius AE, Hunger PM. Biomaterials by freeze casting. Phil Trans R Soc A 2010;368:2099-121.

[58] Porter MM, McKittrick J, Meyers MA. Biomimetic materials by freeze casting. JOM 2013;65:720-7.

[59] Deville S. Ice-templating, freeze casting: Beyond materials processing. J Mater Res 2013;28:2202-19.

[60] Lavoine N, Bergström L. Nanocellulose-based foams and aerogels: processing, properties, and applications. J Mater Chem A 2017;5:16105-17.

[61] Gupta S, Martoïa F, Orgéas L, Dumont P. Ice-templated porous nanocellulose-based materials: current progress and opportunities for materials engineering. Appl Sci 2018;8:2463/1-29.

[62] Li B, Meng M, Cui Y, Wu Y, Zhang Y, Dong H, Zhu Z, Feng Y, Wu C. Changing conventional blending photocatalytic membranes (BPMs): focus on improving photocatalytic performance of Fe_3O_4/g-C_3N_4/PVDF membranes through magnetically induced freezing casting method. Chem Eng J 2019;365:405-14.

[63] Roberts AD, Wang S, Li X, Zhang H. Hierarchical porous nitrogen-rich carbon monoliths via ice-templating: high capacity and high-rate performance as lithium-ion battery anode materials. J Mater Chem A 2014;2:17787-96.

[64] Zhang Y, Bowen CR, Deville S. Ice-templated poly(vinylidene fluoride) ferroelectrets. Soft Matter 2019;15:825-32.

[65] Kim BS, Lee J. Macroporous PVDF/TiO_2 membranes with three-dimensionally interconnected pore structures produced by directional melt crystallization. Chem Eng J 2016;301:158-65.

[66] Deuber F, Mousavi S, Hofer M, Adlhart C. Tailoring pore structure of ultralight electrospun sponges by solid templating. ChemistrySelect 2016;1:5595-8.

[67] Naviroj M, Miller SM, Colombo P, Faber KT. Directionally aligned macroporous SiOC via freeze casting of preceramic polymers. J Eur Ceram Soc 2015;35:2225-32.

[68] Shen H, Yi E, Amores M, Cheng L, Tamura N, Parkinson DY, Chen G, Chen K, Doeff M. Oriented porous LLZO 3D structures obtained by freeze casting for battery applications. J Mater Chem A 2019;7:20861-70.

[69] Zhang X, Li W, Song P, You B, Sun G. Double-cross-linking strategy for preparing flexible, robust, and multifunctional polyimide aerogel. Chem Eng J 2020;381:122784/1-11.

[70] Hou Y, Fang G, Jiang Y, Song H, Zhang Y, Zhao Q. Emulsion lyophilization as a facile pathway to fabricate stretchable polymer foams enabling multishape memory effect and clip application. ACS Appl Mater Interfaces 2019;11:32423-30.

[71] Kwon S-M, Kim H-S, Jin H-J. Multiwalled carbon nanotube cryogels with aligned and non-aligned porous structures. Polymer 2009;50:2786-92.

[72] Du Y, Hedayat N, Panthi D, Ilkhani H, Emley BJ, Woodson T. Freeze-casting for the fabrication of solid oxide fuel cells: a review. Materialia 2018;1:198-210.

[73] Naglieri V, Bale HA, Gludovatz B, Tomsia AP, Ritchie RO. On the development of ice-templated silicon carbide scaffolds for nature-inspired structural materials. Acta Mater 2013;61:6948-57.

[74] Xie X, Zhou Y, Bi H, Yin K, Wan S, Sun L. Large-range control of the microstructures and properties of three-dimensional porous graphene. Sci Rep 2013;3:2117/1-6.

[75] Pot MW, Faraj KA, Adawy A, van Enckevort WJ, van Moerkerk HT, Vlieg E, Daamen WF, van Kuppevelt TH. Versatile wedge-based system for the construction of unidirectional collagen scaffolds by directional freezing: practical and theoretical considerations. ACS Appl Mater Interfaces 2015;7:8495-505.

[76] Gao H-L, Xu L, Long F, Pan Z, Du Y-X, Lu Y, Ge J, Yu S-H. Macroscopic free-standing hierarchical 3D architectures assembled from silver nanowires by ice templating. Angew Chem Int Ed 2014;53:4561-6.

[77] Deville S, Saiz E, Tomsia AP. Ice-templated porous alumina structures. Acta Mater 2007;55:1965-74.

[78] Yang M, Zhao N, Cui Y, Gao W, Zhao Q, Gao C, Bai H, Xie T. Biomimetic architectured graphene aerogel with exceptional strength and resilience. ACS Nano 2017;11:6817-24.

[79] Delattre B, Bai H, Ritchie RO, De Coninck J, Tomsia AP. Unidirectional freezing of ceramic suspensions: in situ x-ray investigation of the effects of additives. ACS Appl Mater Interfaces 2013;6:159-66.

[80] Tang Y, Qiu S, Wu C, Miao Q, Zhao K. Freeze cast fabrication of porous ceramics using tert -butyl alcohol–water crystals as template. J Eur Ceram Soc 2016;36:1513-8.

[81] Munch E, Saiz E, Tomsia AP, Deville S. Architectural control of freeze-cast ceramics through additives and templating. J Am Ceram Soc 2009;92:1534-9.

[82] Zhang P, Li J, Lv L, Zhao Y, Qu L. Vertically aligned graphene sheets membrane for highly efficient solar thermal generation of clean water. ACS Nano 2017;11:5087-93.

[83] Huang C, Peng J, Cheng Y, Zhao Q, Du Y, Dou S, Tomsia AP, Wagner HD, Jiang L, Cheng Q. Ultratough nacre-inspired epoxy–graphene composites with shape memory properties. J Mater Chem A 2019;7:2787-94.

[84] Porter MM, Imperio R, Wen M, Meyers MA, McKittrick J. Bioinspired scaffolds with varying pore architectures and mechanical properties. Adv Funct Mater 2014;24:1978-87.

[85] Hastürk E, Höfert S-P, Topalli B, Schlüsener C, Janiak C. Shaping of MOFs via freeze-casting method with hydrophilic polymers and their effect on textural properties. Microporous Mesoporous Mater 2020;295:109907/1-13.

[86] Munier P, Gordeyeva K, Bergström L, Fall AB. Directional freezing of nanocellulose dispersions aligns the rod-like particles and produces low-density and robust particle networks. Biomacromolecules 2016;17:1875-81.

[87] Qiu L, Liu JZ, Chang SL, Wu Y, Li D. Biomimetic superelastic graphene-based cellular monoliths. Nat Commun 2012;3:1241/1-7.

[88] Wang Z, Shen X, Han NM, Liu X, Wu Y, Ye W, Kim J-K. Ultralow electrical percolation in graphene aerogel/epoxy composites. Chem Mater 2016;28:6731-41.

[89] Pan ZZ, Nishihara H, Iwamura S, Sekiguchi T, Sato A, Isogai A, Kang F, Kyotani T, Yang QH. Cellulose nanofiber as a distinct structure-directing agent for xylem-like microhoneycomb monoliths by unidirectional freeze-drying. ACS Nano 2016;10:10689-97.

[90] Si Y, Wang X, Dou L, Yu J, Ding B. Ultralight and fire-resistant ceramic nanofibrous aerogels with temperature-invariant superelasticity. Sci Adv 2018;4:eaas8925/1-9.

[91] Gao H-L, Lu Y, Mao L-B, An D, Xu L, Gu J-T, Long F, Yu S-H. A shape-memory scaffold for macroscale assembly of functional nanoscale building blocks. Mater Horiz 2014;1:69-73.

[92] Kim J, Nese V, Joos J, Jeske K, Duyckaerts N, Pfänder N, Prieto G. Directional freeze-cast hybrid-backbone meso-macroporous bodies as micromonolith catalysts for gas-to-liquid processes. J Mater Chem A 2018;6:21978-89.

[93] Zhang H, Cooper AI. Aligned porous structures by directional freezing. Adv Mater 2007;19:1529-33.

[94] Reyes Tirado FL, Huang J, Dunand DC. Ice-templated silicon foams with aligned lamellar channels. MRS Commun 2017;7:928-32.

[95] Yang W, Li X, Han X, Zhang W, Wang Z, Ma X, Li M, Li C. Asymmetric ionic aerogel of biologic nanofibrils for harvesting electricity from moisture. Nano Energy 2020;71:104610/1-7.

[96] Zhou Y, Fu S, Pu Y, Pan S, Ragauskas AJ. Preparation of aligned porous chitin nanowhisker foams by directional freeze–casting technique. Carbohydr polym 2014;112:277-83.

[97] Ghorbani F, Nojehdehian H, Zamanian A. Physicochemical and mechanical properties of freeze cast hydroxyapatite-gelatin scaffolds with dexamethasone loaded PLGA microspheres for hard tissue engineering applications. Mater Sci Eng C 2016;69:208-20.

[98] Xu T, Wang C-A. Control of pore size and wall thickness of 3-1 type porous PZT ceramics during freeze-casting process. Mater Des 2016;91:242-7.

[99] Serrano MC, Nardecchia S, Garcia-Rama C, Ferrer ML, Collazos-Castro JE, del Monte F, Gutierrez MC. Chondroitin sulphate-based 3D scaffolds containing MWCNTs for nervous tissue repair. Biomaterials 2014;35:1543-51.

[100] Zhang X, Liu M, Wang H, Yan N, Cai Z, Yu Y. Ultralight, hydrophobic, anisotropic bamboo-derived cellulose nanofibrils aerogels with excellent shape recovery via freeze-casting. Carbohydr Polym 2019;208:232-40.

[101] Xu T, Wang C-A, Feteira A. Piezoelectric properties of a pioneering 3-1 type PZT/epoxy composites based on freeze-casting processing. J Am Ceram Soc 2014;97:1511-6.

[102] Yang X-H, Yao Y-Q, Huang M-H, Chai C-P. Preparation and characterization of poly(vinyl alcohol)/ZIF-8 porous composites by ice-templating method with high ZIF-8 loading amount. Chin J Polym Sci 2020;38:638-43.

[103] Cativa NM, Alvarez Cerimedo MS, Puig J, Arenas GF, Trabadelo F, Ayude MA, Zensich MA, Morales GM, Schroeder WF, Romeo HE, Hoppe CE. PEG-based cross-linked films with aligned channels: combining cryogenic processing and photopolymerization for the design of micro-patterned oriented platforms. Mol Syst Des Eng 2019;4:133-43.

[104] Gaudillere C, Garcia-Fayos J, Serra JM. Enhancing oxygen permeation through hierarchically-structured perovskite membranes elaborated by freeze-casting. J Mater Chem A 2014;2:3828-33.

[105] Bai H, Walsh F, Gludovatz B, Delattre B, Huang C, Chen Y, Tomsia AP, Ritchie RO. Bioinspired Hydroxyapatite/poly(methyl methacrylate) composite with a nacre-mimetic architecture by a bidirectional freezing method. Adv Mater 2016;28:50-6.

[106] Bai H, Chen Y, Delattre B, Tomsia AP, Ritchie RO. Bioinspired large-scale aligned porous materials assembled with dual temperature gradients. Sci Adv 2015;1:e1500849/1-8.

[107] Kim J, Han NM, Kim J, Lee J, Kim JK, Jeon S. Highly conductive and fracture-resistant epoxy composite based on non-oxidized graphene flake aerogel. ACS Appl Mater Interfaces 2018;10:37507-16.

[108] Sambyal P, Iqbal A, Hong J, Kim H, Kim M-K, Hong SM, Han M, Gogotsi Y, Koo CM. Ultralight and mechanically robust $Ti_3C_2T_x$ hybrid aerogel reinforced by carbon nanotubes for electromagnetic interference shielding. ACS Appl Mater Interfaces 2019;11:38046-54.

[109] Algharaibeh S, Ireland AJ, Su B. Bi-directional freeze casting of porous alumina ceramics: a study of the effects of different processing parameters on microstructure. J Eur Ceram Soc 2019;39:514-21.

[110] Divakar P, Yin K, Wegst UGK. Anisotropic freeze-cast collagen scaffolds for tissue regeneration: How processing conditions affect structure and properties in the dry and fully hydrated states. J Mech Behav Biomed Mater 2019;90:350-64.

[111] Fan L, Li JL, Cai Z, Wang X. Creating biomimetic anisotropic architectures with co-aligned nanofibers and macrochannels by manipulating ice crystallization. ACS Nano 2018;12:5780-90.

[112] Tang Y, Miao Q, Qiu S, Zhao K, Hu L. Novel freeze-casting fabrication of aligned lamellar porous alumina with a centrosymmetric structure. J Eur Ceram Soc 2014;34:4077-82.

[113] Fukushima M, Fujiwara T, Fey T, Kakimoto K-i. One- or two-dimensional channel structures and properties of piezoelectric composites via freeze-casting. J Am Ceram Soc 2017;100:5400-8.

[114] Yang D, Zhao Z, Bai F, Wang S, Tomsia AP, Bai H. Promoting cell migration in tissue engineering scaffolds with graded channels. Adv Healthc Mater 2017;6:1700472/1-7.

[115] Bai H, Wang D, Delattre B, Gao W, De Coninck J, Li S, Tomsia AP. Biomimetic gradient scaffold from ice-templating for self-seeding of cells with capillary effect. Acta Biomater 2015;20:113-9.

[116] Liao W, Zhao H-B, Liu Z, Xu S, Wang Y-Z. On controlling aerogel microstructure by freeze casting. Compos Part B Eng 2019;173:107036/1-15.

[117] Tang Y, Zhao K, Hu L, Wu Z. Two-step freeze casting fabrication of hydroxyapatite porous scaffolds with bionic bone graded structure. Ceram Int 2013;39:9703-7.

[118] Arai N, Faber KT. Hierarchical porous ceramics via two-stage freeze casting of preceramic polymers. Scr Mater 2019;162:72-6.

[119] Ouyang A, Wang C, Wu S, Shi E, Zhao W, Cao A, Wu D. Highly porous core–shell structured graphene-chitosan beads. ACS Appl Mater Interfaces 2015;7:14439-45.

[120] Zeng Z, Jin H, Chen M, Li W, Zhou L, Xue X, Zhang Z. Microstructure design of lightweight, flexible, and high electromagnetic shielding porous multiwalled carbon nanotube/polymer composites. Small 2017;13:1701388/1-9.

[121] Wei X, Cao X, Wang Y, Zheng G, Dai K, Liu C, Shen C. Conductive herringbone structure carbon nanotube/thermoplastic polyurethane porous foam tuned by epoxy for high performance flexible piezoresistive sensor. Compos Sci Technol 2017;149:166-77.

[122] Ouyang A, Gong Q, Liang J. Carbon nanotube–chitosan composite beads with radially aligned channels and nanotube-exposed walls for bilirubin adsorption. Adv Eng Mater 2015;17:460-6.

[123] Yu R, Shi Y, Yang D, Liu Y, Qu J, Yu Z-Z. Graphene oxide/chitosan aerogel microspheres with honeycomb-cobweb and radially oriented microchannel structures for broad-spectrum and rapid adsorption of water contaminants. ACS Appl Mater Interfaces 2017;9:21809-19.

[124] Xie Y, Lan X-R, Bao R-Y, Lei Y, Cao Z-Q, Yang M-B, Yang W, Wang Y-B. High-performance porous polylactide stereocomplex crystallite scaffolds prepared by solution blending and salt leaching. Mater Sci Eng C 2018;90:602-9.

[125] Sang Z, Ke K, Manas-Zloczower I. Design strategy for porous composites aimed at pressure sensor application. Small 2019;15:1903487/1-9.

[126] Choi SJ, Kwon TH, Im H, Moon DI, Baek DJ, Seol ML, Duarte JP, Choi YK. A polydimethylsiloxane (PDMS) sponge for the selective absorption of oil from water. ACS Appl Mater Interfaces 2011;3:4552-6.

[127] Chen F, Lu Y, Liu X, Song J, He G, Tiwari MK, Carmalt CJ, Parkin IP. Table salt as a template to prepare reusable porous PVDF-MWCNT foam for separation of immiscible oils/organic solvents and corrosive aqueous solutions. Adv Funct Mater 2017;27:1702926/1-11.

[128] Hunger PM, Donius AE, Wegst UG. Platelets self-assemble into porous nacre during freeze casting. J Mech Behav Biomed Mater 2013;19:87-93.

[129] Gutiérrez MC, Jobbágy M, Rapún N, Ferrer ML, del Monte F. A biocompatible bottom-up route for the preparation of hierarchical biohybrid materials. Adv Mater 2006;18:1137-40.

[130] Wang Y, Gawryla MD, Schiraldi DA. Effects of freezing conditions on the morphology and mechanical properties of clay and polymer/clay aerogels. J Appl Polym Sci 2013;129:1637-41.

[131] Mi H-Y, Jing X, Politowicz AL, Chen E, Huang H-X, Turng L-S. Highly compressible ultra-light anisotropic cellulose/graphene aerogel fabricated by bidirectional freeze drying for selective oil absorption. Carbon 2018;132:199-209.

[132] Bouville F, Portuguez E, Chang Y, Messing GL, Stevenson AJ, Maire E, Courtois L, Deville S, Chan H. Templated grain growth in macroporous materials. J Am Ceram Soc 2014;97:1736-42.

[133] Chen Y, Yang S, Fan D, Li G, Wang S. Dual-enhanced hydrophobic and mechanical properties of long-range 3D anisotropic binary-composite nanocellulose foams via bidirectional gradient freezing. ACS Sustainable Chem Eng 2019;7:12878-86.

[134] Yin K, Divakar P, Wegst UGK. Freeze-casting porous chitosan ureteral stents for improved drainage. Acta Biomater 2019;84:231-41.

[135] Su F, Mok J, McKittrick J. Radial-concentric freeze casting inspired by porcupine fish spines. Ceramics 2019;2:161-79.

[136] Cheng Z, Zhao K, Wu ZP. Structure control of hydroxyapatite ceramics via an electric field assisted freeze casting method. Ceram Int 2015;41:8599-604.

[137] Zhang Y, Hu L, Han J. Preparation of a dense/porous bilayered ceramic by applying an electric field during freeze casting. J Am Ceram Soc 2009;92:1874-6.

[138] Tang YF, Zhao K, Wei JQ, Qin YS. Fabrication of aligned lamellar porous alumina using directional solidification of aqueous slurries with an applied electrostatic field. J Eur Ceram Soc 2010;30:1963-5.

[139] Niksiar P, Frank MB, McKittrick J, Porter MM. Microstructural evolution of paramagnetic materials by magnetic freeze casting. J Mater Res Technol 2019;8:2247-54.

[140] Nelson I, Ogden TA, Al Khateeb S, Graser J, Sparks TD, Abbott JJ, Naleway SE. Freeze-casting of surface-magnetized iron(II,III) oxide particles in a uniform static magnetic field generated by a helmholtz coil. Adv Eng Mater 2019;21:1801092/1-11.

[141] Porter MM, Yeh M, Strawson J, Goehring T, Lujan S, Siripasopsotorn P, Meyers MA, McKittrick J. Magnetic freeze casting inspired by nature. Mater Sci Eng A 2012;556:741-50.

[142] Porter MM, Meraz L, Calderon A, Choi H, Chouhan A, Wang L, Meyers MA, McKittrick J. Torsional properties of helix-reinforced composites fabricated by magnetic freeze casting. Compos Struct 2015;119:174-84.

[143] Frank MB, Hei Siu S, Karandikar K, Liu CH, Naleway SE, Porter MM, Graeve OA, McKittrick J. Synergistic structures from magnetic freeze casting with surface magnetized alumina particles and platelets. J Mech Behav Biomed Mater 2017;76:153-63.

[144] Nelson I, Varga J, Wadsworth P, Mroz M, Kruzic JJ, Kingstedt OT, Naleway SE. Helical and bouligand porous scaffolds fabricated by dynamic low strength magnetic field freeze casting. JOM 2020;72:1498-508.

[145] Ogden TA, Prisbrey M, Nelson I, Raeymaekers B, Naleway SE. Ultrasound freeze casting: fabricating bioinspired porous scaffolds through combining freeze casting and ultrasound directed self-assembly. Mater Des 2019;164:107561/1-10.

[146] Tang Y, Qiu S, Miao Q, Wu C. Fabrication of lamellar porous alumina with axisymmetric structure by directional solidification with applied electric and magnetic fields. J Eur Ceram Soc 2016;36:1233-40.

[147] Porter MM, Niksiar P, McKittrick J, Franks G. Microstructural control of colloidal-based ceramics by directional solidification under weak magnetic fields. J Am Ceram Soc 2016;99:1917-26.

[148] Frank MB, Naleway SE, Haroush T, Liu CH, Siu SH, Ng J, Torres I, Ismail A, Karandikar K, Porter MM, Graeve OA, McKittrick J. Stiff, porous scaffolds from magnetized alumina particles aligned by magnetic freeze casting. Mater Sci Eng C 2017;77:484-92.

[149] Nelson I, Gardner L, Carlson K, Naleway SE. Freeze casting of iron oxide subject to a tri-axial nested Helmholtz-coils driven uniform magnetic field for tailored porous scaffolds. Acta Mater 2019;173:106-16.

[150] Niksiar P, Su F, Frank M, Ogden T, Naleway S, Meyers M, McKittrick J, Porter M. External field assisted freeze casting. Ceramics 2019;2:208-34.

[151] Dalvi-Isfahan M, Hamdami N, Xanthakis E, Le-Bail A. Review on the control of ice nucleation by ultrasound waves, electric and magnetic fields. J Food Eng 2017;195:222-34.

[152] Nelson I, Naleway SE. Intrinsic and extrinsic control of freeze casting. J Mater Res Technol 2019;8:2372-85.

[153] Yang M, Wu J, Bai H, Xie T, Zhao Q, Wong T-W. Controlling three-dimensional ice template via two-dimensional surface wetting. AIChE J 2016;62:4186-92.

[154] Wang Z, Liu Y, Guo P, Heng L, Jiang L. Photoelectric synergetic responsive slippery surfaces based on tailored anisotropic films generated by interfacial directional freezing. Adv Funct Mater 2018;28:1801310/1-10.

[155] Song X, Tetik H, Jirakittsonthon T, Parandoush P, Yang G, Lee D, Ryu S, Lei S, Weiss ML, Lin D. Biomimetic 3D printing of hierarchical and interconnected porous hydroxyapatite structures with high mechanical strength for bone cell culture. Adv Eng Mater 2019;21:1800678/1-6.

[156] Peng M, Wen Z, Xie L, Cheng J, Jia Z, Shi D, Zeng H, Zhao B, Liang Z, Li T, Jiang L. 3D printing of ultralight biomimetic hierarchical graphene materials with exceptional stiffness and resilience. Adv Mater 2019;31:1902930/1-9.

[157] Barg S, Perez FM, Ni N, do Vale Pereira P, Maher RC, Garcia-Tunon E, Eslava S, Agnoli S, Mattevi C, Saiz E. Mesoscale assembly of chemically modified graphene into complex cellular networks. Nat Commun 2014;5:4328/1-10.

[158] Liao S, Zhai T, Xia H. Highly adsorptive graphene aerogel microspheres with center-diverging microchannel structures. J Mater Chem A 2016;4:1068-77.

[159] Chi S, Lee J. In situ incorporation of pores and nanoparticles into polymer surfaces using melt crystallization. Macromol Rapid Commun 2019;40:1900131/1-5.

[160] Li X-H, Li X, Liao K-N, Min P, Liu T, Dasari A, Yu Z-Z. Thermally annealed anisotropic graphene aerogels and their electrically conductive epoxy composites with excellent electromagnetic interference shielding efficiencies. ACS Appl Mater Interfaces 2016;8:33230-9.

[161] Huang W, Dai K, Zhai Y, Liu H, Zhan P, Gao J, Zheng G, Liu C, Shen C. Flexible and lightweight pressure sensor based on carbon nanotube/thermoplastic polyurethane-aligned conductive foam with superior compressibility and stability. ACS Appl Mater Interfaces 2017;9:42266-77.

[162] Hu J, Huang Y, Yao Y, Pan G, Sun J, Zeng X, Sun R, Xu JB, Song B, Wong CP. Polymer composite with improved thermal conductivity by constructing a hierarchically ordered three-dimensional interconnected network of BN. ACS Appl Mater Interfaces 2017;9:13544-53.

[163] Xiao J, Lv W, Song Y, Zheng Q. Graphene/nanofiber aerogels: performance regulation towards multiple applications in dye adsorption and oil/water separation. Chem Eng J 2018;338:202-10.

[164] Xu W, Xing Y, Liu J, Wu H, Cui Y, Li D, Guo D, Li C, Liu A, Bai H. Efficient water transport and solar steam generation via radially, hierarchically structured aerogels. ACS Nano 2019;13:7930-8.

[165] Li T, Ma B, Xue J, Zhai D, Zhao P, Chang J, Wu C. Bioinspired biomaterials with a brick-and-mortar microstructure combining mechanical and biological performance. Adv Healthc Mater 2020;9:1901211/1-9.

[166] Shao Y, Luo C, Deng B-w, Yin B, Yang M-b. Flexible porous silicone rubber-nanofiber nanocomposites generated by supercritical carbon dioxide foaming for harvesting mechanical energy. Nano Energy 2020;67:104290/1-7.

[167] Wang X, Jiang M, Zhou Z, Gou J, Hui D. 3D printing of polymer matrix composites: a review and prospective. Compos Part B Eng 2017;110:442-58.

[168] Zhang X, Xu Y, Zhang X, Wu H, Shen J, Chen R, Xiong Y, Li J, Guo S. Progress on the layer-by-layer assembly of multilayered polymer composites: strategy, structural control and applications. Prog Polym Sci 2019;89:76-107.

[169] Zhang X, Zhang J, Xia L, Wang J, Li C, Xu F, Zhang X, Wu H, Guo S. Achieving high-efficiency and robust 3D thermally conductive while electrically insulating hybrid filler network with high orientation and ordered distribution. Chem Eng J 2018;334:247-56.

[170] Zhang Y, Zheng J, Yue Y, Zhao H, Li F, Guo L. Bioinspired LDH-based hierarchical structural hybrid materials with adjustable mechanical performance. Adv Funct Mater 2018;28:1801614/1-6.

[171] Tang Z, Kotov NA, Magonov S, Ozturk B. Nanostructured artificial nacre. Nat Mater 2003;2:413-8.

[172] Wegst UG, Bai H, Saiz E, Tomsia AP, Ritchie RO. Bioinspired structural materials. Nat Mater 2015;14:23-36.

[173] Huang W, Restrepo D, Jung JY, Su FY, Liu Z, Ritchie RO, McKittrick J, Zavattieri P, Kisailus D. Multiscale toughening mechanisms in biological materials and bioinspired designs. Adv Mater 2019;31:1901561/1-37.

[174] Corni I, Harvey TJ, Wharton JA, Stokes KR, Walsh FC, Wood RJK. A review of experimental techniques to produce a nacre-like structure. Bioinspir Biomim 2012;7:031001/1-23.

[175] Meyers MA, McKittrick J, Chen PY. Structural biological materials: critical mechanics-materials connections. Science 2013;339:773-9.

[176] Yao H-B, Tan Z-H, Fang H-Y, Yu S-H. Artificial nacre-like bionanocomposite films from the self-assembly of chitosan-montmorillonite hybrid building blocks. Angew Chem Int Ed 2010;49:10127-31.

[177] Cheng Q, Wu M, Li M, Jiang L, Tang Z. Ultratough artificial nacre based on conjugated cross-linked graphene oxide. Angew Chem Int Ed 2013;52:3750-5.

[178] Bonderer LJ, Studart AR, Gauckler LJ. Bioinspired design and assembly of platelet reinforced polymer films. Science 2008;319:1069-73.

[179] Laaksonen P, Walther A, Malho J-M, Kainlauri M, Ikkala O, Linder MB. Genetic engineering of biomimetic nanocomposites: diblock proteins, graphene, and nanofibrillated cellulose. Angew Chem Int Ed 2011;50:8688-91.

[180] Das P, Malho J-M, Rahimi K, Schacher FH, Wang B, Demco DE, Walther A. Nacre-mimetics with synthetic nanoclays up to ultrahigh aspect ratios. Nat Commun 2015;6:5967/1-14.

[181] Zhu B, Jasinski N, Benitez A, Noack M, Park D, Goldmann AS, Barner-Kowollik C, Walther A. Hierarchical nacre mimetics with synergistic mechanical properties by control of molecular interactions in self-healing polymers. Angew Chem Int Ed 2015;54:8653-7.

[182] Podsiadlo P, Kaushik AK, Arruda EM, Waas AM, Shim BS, Xu J, Nandivada H, Pumplin BG, Lahann J, Ramamoorthy A, Kotov NA. Ultrastrong and stiff layered polymer nanocomposites. Science 2007;318:80-3.

[183] Chen K, Ding J, Li L, Shang G, Yue Y, Guo L. Amorphous alumina nanosheets/polylactic acid artificial nacre. Matter 2019;1:1385-98.

[184] Wang J, Cheng Q, Tang Z. Layered nanocomposites inspired by the structure and mechanical properties of nacre. Chem Soc Rev 2012;41:1111-29.

[185] Bouville F, Maire E, Meille S, Van de Moortèle B, Stevenson AJ, Deville S. Strong, tough and stiff bioinspired ceramics from brittle constituents. Nat Mater 2014;13:508-14.

[186] Mao L-B, Gao H-L, Yao H-B, Liu L, Cölfen H, Liu G, Chen S-M, Li S-K, Yan Y-X, Liu Y-Y, Yu S-H. Synthetic nacre by predesigned matrix-directed mineralization. Science 2016;354:107-10.

[187] Cheng Q, Jiang L. Mimicking nacre by ice templating. Angew Chem Int Ed 2017;56:934-5.

[188] Studart AR. Bioinspired ceramics: turning brittleness into toughness. Nat Mater 2014;13:433-5.

[189] Askarinejad S, Rahbar N. Mechanics of bioinspired lamellar structured ceramic/polymer composites: experiments and models. Int J Plast 2018;107:122-49.

[190] Cheng Q, Huang C, Tomsia AP. Freeze casting for assembling bioinspired structural materials. Adv Mater 2017;29:1703155/1-11.

[191] Munch E, Launey ME, Alsem DH, Saiz E, Tomsia AP, Ritchie RO. Tough, bio-inspired hybrid materials. Science 2008;322:1516-20.

[192] Naglieri V, Gludovatz B, Tomsia AP, Ritchie RO. Developing strength and toughness in bio-inspired silicon carbide hybrid materials containing a compliant phase. Acta Mater 2015;98:141-51.

[193] Liu J, Bai R, Lei Z, Xu C, Ye Q, Martens W, Yarlagadda PKDV, Yan C. Experimental and numerical investigation of the toughening mechanisms in bioinspired composites prepared by freeze casting. Compos Sci Technol 2019;182:107768/1-7.

[194] Launey ME, Munch E, Alsem DH, Barth HB, Saiz E, Tomsia AP, Ritchie RO. Designing highly toughened hybrid composites through nature-inspired hierarchical complexity. Acta Mater 2009;57:2919-32.

[195] Zhao H, Yue Y, Guo L, Wu J, Zhang Y, Li X, Mao S, Han X. Cloning nacre's 3D interlocking skeleton in engineering composites to achieve exceptional mechanical properties. Adv Mater 2016;28:5099-105.

[196] Huang J, Xu Z, Moreno S, Morsali S, Zhou Z, Daryadel S, Baniasadi M, Qian D, Minary-Jolandan M. Lamellar ceramic semicrystalline-polymer composite fabricated by freeze casting. Adv Eng Mater 2017;19:1700214/1-12.

[197] Huang C, Peng J, Wan S, Du Y, Dou S, Wagner HD, Tomsia AP, Jiang L, Cheng Q. Ultra-tough inverse artificial nacre based on epoxy-graphene by freeze-casting. Angew Chem Int Ed 2019;58:7636-40.

[198] Peng J, Huang C, Cao C, Saiz E, Du Y, Dou S, Tomsia AP, Wagner HD, Jiang L, Cheng Q. Inverse nacre-like epoxy-graphene layered nanocomposites with integration of high toughness and self-monitoring. Matter 2020;2:220-32.

[199] Petrini M, Ferrante M, Su B. Fabrication and characterization of biomimetic ceramic/polymer composite materials for dental restoration. Dent Mater 2013;29:375-81.

[200] Akurati S, Tennant N, Ghosh D. Characterization of dynamic and quasistatic compressive mechanical properties of ice-templated alumina–epoxy composites. J Mater Res 2019;34:959-71.

[201] Naleway SE, Yu CF, Hsiong RL, Sengupta A, Iovine PM, Hildebrand JA, Meyers MA, McKittrick J. Bioinspired intrinsic control of freeze cast composites: harnessing hydrophobic hydration and clathrate hydrates. Acta Mater 2016;114:67-79.

[202] Tan G, Zhang J, Zheng L, Jiao D, Liu Z, Zhang Z, Ritchie RO. Nature-inspired nacre-like composites combining human tooth-matching elasticity and hardness with exceptional damage tolerance. Adv Mater 2019;31:1904603/1-9.

[203] Mayer G. Rigid biological systems as models for synthetic composites. Science 2005;310:1144-7.

[204] Yao H-B, Ge J, Mao L-B, Yan Y-X, Yu S-H. 25th anniversary article: artificial carbonate nanocrystals and layered structural nanocomposites inspired by nacre: synthesis, fabrication and applications. Adv Mater 2014;26:163-88.

[205] Roleček J, Salamon D, Chlup Z. Mechanical properties of hybrid composites prepared by ice-templating of alumina. J Eur Ceram Soc 2017;37:4279-86.

[206] Li C, Ding YW, Hu BC, Wu ZY, Gao HL, Liang HW, Chen JF, Yu SH. Temperature-invariant superelastic and fatigue resistant carbon nanofiber aerogels. Adv Mater 2019;32:1904331/1-7.

[207] Gao W, Zhao N, Yao W, Xu Z, Bai H, Gao C. Effect of flake size on the mechanical properties of graphene aerogels prepared by freeze casting. RSC Adv 2017;7:33600-5.

[208] Gao H-L, Zhu Y-B, Mao L-B, Wang F-C, Luo X-S, Liu Y-Y, Lu Y, Pan Z, Ge J, Shen W, Zheng Y-R, Xu L, Wang L-J, Xu W-H, Wu H-A, Yu S-H. Super-elastic and fatigue resistant carbon material with lamellar multi-arch microstructure. Nature Commun 2016;7:12920/1-8.

[209] Ferraro C, Garcia-Tuñon E, Rocha VG, Barg S, Fariñas MD, Alvarez-Arenas TEG, Sernicola G, Giuliani F, Saiz E. Light and strong SiC networks. Adv Funct Mater 2016;26:1636-45.

[210] Knoller A, Kilper S, Diem AM, Widenmeyer M, Runcevski T, Dinnebier RE, Bill J, Burghard Z. Ultrahigh damping capacities in lightweight structural materials. Nano Lett 2018;18:2519-24.

[211] Han M, Yin X, Hantanasirisakul K, Li X, Iqbal A, Hatter CB, Anasori B, Koo CM, Torita T, Soda Y, Zhang L, Cheng L, Gogotsi Y. Anisotropic MXene aerogels with a mechanically tunable ratio of electromagnetic wave reflection to absorption. Adv Opt Mater 2019;7:1900267/1-7.

[212] Chen Y, Yu Z, Han Y, Yang S, Fan D, Li G, Wang S. Combination of water-soluble chemical grafting and gradient freezing to fabricate elasticity-enhanced and anisotropic nanocellulose aerogels. Appl Nanosci 2019;10:411-9.

[213] Köhnke T, Lin A, Elder T, Theliander H, Ragauskas AJ. Nanoreinforced xylan–cellulose composite foams by freeze-casting. Green Chem 2012;14:1864-9.

[214] Donius AE, Liu A, Berglund LA, Wegst UGK. Superior mechanical performance of highly porous, anisotropic nanocellulose–montmorillonite aerogels prepared by freeze casting. J Mech Behav Biomed Mater 2014;37:88-99.

[215] Ye S, Feng J, Wu P. Highly elastic graphene oxide–epoxy composite aerogels via simple freeze-drying and subsequent routine curing. J Mater Chem A 2013;1:3495-502.

[216] Liu A, Medina L, Berglund LA. High-strength nanocomposite aerogels of ternary composition: poly(vinyl alcohol), clay, and cellulose nanofibrils. ACS Appl Mater Interfaces 2017;9:6453-61.

[217] Zeng X, Ye L, Yu S, Sun R, Xu J, Wong C-P. Facile preparation of superelastic and ultralow dielectric boron nitride nanosheet aerogels via freeze-casting process. Chem Mater 2015;27:5849-55.

[218] Wang F, Dou L, Dai J, Li Y, Huang L, Si Y, Yu J, Ding B. In situ synthesis of biomimetic silica nanofibrous aerogels with temperature-invariant superelasticity over one million compressions. Angew Chem Int Ed 2020;59:8285-92.

[219] Shearouse WC, Lillie LM, Reineke TM, Tolman WB. Sustainable polyesters derived from glucose and castor oil: building block structure impacts properties. ACS Macro Lett 2015;4:284-8.

[220] Bellin I, Kelch S, Langer R, Lendlein A. Polymeric triple-shape materials. Proc Natl Acad Sci 2006;103:18043-7.

[221] Xie T. Tunable polymer multi-shape memory effect. Nature 2010;464:267-70.

[222] Zheng N, Hou J, Xu Y, Fang Z, Zou W, Zhao Q, Xie T. Catalyst-free thermoset polyurethane with permanent shape reconfigurability and highly tunable triple-shape memory performance. ACS Macro Lett 2017;6:326-30.

[223] Behl M, Kratz K, Zotzmann J, Nochel U, Lendlein A. Reversible bidirectional shape-memory polymers. Adv Mater 2013;25:4466-9.

[224] Zhao Q, Zou W, Luo Y, Xie T. Shape memory polymer network with thermally distinct elasticity and plasticity. Sci Adv 2016;2:e1501297/1-7.

[225] Lendlein A, Langer R. Biodegradable, elastic shape-memory polymers for potential biomedical applications. Science 2002;296:1673-6.

[226] Gautrot JE, Zhu XX. Shape memory polymers based on naturally-occurring bile acids. Macromolecules 2009;42:7324-31.

[227] Lendlein A, Jiang H, Jünger O, Langer R. Light-induced shape-memory polymers. Nature 2005;434:879-82.

[228] Zhang Z-x, Dou J-x, He J-h, Xiao C-x, Shen L-y, Yang J-h, Wang Y, Zhou Z-w. Electrically/infrared actuated shape memory composites based on a bio-based polyester blend and graphene nanoplatelets and their excellent self-driven ability. J Mater Chem C 2017;5:4145-58.

[229] Huang WM, Yang B, Zhao Y, Ding Z. Thermo-moisture responsive polyurethane shape-memory polymer and composites: a review. J Mater Chem 2010;20:3367-81.

[230] Zhang P, Behl M, Peng X, Razzaq MY, Lendlein A. Ultrasonic cavitation induced shape-memory effect in porous polymer networks. Macromol Rapid Commun 2016;37:1897-903.

[231] Han XJ, Dong ZQ, Fan MM, Liu Y, li JH, Wang YF, Yuan QJ, Li BJ, Zhang S. pH-induced shape-memory polymers. Macromol Rapid Commun 2012;33:1055-60.

[232] Xu B, Zhang Y, Liu W. Hydrogen-Bonding Toughened Hydrogels and Emerging CO2-Responsive Shape Memory Effect. Macromol Rapid Commun 2015;36:1585-91.

[233] Quitmann D, Gushterov N, Sadowski G, Katzenberg F, Tiller JC. Solvent-sensitive reversible stress-response of shape memory natural rubber. ACS Appl Mater Interfaces 2013;5:3504-7.

[234] Yasin A, Li H, Lu Z, ur Rehman S, Siddiq M, Yang H. A shape memory hydrogel induced by the interactions between metal ions and phosphate. Soft Matter 2014;10:972-7.

[235] Ze Q, Kuang X, Wu S, Wong J, Montgomery SM, Zhang R, Kovitz JM, Yang F, Qi HJ, Zhao R. Magnetic shape memory polymers with integrated multifunctional shape manipulation. Adv Mater 2020;32:1906657/1-8.

[236] Leng J, Lan X, Liu Y, Du S. Shape-memory polymers and their composites: stimulus methods and applications. Prog Mater Sci 2011;56:1077-135.

[237] Lendlein A, Gould OEC. Reprogrammable recovery and actuation behaviour of shape-memory polymers. Nat Rev Mater 2019;4:116-33.

[238] Wang K, Jia Y-G, Zhao C, Zhu XX. Multiple and two-way reversible shape memory polymers: Design strategies and applications. Prog Mater Sci 2019;105:100572/1-39.

[239] Lendlein A, Balk M, Tarazona NA, Gould OEC. Bioperspectives for shape-memory polymers as shape programmable, active materials. Biomacromolecules 2019;20:3627-40.

[240] Liu Y, Du H, Liu L, Leng J. Shape memory polymers and their composites in aerospace applications: a review. Smart Mater Struct 2014;23:023001/1-22.

[241] Jin B, Song H, Jiang R, Song J, Zhao Q, Xie T. Programming a crystalline shape memory polymer network with thermo- and photo-reversible bonds toward a single-component soft robot. Sci Adv 2018;4:eaao3865/1-6.

[242] Gao H, Li J, Zhang F, Liu Y, Leng J. The research status and challenges of shape memory polymer-based flexible electronics. Mater Horiz 2019;6:931-44.

[243] Zhang X, Tan BH, Li Z. Biodegradable polyester shape memory polymers: Recent advances in design, material properties and applications. Mater Sci Eng C 2018;92:1061-74.

[244] Mu T, Liu L, Lan X, Liu Y, Leng J. Shape memory polymers for composites. Compos Sci Technol 2018;160:169-98.

[245] Li C, Qiu L, Zhang B, Li D, Liu CY. Robust vacuum-/air-dried graphene aerogels and fast recoverable shape-memory hybrid foams. Adv Mater 2016;28:1510-6.

[246] D'Elia E, Ahmed HS, Feilden E, Saiz E. Electrically-responsive graphene-based shape-memory composites. Appl Mater Today 2019;15:185-91.

[247] Kang S, Kang T-H, Kim BS, Oh J, Park S, Choi IS, Lee J, Son JG. 2D reentrant micro-honeycomb structure of graphene-CNT in polyurethane: high stretchability, superior electrical/thermal conductivity, and improved shape memory properties. Compos Part B Eng 2019;162:580-8.

[248] Du G, Mao A, Yu J, Hou J, Zhao N, Han J, Zhao Q, Gao W, Xie T, Bai H. Nacre-mimetic composite with intrinsic self-healing and shape-programming capability. Nature Commun 2019;10:800/1-8.

[249] Yan K, Xu F, Li S, Li Y, Chen Y, Wang D. Ice-templating of chitosan/agarose porous composite hydrogel with adjustable water-sensitive shape memory property and multi-staged degradation performance. Colloids Surf B Biointerfaces 2020;190:110907/1-8.

[250] Zhang R, Moon K-s, Lin W, Wong CP. Preparation of highly conductive polymer nanocomposites by low temperature sintering of silver nanoparticles. J Mater Chem 2010;20:2018-23.

[251] Gong T, Peng S-P, Bao R-Y, Yang W, Xie B-H, Yang M-B. Low percolation threshold and balanced electrical and mechanical performances in polypropylene/carbon black composites with a continuous segregated structure. Compos Part B Eng 2016;99:348-57.

[252] Zhang X, Zheng S, Zou H, Zheng X, Liu Z, Yang W, Yang M. Two-step positive temperature coefficient effect with favorable reproducibility achieved by specific “island-bridge” electrical conductive networks in HDPE/PVDF/CNF composite. Compos Part A Appl Sci Manuf 2017;94:21-31.

[253] Chen J, Cui X, Zhu Y, Jiang W, Sui K. Design of superior conductive polymer composite with precisely controlling carbon nanotubes at the interface of a co-continuous polymer blend via a balance of π-π interactions and dipole-dipole interactions. Carbon 2017;114:441-8.

[254] Wang Z, Shen X, Akbari Garakani M, Lin X, Wu Y, Liu X, Sun X, Kim JK. Graphene aerogel/epoxy composites with exceptional anisotropic structure and properties. ACS Appl Mater Interfaces 2015;7:5538-49.

[255] Song P, Qin H, Gao HL, Cong HP, Yu SH. Self-healing and superstretchable conductors from hierarchical nanowire assemblies. Nature Commun 2018;9:2786/1-9.

[256] Wang Q, Cheng L, Wang J, Qian Z, Wei T, Guo W. High performance antistatic HDPE composites with bridging effect of hybrid carbon black and multi-walled carbon nanotubes fillers. Adv Eng Mater 2019;21:1800609/1-9.

[257] Sun R, Zhang H-B, Liu J, Xie X, Yang R, Li Y, Hong S, Yu Z-Z. Highly conductive transition metal carbide/carbonitride(MXene)@polystyrene nanocomposites fabricated by electrostatic assembly for highly efficient electromagnetic interference shielding. Adv Funct Mater 2017;27:1702807/1-11.

[258] Liu H, Li Q, Zhang S, Yin R, Liu X, He Y, Dai K, Shan C, Guo J, Liu C, Shen C, Wang X, Wang N, Wang Z, Wei R, Guo Z. Electrically conductive polymer composites for smart flexible strain sensors: a critical review. J Mater Chem C 2018;6:12121-41.

[259] Zeng Z, Jin H, Zhang L, Zhang H, Chen Z, Gao F, Zhang Z. Low-voltage and high-performance electrothermal actuator based on multi-walled carbon nanotube/polymer composites. Carbon 2015;84:327-34.

[260] Yu C, Choi K, Yin L, Grunlan JC. Light-weight flexible carbon nanotube based organic composites with large thermoelectric power factors. ACS Nano 2011;5:7885-92.

[261] Deng H, Lin L, Ji M, Zhang S, Yang M, Fu Q. Progress on the morphological control of conductive network in conductive polymer composites and the use as electroactive multifunctional materials. Prog Polym Sci 2014;39:627-55.

[262] Pang H, Xu L, Yan D-X, Li Z-M. Conductive polymer composites with segregated structures. Prog Polym Sci 2014;39:1908-33.

[263] Zhai W, Zhao S, Wang Y, Zheng G, Dai K, Liu C, Shen C. Segregated conductive polymer composite with synergistically electrical and mechanical properties. Compos Part A Appl Sci Manuf 2018;105:68-77.

[264] Li T, Ma L-F, Bao R-Y, Qi G-Q, Yang W, Xie B-H, Yang M-B. A new approach to construct segregated structures in thermoplastic polyolefin elastomers towards improved conductive and mechanical properties. J Mater Chem A 2015;3:5482-90.

[265] Yu W-C, Zhang G-Q, Liu Y-H, Xu L, Yan D-X, Huang H-D, Tang J-H, Xu J-Z, Li Z-M. Selective electromagnetic interference shielding performance and superior mechanical strength of conductive polymer composites with oriented segregated conductive networks. Chem Eng J 2019;373:556-64.

[266] Zhao S, Zhang HB, Luo JQ, Wang QW, Xu B, Hong S, Yu ZZ. Highly electrically conductive three-dimensional $Ti_3C_2T_x$ MXene/reduced graphene oxide hybrid aerogels with excellent electromagnetic interference shielding performances. ACS Nano 2018;12:11193-202.

[267] D'Elia E, Barg S, Ni N, Rocha VG, Saiz E. Self-healing graphene-based composites with sensing capabilities. Adv Mater 2015;27:4788-94.

[268] Qian F, Lan PC, Freyman MC, Chen W, Kou T, Olson TY, Zhu C, Worsley MA, Duoss EB, Spadaccini CM, Baumann T, Han TY. Ultralight conductive silver nanowire aerogels. Nano Lett 2017;17:7171-6.

[269] Han NM, Wang Z, Shen X, Wu Y, Liu X, Zheng Q, Kim TH, Yang J, Kim JK. Graphene size-dependent multifunctional properties of unidirectional graphene aerogel/epoxy nanocomposites. ACS Appl Mater Interfaces 2018;10:6580-92.

[270] Jia J, Sun X, Lin X, Shen X, Mai Y-W, Kim J-K. Exceptional electrical conductivity and fracture resistance of 3D interconnected graphene foam/epoxy composites. ACS Nano 2014;8:5774-83.

[271] Wang Z, Han NM, Wu Y, Liu X, Shen X, Zheng Q, Kim J-K. Ultrahigh dielectric constant and low loss of highly-aligned graphene aerogel/poly(vinyl alcohol) composites with insulating barriers. Carbon 2017;123:385-94.

[272] Zhang B, Ye F, Gao Y, Liu Q, Liu S, Liu L. Dielectric properties of BADCy/$Ni_{0.5}Ti_{0.5}NbO_4$ composites with novel structure fabricated by freeze casting combined with vacuum assisted infiltration process. Compos Sci Technol 2015;119:75-84.

[273] Luo S, Shen Y, Yu S, Wan Y, Liao W-H, Sun R, Wong C-P. Construction of a 3D-$BaTiO_3$ network leading to significantly enhanced dielectric permittivity and energy storage density of polymer composites. Energy Environ Sci 2017;10:137-44.

[274] Kim DS, Baek C, Ma HJ, Kim DK. Enhanced dielectric permittivity of $BaTiO_3$/epoxy resin composites by particle alignment. Ceram Int 2016;42:7141-7.

[275] Wu Z, Shang T, Deng Y, Tao Y, Yang QH. The assembly of MXenes from 2D to 3D. Adv Sci 2020;7:1903077/1-16.

[276] Song H, Zhao N, Qin W, Duan B, Ding X, Wen X, Qiu P, Ba X. High-performance ionic liquid-based nanocomposite polymer electrolytes with anisotropic ionic conductivity prepared by coupling liquid crystal self-templating with unidirectional freezing. J Mater Chem A 2015;3:2128-34.

[277] Cao L, Wu H, Yang P, He X, Li J, Li Y, Xu M, Qiu M, Jiang Z. Graphene oxide-based solid electrolytes with 3D prepercolating pathways for efficient proton transport. Adv Funct Mater 2018;28:1804944/1-10.

[278] Zhang Y, Huang Y, Zhang T, Chang H, Xiao P, Chen H, Huang Z, Chen Y. Broadband and tunable high-performance microwave absorption of an ultralight and highly compressible graphene foam. Adv Mater 2015;27:2049-53.

[279] Chen Y, Zhang H-B, Yang Y, Wang M, Cao A, Yu Z-Z. High-performance epoxy nanocomposites reinforced with three-dimensional carbon nanotube sponge for electromagnetic interference shielding. Adv Funct Mater 2016;26:447-55.

[280] Abbasi H, Antunes M, Velasco JI. Recent advances in carbon-based polymer nanocomposites for electromagnetic interference shielding. Prog Mater Sci 2019;103:319-73.

[281] Yousefi N, Sun X, Lin X, Shen X, Jia J, Zhang B, Tang B, Chan M, Kim J-K. Highly aligned graphene/polymer nanocomposites with excellent dielectric properties for high-performance electromagnetic interference shielding. Adv Mater 2014;26:5480-7.

[282] Jiang D, Murugadoss V, Wang Y, Lin J, Ding T, Wang Z, Shao Q, Wang C, Liu H, Lu N, Wei R, Subramania A, Guo Z. Electromagnetic interference shielding polymers and nanocomposites - a review. Polym Rev 2019;59:280-337.

[283] Gupta S, Tai N-H. Carbon materials and their composites for electromagnetic interference shielding effectiveness in X-band. Carbon 2019;152:159-87.

[284] Jiang Y, Xie X, Chen Y, Liu Y, Yang R, Sui G. Hierarchically structured cellulose aerogels with interconnected MXene networks and their enhanced microwave absorption properties. J Mater Chem C 2018;6:8679-87.

[285] Jiang Y, Chen Y, Liu Y-J, Sui G-X. Lightweight spongy bone-like graphene@SiC aerogel composites for high-performance microwave absorption. Chem Eng J 2018;337:522-31.

[286] Oh J-H, Kim J, Lee H, Kang Y, Oh I-K. Directionally antagonistic graphene oxide-polyurethane hybrid aerogel as a sound absorber. ACS Appl Mater Interfaces 2018;10:22650-60.

[287] Yan D-X, Pang H, Li B, Vajtai R, Xu L, Ren P-G, Wang J-H, Li Z-M. Structured reduced graphene oxide/polymer composites for ultra-efficient electromagnetic interference shielding. Adv Funct Mater 2015;25:559-66.

[288] Sharif F, Arjmand M, Moud AA, Sundararaj U, Roberts EPL. Segregated hybrid poly(methyl methacrylate)/graphene/magnetite nanocomposites for electromagnetic interference shielding. ACS Appl Mater Interfaces 2017;9:14171-9.

[289] Zhan Y, Wang J, Zhang K, Li Y, Meng Y, Yan N, Wei W, Peng F, Xia H. Fabrication of a flexible electromagnetic interference shielding Fe_3O_4@reduced graphene oxide/natural rubber composite with segregated network. Chem Eng J 2018;344:184-93.

[290] Feng D, Xu D, Wang Q, Liu P. Highly stretchable electromagnetic interference (EMI) shielding segregated polyurethane/carbon nanotube composites fabricated by microwave selective sintering. J Mater Chem C 2019;7:7938-46.

[291] Wang H, Zheng K, Zhang X, Du T, Xiao C, Ding X, Bao C, Chen L, Tian X. Segregated poly(vinylidene fluoride)/MWCNTs composites for high-performance electromagnetic interference shielding. Compos Part A Appl Sci Manuf 2016;90:606-13.

[292] Liang C, Song P, Qiu H, Zhang Y, Ma X, Qi F, Gu H, Kong J, Cao D, Gu J. Constructing interconnected spherical hollow conductive networks in silver platelets/reduced graphene oxide foam/epoxy nanocomposites for superior electromagnetic interference shielding effectiveness. Nanoscale 2019;11:22590-8.

[293] Gao W, Zhao N, Yu T, Xi J, Mao A, Yuan M, Bai H, Gao C. High-efficiency electromagnetic interference shielding realized in nacre-mimetic graphene/polymer composite with extremely low graphene loading. Carbon 2020;157:570-7.

[294] Wang G, Wang L, Mark LH, Shaayegan V, Wang G, Li H, Zhao G, Park CB. Ultralow-threshold and lightweight biodegradable porous PLA/MWCNT with segregated conductive networks for high-performance thermal insulation and electromagnetic interference shielding applications. ACS Appl Mater Interfaces 2018;10:1195-203.

[295] Chen J, Liao X, Xiao W, Yang J, Jiang Q, Li G. Facile and green method to structure ultralow-threshold and lightweight polystyrene/MWCNT composites with segregated conductive networks for efficient electromagnetic interference shielding. ACS Sustainable Chem Eng 2019;7:9904-15.

[296] Bian R, He G, Zhi W, Xiang S, Wang T, Cai D. Ultralight MXene-based aerogels with high electromagnetic interference shielding performance. J Mater Chem C 2019;7:474-8.

[297] Zeng Z, Jin H, Chen M, Li W, Zhou L, Zhang Z. Lightweight and anisotropic porous MWCNT/WPU composites for ultrahigh performance electromagnetic interference shielding. Adv Funct Mater 2016;26:303-10.

[298] Zeng Z, Chen M, Pei Y, Seyed Shahabadi SI, Che B, Wang P, Lu X. Ultralight and flexible polyurethane/silver nanowire nanocomposites with unidirectional pores for highly effective electromagnetic shielding. ACS Appl Mater Interfaces 2017;9:32211-9.

[299] Li MZ, Jia LC, Zhang XP, Yan DX, Zhang QC, Li ZM. Robust carbon nanotube foam for efficient electromagnetic interference shielding and microwave absorption. J Colloid Interface Sci 2018;530:113-9.

[300] Zhang LQ, Yang SG, Li L, Yang B, Huang HD, Yan DX, Zhong GJ, Xu L, Li ZM. Ultralight cellulose porous composites with manipulated porous structure and carbon nanotube distribution for promising electromagnetic interference shielding. ACS Appl Mater Interfaces 2018;10:40156-67.

[301] Zeng Z, Wu T, Han D, Ren Q, Siqueira G, Nystrom G. Ultralight, flexible and biomimetic nanocellulose/silver nanowire aerogels for electromagnetic interference shielding. ACS Nano 2020;14:2927-38.

[302] Shuck CE, Gogotsi Y. Taking MXenes from the lab to commercial products. Chem Eng J 2020;401:125786/1-6.

[303] Zhou ZH, Li MZ, Huang HD, Li L, Yang B, Yan DX, Li ZM. Structuring hierarchically porous architecture in biomass-derived carbon aerogels for simultaneously achieving high electromagnetic interference shielding effectiveness and high absorption coefficient. ACS Appl Mater Interfaces 2020;12:18840-9.

[304] Duan H, Zhu H, Gao J, Yan D-X, Dai K, Yang Y, Zhao G, Liu Y, Li Z-M. Asymmetric conductive polymer composite foam for absorption dominated ultra-efficient electromagnetic interference shielding with extremely low reflection characteristics. J Mater Chem A 2020;8:9146-59.

[305] Ha M, Lim S, Ko H. Wearable and flexible sensors for user-interactive health-monitoring devices. J Mater Chem B 2018;6:4043-64.

[306] Amjadi M, Kyung K-U, Park I, Sitti M. Stretchable, skin-mountable, and wearable strain sensors and their potential applications: a review. Adv Funct Mater 2016;26:1678-98.

[307] Pu J-H, Zhao X, Zha X-J, Bai L, Ke K, Bao R-Y, Liu Z-Y, Yang M-B, Yang W. Multilayer structured AgNW/WPU-MXene fiber strain sensors with ultrahigh sensitivity and a wide operating range for wearable monitoring and healthcare. J Mater Chem A 2019;7:15913-23.

[308] Qiu A, Li P, Yang Z, Yao Y, Lee I, Ma J. A path beyond metal and silicon: polymer/nanomaterial composites for stretchable strain sensors. Adv Funct Mater 2019;29:1806306/1-21.

[309] Wu S, Ladani RB, Zhang J, Ghorbani K, Zhang X, Mouritz AP, Kinloch AJ, Wang CH. Strain sensors with adjustable sensitivity by tailoring the microstructure of graphene aerogel/PDMS nanocomposites. ACS Appl Mater Interfaces 2016;8:24853-61.

[310] Wang C, Pan ZZ, Lv W, Liu B, Wei J, Lv X, Luo Y, Nishihara H, Yang QH. A directional strain sensor based on anisotropic microhoneycomb cellulose nanofiber-carbon nanotube hybrid aerogels prepared by unidirectional freeze drying. Small 2019;15:1805363/1-8.

[311] Zeng Z, Seyed Shahabadi SI, Che B, Zhang Y, Zhao C, Lu X. Highly stretchable, sensitive strain sensors with a wide linear sensing region based on compressed anisotropic graphene foam/polymer nanocomposites. Nanoscale 2017;9:17396-404.

[312] Xie M, Zhang Y, Kraśny MJ, Bowen C, Khanbareh H, Gathercole N. Flexible and active self-powered pressure, shear sensors based on freeze casting ceramic–polymer composites. Energy Environ Sci 2018;11:2919-27.

[313] Pu JH, Zha XJ, Zhao M, Li S, Bao RY, Liu ZY, Xie BH, Yang MB, Guo Z, Yang W. 2D end-to-end carbon nanotube conductive networks in polymer nanocomposites: a conceptual design to dramatically enhance the sensitivities of strain sensors. Nanoscale 2018;10:2191-8.

[314] Giri A, Hopkins PE, Wessel JG, Duda JC. Kapitza resistance and the thermal conductivity of amorphous superlattices. J Appl Phys 2015;118:165303/1-6.

[315] Xiao Y-j, Wang W-y, Lin T, Chen X-j, Zhang Y-t, Yang J-h, Wang Y, Zhou Z-w. Largely enhanced thermal conductivity and high dielectric constant of poly(vinylidene fluoride)/boron nitride composites achieved by adding a few carbon nanotubes. J Phys Chem C 2016;120:6344-55.

[316] Chen H, Ginzburg VV, Yang J, Yang Y, Liu W, Huang Y, Du L, Chen B. Thermal conductivity of polymer-based composites: fundamentals and applications. Prog Polym Sci 2016;59:41-85.

[317] Burger N, Laachachi A, Ferriol M, Lutz M, Toniazzo V, Ruch D. Review of thermal conductivity in composites: mechanisms, parameters and theory. Prog Polym Sci 2016;61:1-28.

[318] Yuan K, Shi J, Aftab W, Qin M, Usman A, Zhou F, Lv Y, Gao S, Zou R. Engineering the thermal conductivity of functional phase-change materials for heat energy conversion, storage, and utilization. Adv Funct Mater 2020;30:1904228/1-31.

[319] Zhang P, Yuan P, Jiang X, Zhai S, Zeng J, Xian Y, Qin H, Yang D. A theoretical review on interfacial thermal transport at the nanoscale. Small 2018;14:1702769/1-19.

[320] Singh V, Bougher TL, Weathers A, Cai Y, Bi K, Pettes MT, McMenamin SA, Lv W, Resler DP, Gattuso TR, Altman DH, Sandhage KH, Shi L, Henry A, Cola BA. High thermal conductivity of chain-oriented amorphous polythiophene. Nat Nanotechnol 2014;9:384-90.

[321] Kim GH, Lee D, Shanker A, Shao L, Kwon MS, Gidley D, Kim J, Pipe KP. High thermal conductivity in amorphous polymer blends by engineered interchain interactions. Nat Mater 2015;14:295-300.

[322] Wang S, Cheng Y, Wang R, Sun J, Gao L. Highly thermal conductive copper nanowire composites with ultralow loading: toward applications as thermal interface materials. ACS Appl Mater Interfaces 2014;6:6481-6.

[323] Chen C, Wang H, Xue Y, Xue Z, Liu H, Xie X, Mai Y-W. Structure, rheological, thermal conductive and electrical insulating properties of high-performance hybrid epoxy/nanosilica/AgNWs nanocomposites. Compos Sci Technol 2016;128:207-14.

[324] Han Z, Fina A. Thermal conductivity of carbon nanotubes and their polymer nanocomposites: a review. Prog Polym Sci 2011;36:914-44.

[325] Feng C, Ni H, Chen J, Yang W. Facile method to fabricate highly thermally conductive graphite/PP composite with network structures. ACS Appl Mater interfaces 2016;8:19732-8.

[326] Shtein M, Nadiv R, Buzaglo M, Kahil K, Regev O. Thermally conductive graphene-polymer composites: size, percolation, and synergy effects. Chem Mater 2015;27:2100-6.

[327] Song SH, Park KH, Kim BH, Choi YW, Jun GH, Lee DJ, Kong BS, Paik KW, Jeon S. Enhanced thermal conductivity of epoxy-graphene composites by using non-oxidized graphene flakes with non-covalent functionalization. Adv Mater 2013;25:732-7.

[328] Lule Z, Kim J. Thermally conductive and highly rigid polylactic acid (PLA) hybrid composite filled with surface treated alumina/nano-sized aluminum nitride. Compos Part A Appl Sci Manuf 2019;124:105506/1-8.

[329] Chen J, Huang X, Zhu Y, Jiang P. Cellulose nanofiber supported 3D interconnected BN nanosheets for epoxy nanocomposites with ultrahigh thermal management capability. Adv Funct Mater 2017;27:1604754/1-9.

[330] Chen J, Huang X, Sun B, Wang Y, Zhu Y, Jiang P. Vertically aligned and interconnected boron nitride nanosheets for advanced flexible nanocomposite thermal interface materials. ACS Appl Mater Interfaces 2017;9:30909-17.

[331] Huang Y, Hu J, Yao Y, Zeng X, Sun J, Pan G, Sun R, Xu J-B, Wong C-P. Manipulating orientation of silicon carbide nanowire in polymer composites to achieve high thermal conductivity. Adv Mater Interfaces 2017;4:1700446/1-8.

[332] Lin Z, Liu Y, Raghavan S, Moon K-s, Sitaraman SK, Wong C-p. Magnetic alignment of hexagonal boron nitride platelets in polymer matrix: toward high performance anisotropic polymer composites for electronic encapsulation. ACS Appl Mater Interfaces 2013;5:7633-40.

[333] Yuan C, Duan B, Li L, Xie B, Huang M, Luo X. Thermal conductivity of polymer-based composites with magnetic aligned hexagonal boron nitride platelets. ACS Appl Mater Interfaces 2015;7:13000-6.

[334] Kuang Z, Chen Y, Lu Y, Liu L, Hu S, Wen S, Mao Y, Zhang L. Fabrication of highly oriented hexagonal boron nitride nanosheet/elastomer nanocomposites with high thermal conductivity. Small 2015;11:1655-9.

[335] Shen H, Guo J, Wang H, Zhao N, Xu J. Bioinspired modification of h-BN for high thermal conductive composite films with aligned structure. ACS Appl Mater Interfaces 2015;7:5701-8.

[336] Zeng X, Sun J, Yao Y, Sun R, Xu JB, Wong CP. A combination of boron nitride nanotubes and cellulose nanofibers for the preparation of a nanocomposite with high thermal conductivity. ACS Nano 2017;11:5167-78.

[337] Zhu H, Li Y, Fang Z, Xu J, Cao F, Wan J, Preston C, Yang B, Hu L. Highly thermally conductive papers with percolative layered boron nitride nanosheets. ACS Nano 2014;8:3606-13.

[338] Lim HS, Oh JW, Kim SY, Yoo M-J, Park S-D, Lee WS. Anisotropically alignable magnetic boron nitride platelets decorated with iron oxide nanoparticles. Chem Mater 2013;25:3315-9.

[339] Cho H-B, Nakayama T, Suematsu H, Suzuki T, Jiang W, Niihara K, Song E, Eom NSA, Kim S, Choa Y-H. Insulating polymer nanocomposites with high-thermal-conduction routes via linear densely packed boron nitride nanosheets. Compos Sci Technol 2016;129:205-13.

[340] Lian G, Tuan C-C, Li L, Jiao S, Wang Q, Moon K-S, Cui D, Wong C-P. Vertically aligned and interconnected graphene networks for high thermal conductivity of epoxy composites with ultralow loading. Chem Mater 2016;28:6096-104.

[341] Li X-H, Liu P, Li X, An F, Min P, Liao K-N, Yu Z-Z. Vertically aligned, ultralight and highly compressive all-graphitized graphene aerogels for highly thermally conductive polymer composites. Carbon 2018;140:624-33.

[342] Yang J, Li X, Han S, Yang R, Min P, Yu Z-Z. High-quality graphene aerogels for thermally conductive phase change composites with excellent shape stability. J Mater Chem A 2018;6:5880-6.

[343] Xin G, Sun H, Scott SM, Yao T, Lu F, Shao D, Hu T, Wang G, Ran G, Lian J. Advanced phase change composite by thermally annealed defect-free graphene for thermal energy storage. ACS Appl Mater Interfaces 2014;6:15262-71.

[344] Kim KH, Oh Y, Islam MF. Graphene coating makes carbon nanotube aerogels superelastic and resistant to fatigue. Nat Nanotechnol 2012;7:562-6.

[345] An F, Li X, Min P, Li H, Dai Z, Yu Z-Z. Highly anisotropic graphene/boron nitride hybrid aerogels with long-range ordered architecture and moderate density for highly thermally conductive composites. Carbon 2018;126:119-27.

[346] Bryning MB, Milkie DE, Islam MF, Hough LA, Kikkawa JM, Yodh AG. Carbon nanotube aerogels. Adv Mater 2007;19:661-4.

[347] Li Y, Zhao M, Chen J, Fan S, Liang J, Ding L, Chen S. Flexible chitosan/carbon nanotubes aerogel, a robust matrix for in-situ growth and non-enzymatic biosensing applications. Sens Actuators B Chem 2016;232:750-7.

[348] Yan J, Wang H, Wu T, Li X, Ding Z. Elastic and electrically conductive carbon nanotubes/chitosan composites with lamellar structure. Compos Part A Appl Sci Manuf 2014;67:1-7.

[349] Yao Y, Sun J, Zeng X, Sun R, Xu JB, Wong CP. Construction of 3D skeleton for polymer composites achieving a high thermal conductivity. Small. 2018;14:1704044/1-12.

[350] Zeng X, Yao Y, Gong Z, Wang F, Sun R, Xu J, Wong CP. Ice-templated assembly strategy to construct 3D boron nitride nanosheet networks in polymer composites for thermal conductivity improvement. Small. 2015;11:6205-13.

[351] Wang X, Wu P. 3D vertically aligned BNNS network with long-range continuous channels for achieving a highly thermally conductive composite. ACS Appl Mater Interfaces 2019;11:28943-52.

[352] Vu MC, Choi WK, Lee SG, Park P, Kim D-H, Islam MA, Kim SR. High thermal conductivity enhancement of polymer composites with vertically aligned silicon carbide sheet scaffold. ACS Appl Mater Interfaces 2020;12:23388-98.

[353] Shen Z, Feng J. Achieving vertically aligned SiC microwires networks in a uniform cold environment for polymer composites with high through-plane thermal conductivity enhancement. Compos Sci Technol 2019;170:135-40.

[354] Yao Y, Zhu X, Zeng X, Sun R, Xu J-B, Wong C-P. Vertically aligned and interconnected SiC nanowire networks leading to significantly enhanced thermal conductivity of polymer composites. ACS Appl Mater Interfaces 2018;10:9669-78.

[355] Ma J, Shang T, Ren L, Yao Y, Zhang T, Xie J, Zhang B, Zeng X, Sun R, Xu J-B, Wong C-P. Through-plane assembly of carbon fibers into 3D skeleton achieving enhanced thermal conductivity of a thermal interface material. Chem Eng J 2020;380:122550/1-8.

[356] Thieu NAT, Vu MC, Kim DH, Choi WK, Kim SR. Effect of aspect ratio of vertically aligned copper nanowires in the presence of cellulose nanofibers on the thermal conductivity of epoxy composites. Polym Adv Technol 2020;31:4954/1-9.

[357] Wei Z, Xie W, Ge B, Zhang Z, Yang W, Xia H, Wang B, Jin H, Gao N, Shi Z. Enhanced thermal conductivity of epoxy composites by constructing aluminum nitride honeycomb reinforcements. Compos Sci Technol 2020; doi: https://doi.org/10.1016/j.compscitech.2020.108304.

[358] Chen J, Huang X, Sun B, Jiang P. Highly thermally conductive yet electrically insulating polymer/boron nitride nanosheets nanocomposite films for improved thermal management capability. ACS Nano 2019;13:337-45.

[359] Cui S, Jiang F, Song N, Shi L, Ding P. Flexible films for smart thermal management: influence of structure construction of a two-dimensional graphene network on active heat dissipation response behavior. ACS Appl Mater Interfaces 2019;11:30352-9.

[360] Dong J, Cao L, Li Y, Wu Z, Teng C. Largely improved thermal conductivity of PI/BNNS nanocomposites obtained by constructing a 3D BNNS network and filling it with AgNW as the thermally conductive bridges. Compos Sci Technol 2020;196:108242/1-11.

[361] Guo F, Shen X, Zhou J, Liu D, Zheng Q, Yang J, Jia B, Lau AKT, Kim JK. Highly thermally conductive dielectric nanocomposites with synergistic alignments of graphene and boron nitride nanosheets. Adv Funct Mater 2020;30:1910826/1-13.

[362] Han J, Du G, Gao W, Bai H. An anisotropically high thermal conductive boron nitride/epoxy composite based on nacre-mimetic 3D network. Adv Funct Mater 2019;29:1900412/1-9.

[363] Hou X, Chen Y, Dai W, Wang Z, Li H, Lin C-T, Nishimura K, Jiang N, Yu J. Highly thermal conductive polymer composites via constructing micro-phragmites communis structured carbon fibers. Chem Eng J 2019;375:121921/1-6.

[364] Shen H, Cai C, Guo J, Qian Z, Zhao N, Xu J. Fabrication of oriented hBN scaffolds for thermal interface materials. RSC Adv 2016;6:16489-94.

[365] Hou X, Chen Y, Lv L, Dai W, Zhao S, Wang Z, Fu L, Lin C-T, Jiang N, Yu J. High-thermal-transport-channel construction within flexible composites via the welding of boron nitride nanosheets. ACS Appl Nano Mater 2019;2:360-8.

[366] Wang D, Lin Y, Hu D, Jiang P, Huang X. Multifunctional 3D-MXene/PDMS nanocomposites for electrical, thermal and triboelectric applications. Compos Part A Appl Sci Manuf 2020;130:105754/1-8.

[367] Song J, Zhang Y. Vertically aligned silicon carbide nanowires/reduced graphene oxide networks for enhancing the thermal conductivity of silicone rubber composites. Compos Part A Appl Sci Manuf 2020;133:105873/1-8.

[368] An D, Cheng S, Zhang Z, Jiang C, Fang H, Li J, Liu Y, Wong C-P. A polymer-based thermal management material with enhanced thermal conductivity by introducing three-dimensional networks and covalent bond connections. Carbon 2019;155:258-67.

[369] An D, Duan X, Cheng S, Zhang Z, Yang B, Lian Q, Li J, Sun Z, Liu Y, Wong C-P. Enhanced thermal conductivity of natural rubber based thermal interfacial materials by constructing covalent bonds and three-dimensional networks. Compos Part A Appl Sci Manuf 2020;135:105928/1-10.

[370] Feng CP, Bai L, Bao R-Y, Wang S-W, Liu Z, Yang M-B, Chen J, Yang W. Superior thermal interface materials for thermal management. Compos Commun 2019;12:80-5.

[371] Shahil KM, Balandin AA. Graphene-multilayer graphene nanocomposites as highly efficient thermal interface materials. Nano Lett 2012;12:861-7.

[372] Wang H, Feng JY, Hu XJ, Ng KM. Reducing thermal contact resistance using a bilayer aligned CNT thermal interface material. Chem Eng Sci 2010;65:1101-8.

[373] Yang J, Tang L-S, Bai L, Bao R-Y, Liu Z, Xie B-H, Yang M-B, Yang W. Photodriven shape-stabilized phase change materials with optimized thermal conductivity by tailoring the microstructure of hierarchically ordered hybrid porous scaffolds. ACS Sustainable Chem Eng 2018;6:6761-70.

[374] Wu K, Lei C, Huang R, Yang W, Chai S, Geng C, Chen F, Fu Q. Design and preparation of a unique segregated double network with excellent thermal conductive property. ACS Appl Mater Interfaces 2017;9:7637-47.

[375] Chen X, Lim JSK, Yan W, Guo F, Liang YN, Chen H, Lambourne A, Hu X. Salt template assisted BN scaffold fabrication toward highly thermally conductive epoxy composites. ACS Appl Mater Interfaces 2020;12:16987-96.

[376] Jia X, Li Q, Ao C, Hu R, Xia T, Xue Z, Wang Q, Deng X, Zhang W, Lu C. High thermal conductive shape-stabilized phase change materials of polyethylene glycol/boron nitride@chitosan composites for thermal energy storage. Compos Part A Appl Sci Manuf 2020;129:105710/1-10.

[377] Wei X, Xue F, Qi X-d, Yang J-h, Zhou Z-w, Yuan Y-p, Wang Y. Photo- and electro-responsive phase change materials based on highly anisotropic microcrystalline cellulose/graphene nanoplatelet structure. Appl Energy 2019;236:70-80.

[378] Zhang L, Liu X, Deb A, Feng G. Ice-templating synthesis of hierarchical and anisotropic silver-nanowire-fabric aerogel and its application for enhancing thermal energy storage composites. ACS Sustainable Chem Eng 2019;7:19910-7.

[379] Balandin AA, Ghosh S, Bao W, Calizo I, Teweldebrhan D, Miao F, Lau CN. Superior thermal conductivity of single-layer graphene. Nano Lett 2008;8:902-7.

[380] Dai W, Ma T, Yan Q, Gao J, Tan X, Lv L, Hou H, Wei Q, Yu J, Wu J, Yao Y, Du S, Sun R, Jiang N, Wang Y, Kong J, Wong C, Maruyama S, Lin CT. Metal-level thermally conductive yet soft graphene thermal interface materials. ACS Nano 2019;13:11561-71.

[381] Wu S, Li T, Tong Z, Chao J, Zhai T, Xu J, Yan T, Wu M, Xu Z, Bao H, Deng T, Wang R. High-performance thermally conductive phase change composites by large-size oriented graphite sheets for scalable thermal energy harvesting. Adv Mater 2019;31:1905099/1-9.

[382] Qi G, Yang J, Bao R, Xia D, Cao M, Yang W, Yang M, Wei D. Hierarchical graphene foam-based phase change materials with enhanced thermal conductivity and shape stability for efficient solar-to-thermal energy conversion and storage. Nano Res 2016;10:802-13.

[383] Yang J, Qi G-Q, Bao R-Y, Yi K, Li M, Peng L, Cai Z, Yang M-B, Wei D, Yang W. Hybridizing graphene aerogel into three-dimensional graphene foam for high-performance composite phase change materials. Energy Storage Mater 2018;13:88-95.

[384] Feng CP, Chen LB, Tian GL, Wan SS, Bai L, Bao RY, Liu ZY, Yang MB, Yang W. Multifunctional thermal management materials with excellent heat dissipation and generation capability for future electronics. ACS Appl Mater Interfaces 2019;11:18739-45.

[385] Wu K, Liu D, Lei C, Xue S, Fu Q. Is filler orientation always good for thermal management performance: a visualized study from experimental results to simulative analysis. Chem Eng J 2020;394:124929/1-8.

[386] Cuce E, Cuce PM, Wood CJ, Riffat SB. Toward aerogel based thermal superinsulation in buildings: a comprehensive review. Renewable Sustainable Energy Rev 2014;34:273-99.

[387] Randall JP, Meador MAB, Jana SC. Tailoring mechanical properties of aerogels for aerospace applications. ACS Appl Mater Interfaces 2011;3:613-26.

[388] Bai F, Wu J, Gong G, Guo L. A flexible, sandwiched high-performance super-insulation fabric. J Mater Chem A 2015;3:13198-202.

[389] Rizvi A, Chu RKM, Park CB. Scalable fabrication of thermally insulating mechanically resilient hierarchically porous polymer foams. ACS Appl Mater Interfaces 2018;10:38410-7.

[390] Han Y, Zhang X, Wu X, Lu C. Flame retardant, heat insulating cellulose aerogels from waste cotton fabrics by in situ formation of magnesium hydroxide nanoparticles in cellulose gel nanostructures. ACS Sustainable Chem Eng 2015;3:1853-9.

[391] Gong P, Wang G, Tran M-P, Buahom P, Zhai S, Li G, Park CB. Advanced bimodal polystyrene/multi-walled carbon nanotube nanocomposite foams for thermal insulation. Carbon 2017;120:1-10.

[392] Wang G, Zhao G, Dong G, Song L, Park CB. Lightweight, thermally insulating, and low dielectric microcellular high-impact polystyrene (HIPS) foams fabricated by high-pressure foam injection molding with mold opening. J Mater Chem C 2018;6:12294-305.

[393] Koebel M, Rigacci A, Achard P. Aerogel-based thermal superinsulation: an overview. J Sol-Gel Sci Technol 2012;63:315-39.

[394] Fan W, Zhang X, Zhang Y, Zhang Y, Liu T. Lightweight, strong, and super-thermal insulating polyimide composite aerogels under high temperature. Compos Sci Technol 2019;173:47-52.

[395] Huber L, Zhao S, Malfait WJ, Vares S, Koebel MM. Fast and minimal-solvent production of superinsulating silica aerogel granulate. Angew Chem Int Ed 2017;56:4753-6.

[396] Hayase G, Kugimiya K, Ogawa M, Kodera Y, Kanamori K, Nakanishi K. The thermal conductivity of polymethylsilsesquioxane aerogels and xerogels with varied pore sizes for practical application as thermal superinsulators. J Mater Chem A 2014;2:6525-31.

[397] Zou F, Yue P, Zheng X, Tang D, Fu W, Li Z. Robust and superhydrophobic thiourethane bridged polysilsesquioxane aerogels as potential thermal insulation materials. J Mater Chem A 2016;4:10801-5.

[398] Tang L, Zhuang S, Hong B, Cai Z, Chen Y, Huang B. Synthesis of light weight, high strength biomass-derived composite aerogels with low thermal conductivities. Cellulose 2019;26:8699-712.

[399] Wicklein B, Kocjan A, Salazar-Alvarez G, Carosio F, Camino G, Antonietti M, Bergström L. Thermally insulating and fire-retardant lightweight anisotropic foams based on nanocellulose and graphene oxide. Nat Nanotechnol 2014;10:277-83.

[400] Yu Z-L, Yang N, Zhou L-C, Ma Z-Y, Zhu Y-B, Lu Y-Y, Qin B, Xing W-Y, Ma T, Li S-C, Gao H-L, Wu H-A, Yu S-H. Bioinspired polymeric woods. Sci Adv 2018;4:eaat7223/1-10.

[401] Qin Y, Peng Q, Zhu Y, Zhao X, Lin Z, He X, Li Y. Lightweight, mechanically flexible and thermally superinsulating rGO/polyimide nanocomposite foam with an anisotropic microstructure. Nanoscale Adv 2019;1:4895-903.

[402] Peng Q, Qin Y, Zhao X, Sun X, Chen Q, Xu F, Lin Z, Yuan Y, Li Y, Li J, Yin W, Gao C, Zhang F, He X, Li Y. Superlight, mechanically flexible, thermally superinsulating, and antifrosting anisotropic nanocomposite foam based on hierarchical graphene oxide assembly. ACS Appl Mater Interfaces 2017;9:44010-7.

[403] Zhang X, Zhao X, Xue T, Yang F, Fan W, Liu T. Bidirectional anisotropic polyimide/bacterial cellulose aerogels by freeze-drying for super-thermal insulation. Chem Eng J 2020;385:123963/1-9.

[404] Yang Y, Gao W. Wearable and flexible electronics for continuous molecular monitoring. Chem Soc Rev 2019;48:1465-91.

[405] Peng Y, Chen J, Song AY, Catrysse PB, Hsu P-C, Cai L, Liu B, Zhu Y, Zhou G, Wu DS, Lee HR, Fan S, Cui Y. Nanoporous polyethylene microfibres for large-scale radiative cooling fabric. Nat Sustain 2018;1:105-12.

[406] Tao X. Study of fiber-based wearable energy systems. Acc Chem Res 2019;52:307-15.

[407] Seyedin S, Zhang P, Naebe M, Qin S, Chen J, Wang X, Razal JM. Textile strain sensors: a review of the fabrication technologies, performance evaluation and applications. Mater Horiz 2019;6:219-49.

[408] Yang H, Wang Z, Liu Z, Cheng H, Li C. Continuous, strong, porous silk firoin-based aerogel fibers toward textile thermal insulation. Polymers 2019;11:1899/1-14.

[409] Zhou J, Hsieh Y-L. Nanocellulose aerogel-based porous coaxial fibers for thermal insulation. Nano Energy 2020;68:104305/1-9.

[410] Wang Z, Yang H, Li Y, Zheng X. Robust silk fibroin/graphene oxide aerogel fiber for radiative heating textiles. ACS Appl Mater Interfaces 2020;12:15726-36.

[411] Ge J, Zhao HY, Zhu HW, Huang J, Shi LA, Yu SH. Advanced sorbents for oil-spill cleanup: recent advances and future perspectives. Adv Mater 2016;28:10459-90.

[412] Mohammadzadeh Pakdel P, Peighambardoust SJ. Review on recent progress in chitosan-based hydrogels for wastewater treatment application. Carbohydr Polym 2018;201:264-79.

[413] Wang M, Payne KA, Tong S, Ergas SJ. Hybrid algal photosynthesis and ion exchange (HAPIX) process for high ammonium strength wastewater treatment. Water Res 2018;142:65-74.

[414] Mudhoo A, Bhatnagar A, Rantalankila M, Srivastava V, Sillanpää M. Endosulfan removal through bioremediation, photocatalytic degradation, adsorption and membrane separation processes: a review. Chem Eng J 2019;360:912-28.

[415] Volpin F, Fons E, Chekli L, Kim JE, Jang A, Shon HK. Hybrid forward osmosis-reverse osmosis for wastewater reuse and seawater desalination: understanding the optimal feed solution to minimise fouling. Process Saf Environ Prot 2018;117:523-32.

[416] Wu Y, Xu M, Chen X, Yang S, Wu H, Pan J, Xiong X. CTAB-assisted synthesis of novel ultrathin $MoSe_2$ nanosheets perpendicular to graphene for the adsorption and photodegradation of organic dyes under visible light. Nanoscale 2016;8:440-50.

[417] Dong Z, Wang D, Liu X, Pei X, Chen L, Jin J. Bio-inspired surface-functionalization of graphene oxide for the adsorption of organic dyes and heavy metal ions with a superhigh capacity. J Mater Chem A 2014;2:5034-40.

[418] Yu P, Wang H-Q, Bao R-Y, Liu Z, Yang W, Xie B-H, Yang M-B. Self-assembled sponge-like chitosan/reduced graphene oxide/montmorillonite composite hydrogels without cross-linking of chitosan for effective Cr(VI) sorption. ACS Sustainable Chem Eng 2017;5:1557-66.

[419] Phetphaisit CW, Yuanyang S, Chaiyasith WC. Polyacrylamido-2-methyl-1-propane sulfonic acid-grafted-natural rubber as bio-adsorbent for heavy metal removal from aqueous standard solution and industrial wastewater. J Hazard Mater 2016;301:163-71.

[420] Jiang N, Shang R, Heijman SGJ, Rietveld LC. High-silica zeolites for adsorption of organic micro-pollutants in water treatment: a review. Water Res 2018;144:145-61.

[421] Kyzas GZ, Bomis G, Kosheleva RI, Efthimiadou EK, Favvas EP, Kostoglou M, Mitropoulos AC. Nanobubbles effect on heavy metal ions adsorption by activated carbon. Chem Eng J 2019;356:91-7.

[422] Ge J, Shi LA, Wang YC, Zhao HY, Yao HB, Zhu YB, Zhang Y, Zhu HW, Wu HA, Yu SH. Joule-heated graphene-wrapped sponge enables fast clean-up of viscous crude-oil spill. Nat Nanotechnol 2017;12:434-40.

[423] Liu Y, Li F, Xia Q, Wu J, Liu J, Huang M, Xie J. Conductive 3D sponges for affordable and highly-efficient water purification. Nanoscale 2018;10:4771-8.

[424] Fang Q, Zhou X, Deng W, Liu Y, Zheng Z, Liu Z. Nitrogen-doped graphene nanoscroll foam with high diffusion rate and binding affinity for removal of organic pollutants. Small 2017;13:1603779/1-7.

[425] Sun H, Xu Z, Gao C. Multifunctional, ultra-flyweight, synergistically assembled carbon aerogels. Adv Mater 2013;25:2554-60.

[426] Zhan W, Yu S, Gao L, Wang F, Fu X, Sui G, Yang X. Bioinspired assembly of carbon nanotube into graphene aerogel with "cabbagelike" hierarchical porous structure for highly efficient organic pollutants cleanup. ACS Appl Mater Interfaces 2018;10:1093-103.

[427] Liu T, Huang M, Li X, Wang C, Gui C-X, Yu Z-Z. Highly compressible anisotropic graphene aerogels fabricated by directional freezing for efficient absorption of organic liquids. Carbon 2016;100:456-64.

[428] Hou S, Wu X, Lv Y, Jia W, Guo J, Wang L, Tong F, Jia D. Ultralight, highly elastic and bioinspired capillary-driven graphene aerogels for highly efficient organic pollutants absorption. Appl Surf Sci 2019;509:144818/1-9.

[429] Li C, Wu Z-Y, Liang H-W, Chen J-F, Yu S-H. Ultralight multifunctional carbon-based aerogels by combining graphene oxide and bacterial cellulose. Small 2017;13:1700453/1-8.

[430] Rodríguez-Mata V, González-Domínguez JM, Benito AM, Maser WK, García-Bordejé E. Reduced graphene oxide aerogels with controlled continuous microchannels for environmental remediation. ACS Appl Nano Mater 2019;2:1210-22.

[431] Liu X, Pang K, Yang H, Guo X. Intrinsically microstructured graphene aerogel exhibiting excellent mechanical performance and super-high adsorption capacity. Carbon 2020;161:146-52.

[432] Lai KC, Lee LY, Hiew BYZ, Thangalazhy-Gopakumar S, Gan S. Environmental application of three-dimensional graphene materials as adsorbents for dyes and heavy metals: Review on ice-templating method and adsorption mechanisms. J Environ Sci 2019;79:174-99.

[433] Chen T, Li M, Zhou L, Ding X, Lin D, Duan T, Yang G, He R, Zhu W. Bio-inspired biomass-derived carbon aerogels with superior mechanical property for oil–water separation. ACS Sustainable Chem Eng 2020;8:6458-65.

[434] Zeng Z, Ma XYD, Zhang Y, Wang Z, Ng BF, Wan MP, Lu X. Robust lignin-based aerogel filters: high-efficiency capture of ultrafine airborne particulates and the mechanism. ACS Sustainable Chem Eng 2019;7:6959-68.

[435] da Silva LL, Galembeck F. Morphology of latex and nanocomposite adsorbents prepared by freeze-casting. J Mater Chem A 2015;3:7263-72.

[436] Liaw B-S, Chang T-T, Chang H-K, Liu W-K, Chen P-Y. Fish scale-extracted hydroxyapatite/chitosan composite scaffolds fabricated by freeze casting—an innovative strategy for water treatment. J hazard Mater 2020;382:121082/1-13.

[437] Chen J, Shi X, Zhan Y, Qiu X, Du Y, Deng H. Construction of horizontal stratum landform-like composite foams and their methyl orange adsorption capacity. Appl Surf Sci 2017;397:133-43.

[438] Yang J, Xia Y, Xu P, Chen B. Super-elastic and highly hydrophobic/superoleophilic sodium alginate/cellulose aerogel for oil/water separation. Cellulose 2018;25:3533-44.

[439] Cao X, Zhou Y, Wei X, Zhai W, Zheng G, Dai K, Liu C, Shen C. Lightweight, mechanical robust foam with a herringbone-like porous structure for oil/water separation and filtering. Polym Test 2018;72:86-93.

[440] Li Y, Zhang G, Gao A, Cui J, Zhao S, Yan Y. Robust graphene/poly(vinyl alcohol) Janus aerogels with a hierarchical architecture for highly efficient switchable separation of oil/water emulsions. ACS Appl Mater Interfaces 2019;11:36638-48.

[441] Cui Y, Wang Y, Shao Z, Mao A, Gao W, Bai H. Smart sponge for fast liquid absorption and thermal responsive self-squeezing. Adv Mater 2020;32:1908249/1-9.

[442] Li Z, Klein TR, Kim DH, Yang M, Berry JJ, van Hest MFAM, Zhu K. Scalable fabrication of perovskite solar cells. Nat Rev Mater 2018;3:18017/1-20.

[443] Li M, Lu J, Chen Z, Amine K. 30 years of lithium-ion batteries. Adv Mater 2018;30:1800561/1-24.

[444] Xu Y, Shi G, Duan X. Self-assembled three-dimensional graphene macrostructures: synthesis and applications in supercapacitors. Acc Chem Res 2015;48:1666-75.

[445] Jella V, Ippili S, Eom J-H, Pammi SVN, Jung J-S, Tran V-D, Nguyen VH, Kirakosyan A, Yun S, Kim D, Sihn MR, Choi J, Kim Y-J, Kim H-J, Yoon S-G. A comprehensive review of flexible piezoelectric generators based on organic-inorganic metal halide perovskites. Nano Energy 2019;57:74-93.

[446] Wu C, Wang AC, Ding W, Guo H, Wang ZL. Triboelectric nanogenerator: a foundation of the energy for the new era. Adv Energy Mater 2019; ;9:1802906/1-25.

[447] Kroon R, Mengistie DA, Kiefer D, Hynynen J, Ryan JD, Yu L, Muller C. Thermoelectric plastics: from design to synthesis, processing and structure-property relationships. Chem Soc Rev 2016;45:6147-64.

[448] Zhang L, Lin S, Hua T, Huang B, Liu S, Tao X. Fiber-based thermoelectric generators: materials, device structures, fabrication, characterization, and applications. Adv Energy Mater 2018;8:1700524/1-18.

[449] Zhou L, Li X, Ni GW, Zhu S, Zhu J. The revival of thermal utilization from the Sun: interfacial solar vapor generation. Nat Sci Rev 2019;6:562-78.

[450] Qiu B, Xing M, Zhang J. Recent advances in three-dimensional graphene based materials for catalysis applications. Chem Soc Rev 2018;47:2165-216.

[451] Hu R, Zhang J, Kuang Y, Wang K, Cai X, Fang Z, Huang W, Chen G, Wang Z. A Janus evaporator with low tortuosity for long-term solar desalination. J Mater Chem A 2019;7:15333-40.

[452] Li C, Yang Y, Wu Y, Tao X, Chen W. High-performance piezocomposite energy harvesters by constructing bionic ion channels. Adv Mater Technol 2020;5:2000050/1-10.

[453] Wei J, Yin C, Wang H, Wang Q. Polyampholyte-doped aligned polymer hydrogels as anisotropic electrolytes for ultrahigh-capacity supercapacitors. J Mater Chem A 2018;6:58-64.

[454] Yang X, Sun Q, Zhao C, Gao X, Adair KR, Liu Y, Luo J, Lin X, Liang J, Huang H, Zhang L, Yang R, Lu S, Li R, Sun X. High-areal-capacity all-solid-state lithium batteries enabled by rational design of fast ion transport channels in vertically-aligned composite polymer electrodes. Nano Energy 2019;61:567-75.

[455] Dao V-D, Vu NH, Yun S. Recent advances and challenges for solar-driven water evaporation system toward applications. Nano Energy 2020;68:104324/1-18.

[456] Dao VD, Choi HS. Carbon-based sunlight absorbers in solar-driven steam generation devices. Glob Chall 2018; ;2:1700094/1-14.

[457] Li D, Li A, Chen Y, Chen G, Chen X, Zhang D, Zhu H, Samo IA, Song H. Spray-freezing induced multidimensional morphology tuning of assembled spherical carbon for solar-driven steam generation. Carbon 2020;162:481-9.

[458] Hu X, Xu W, Zhou L, Tan Y, Wang Y, Zhu S, Zhu J. Tailoring graphene oxide-based aerogels for efficient solar steam generation under one sun. Adv Mater 2017;29:1604031/1-5.

[459] Jiang F, Liu H, Li Y, Kuang Y, Xu X, Chen C, Huang H, Jia C, Zhao X, Hitz E, Zhou Y, Yang R, Cui L, Hu L. Lightweight, mesoporous, and highly absorptive all-nanofiber aerogel for efficient solar steam generation. ACS Appl Mater Interfaces 2018;10:1104-12.

[460] Zhang P, Liu F, Liao Q, Yao H, Geng H, Cheng H, Li C, Qu L. A microstructured graphene/poly(n-isopropylacrylamide) membrane for intelligent solar water evaporation. Angew Chem Int Ed 2018;57:16343-7.

[461] Zhao F, Zhou X, Shi Y, Qian X, Alexander M, Zhao X, Mendez S, Yang R, Qu L, Yu G. Highly efficient solar vapour generation via hierarchically nanostructured gels. Nat Nanotechnol 2018;13:489-95.

[462] Liu Y, Ai K, Lu L. Polydopamine and its derivative materials: synthesis and promising applications in energy, environmental, and biomedical fields. Chem Rev 2014;114:5057-115.

[463] Li R, Zhang L, Shi L, Wang P. MXene Ti_3C_2: an effective 2D light-to-heat conversion material. ACS Nano 2017;11:3752-9.

[464] Xu D, Li Z, Li L, Wang J. Insights into the photothermal conversion of 2D MXene nanomaterials: synthesis, mechanism, and applications. Adv Funct Mater 2020;30:2000712/1-21.

[465] Zhao X, Zha X-J, Tang L-S, Pu J-H, Ke K, Bao R-Y, Liu Z-y, Yang M-B, Yang W. Self-assembled core-shell polydopamine@MXene with synergistic solar absorption capability for highly efficient solar-to-vapor generation. Nano Res 2019;13:255-64.

[466] Huang L, Lin S, Xu Z, Zhou H, Duan J, Hu B, Zhou J. Fiber-based energy conversion devices for human-body energy harvesting. Adv Mater 2019;32:1902034/1-20.

[467] Chen G, Li Y, Bick M, Chen J. Smart textiles for electricity generation. Chem Rev 2020;120:3668-720.

[468] Wang Y, Gao S, Xu W, Wang Z. Nanogenerators with superwetting surfaces for harvesting water/liquid energy. Adv Funct Mater 2020;30:1908252/1-15.

[469] Li M, Zong L, Yang W, Li X, You J, Wu X, Li Z, Li C. Biological nanofibrous generator for electricity harvest from moist air flow. Adv Funct Mater 2019;29:1901798/1-8.

[470] Zhao F, Wang L, Zhao Y, Qu L, Dai L. Graphene oxide nanoribbon assembly toward moisture-powered information storage. Adv Mater 2017;29:1604972/1-7.

[471] Zhang Y, Bao Y, Zhang D, Bowen CR, Pilon L. Porous PZT ceramics with aligned pore channels for energy harvesting applications. J Am Ceram Soc 2015;98:2980-3.

[472] Zhang Y, Xie M, Roscow J, Bao Y, Zhou K, Zhang D, Bowen CR. Enhanced pyroelectric and piezoelectric properties of PZT with aligned porosity for energy harvesting applications. J Mater Chem A 2017;5:6569-80.

[473] Zhang YZ, Wang Y, Cheng T, Yao LQ, Li X, Lai WY, Huang W. Printed supercapacitors: materials, printing and applications. Chem Soc Rev 2019;48:3229-64.

[474] Hu Y, Tong X, Zhuo H, Zhong L, Peng X. Biomass-based porous N-self-doped carbon framework/polyaniline composite with outstanding supercapacitance. ACS Sustainable Chem Eng 2017;5:8663-74.

[475] Wu X, Tang L, Zheng S, Huang Y, Yang J, Liu Z, Yang W, Yang M. Hierarchical unidirectional graphene aerogel/polyaniline composite for high performance supercapacitors. J Power Sources 2018;397:189-95.

[476] Shao Y, El-Kady MF, Lin C-W, Zhu G, Marsh KL, Hwang JY, Zhang Q, Li Y, Wang H, Kaner RB. 3D freeze-casting of cellular graphene films for ultrahigh-power-density supercapacitors. Adv Mater 2016;28:6719-26.

[477] Bayram V, Ghidiu M, Byun JJ, Rawson SD, Yang P, McDonald SA, Lindley M, Fairclough S, Haigh SJ, Withers PJ, Barsoum MW, Kinloch IA, Barg S. MXene tunable lamellae architectures for supercapacitor electrodes. ACS Appl Energy Mater 2019;3:411-22.

[478] Sahoo PK, Kumar N, Thiyagarajan S, Thakur D, Panda HS. Freeze-Casting of Multifunctional cellular 3D-graphene/Ag nanocomposites: synergistically affect supercapacitor, catalytic, and antibacterial properties. ACS Sustainable Chem Eng 2018;6:7475-87.

[479] Zhang P, Zhu Q, Soomro RA, He S, Sun N, Qiao N, Xu B. In situ ice template approach to fabricate 3D flexible MXene film-based electrode for high performance supercapacitors. Adv Funct Mater 2020;30:2000922/1-10.

[480] Yue Y, Liu N, Ma Y, Wang S, Liu W, Luo C, Zhang H, Cheng F, Rao J, Hu X, Su J, Gao Y. Highly self-healable 3D microsupercapacitor with MXene-graphene composite aerogel. ACS Nano 2018;12:4224-32.

[481] Kong J, Xiong G, Bo Z, Lu X, Yi K, Kuang W, Yang S, Yang H, Tian S, Yan J, Cen K. Well-aligned hierarchical graphene-based electrodes for pseudocapacitors with outstanding low-temperature stability. ChemElectroChem 2019;6:2788-95.

[482] Liu X, Wang B, Jin Z, Wang H, Wang Q. Elastic ionogels with freeze-aligned pores exhibit enhanced electrochemical performances as anisotropic electrolytes of all-solid-state supercapacitors. J Mater Chem A 2015;3:15408-12.

[483] Liu X, Taiwo OO, Yin C, Ouyang M, Chowdhury R, Wang B, Wang H, Wu B, Brandon NP, Wang Q, Cooper SJ. Aligned ionogel electrolytes for high-temperature supercapacitors. Adv Sci 2019;6:1801337/1-7.

[484] Zhao Y, Alsaid Y, Yao B, Zhang Y, Zhang B, Bhuskute N, Wu S, He X. Wood-inspired morphologically tunable aligned hydrogel for high-performance flexible all-solid-state supercapacitors. Adv Funct Mater 2020;30:1909133/1-8.

[485] Li L, Zhang Y, Lu H, Wang Y, Xu J, Zhu J, Zhang C, Liu T. Cryopolymerization enables anisotropic polyaniline hybrid hydrogels with superelasticity and highly deformation-tolerant electrochemical energy storage. Nat Commun 2020;11:62/1-12.

[486] Chen S, Qiu L, Cheng HM. Carbon-based fibers for advanced electrochemical energy storage devices. Chem Rev 2020;120:2811-78.

[487] Huang Y, Wu D, Jiang J, Mai Y, Zhang F, Pan H, Feng X. Highly oriented macroporous graphene hybrid monoliths for lithium ion battery electrodes with ultrahigh capacity and rate capability. Nano Energy 2015;12:287-95.

[488] Roberts AD, Li X, Zhang H. Hierarchically porous sulfur-containing activated carbon monoliths via ice-templating and one-step pyrolysis. Carbon 2015;95:268-78.

[489] Zhang X, Ju Z, Housel LM, Wang L, Zhu Y, Singh G, Sadique N, Takeuchi KJ, Takeuchi ES, Marschilok AC, Yu G. Promoting transport kinetics in Li-ion battery with aligned porous electrode architectures. Nano Lett 2019;19:8255-61.

[490] Liu M, Yang Z, Sun H, Lai C, Zhao X, Peng H, Liu T. A hybrid carbon aerogel with both aligned and interconnected pores as interlayer for high-performance lithium–sulfur batteries. Nano Res 2016;9:3735-46.

[491] Amin R, Delattre B, Tomsia AP, Chiang Y-M. Electrochemical characterization of high energy density graphite electrodes made by freeze-casting. ACS Appl Energy Mater 2018;1:4976-81.

[492] Park H, Choi H, Nam K, Lee S, Um JH, Kim K, Kim J-H, Yoon W-S, Choe H. Anode design based on microscale porous scaffolds for advanced lithium ion batteries. J Electron Mater 2017;46:3789-95.

[493] Um JH, Choi M, Park H, Cho YH, Dunand DC, Choe H, Sung YE. 3D macroporous electrode and high-performance in lithium-ion batteries using SnO_2 coated on Cu foam. Sci Rep 2016;6:18626/1-9.

[494] Ju Z, Zhu Y, Zhang X, Lutz DM, Fang Z, Takeuchi KJ, Takeuchi ES, Marschilok AC, Yu G. Understanding thickness-dependent transport kinetics in nanosheet-based battery electrodes. Chem Mater 2020;32:1684-92.

[495] Delattre B, Amin R, Sander J, De Coninck J, Tomsia AP, Chiang Y-M. Impact of pore tortuosity on electrode kinetics in lithium battery electrodes: study in directionally freeze-cast $LiNi_{0.8}Co_{0.15}Al_{0.05}O_2$(NCA). J Electrochem Soc 2018;165:A388-A95.

[496] Jung WK, Baek C, Kim J-H, Moon S, Kim DS, Jung YH, Kim DK. A highly-aligned lamellar structure of ice-templated $LiFePO_4$ cathode for enhanced rate capability. Mater Des 2018;139:89-95.

[497] Pan ZZ, Lv W, He YB, Zhao Y, Zhou G, Dong L, Niu S, Zhang C, Lyu R, Wang C, Shi H, Zhang W, Kang F, Nishihara H, Yang QH. A nacre-like carbon nanotube sheet for high performance Li-polysulfide batteries with high sulfur loading. Adv Sci 2018;5:1800384/1-7.

[498] Zhai H, Xu P, Ning M, Cheng Q, Mandal J, Yang Y. A flexible solid composite electrolyte with vertically aligned and connected ion-conducting nanoparticles for lithium batteries. Nano Lett 2017;17:3182-7.

[499] Wang X, Zhai H, Qie B, Cheng Q, Li A, Borovilas J, Xu B, Shi C, Jin T, Liao X, Li Y, He X, Du S, Fu Y, Dontigny M, Zaghib K, Yang Y. Rechargeable solid-state lithium metal batteries with vertically aligned ceramic nanoparticle/polymer composite electrolyte. Nano Energy 2019;60:205-12.

[500] Tang W, Tang S, Guan X, Zhang X, Xiang Q, Luo J. High-performance solid polymer electrolytes filled with vertically aligned 2D materials. Adv Funct Mater 2019;29:1900648/1-7.

[501] Stolze C, Janoschka T, Flauder S, Müller FA, Hager MD, Schubert US. Investigation of ice-templated porous electrodes for application in organic batteries. ACS Appl Mater Interfaces 2016;8:23614-23.

[502] Liu M, Zhang P, Qu Z, Yan Y, Lai C, Liu T, Zhang S. Conductive carbon nanofiber interpenetrated graphene architecture for ultra-stable sodium ion battery. Nature Commun 2019;10:3917/1-11.

[503] He Z, Liu J, Qiao Y, Li CM, Tan TT. Architecture engineering of hierarchically porous chitosan/vacuum-stripped graphene scaffold as bioanode for high performance microbial fuel cell. Nano Lett 2012;12:4738-41.

[504] Zhao Z, Sun M, Chen W, Liu Y, Zhang L, Dongfang N, Ruan Y, Zhang J, Wang P, Dong L, Xia Y, Lu H. Sandwich, vertical-channeled thick electrodes with high rate and cycle performance. Adv Funct Mater 2019;29:1809196/1-13.

[505] Huang C, Dontigny M, Zaghib K, Grant PS. Low-tortuosity and graded lithium ion battery cathodes by ice templating. J Mater Chem A 2019;7:21421-31.

[506] Chen H, Pei A, Wan J, Lin D, Vilá R, Wang H, Mackanic D, Steinrück H-G, Huang W, Li Y, Yang A, Xie J, Wu Y, Wang H, Cui Y. Tortuosity effects in lithium-metal host anodes. Joule 2020;4:938-52.

[507] Yin Y-C, Yu Z-L, Ma Z-Y, Zhang T-W, Lu Y-Y, Ma T, Zhou F, Yao H-B, Yu S-H. Bio-inspired low-tortuosity carbon host for high-performance lithium-metal anode. Nat Sci Rev 2019;6:247-56.

[508] Yu Y, Zhang H, Yang X, Gou J, Tong X, Li X, Zhang H. Vertically aligned laminate porous electrode: amaze the performance with a maze structure. Energy Storage Mater 2019;19:88-93.

[509] Deville S. Freeze-casting of porous biomaterials: structure, properties and opportunities. Materials 2010;3:1913-27.

[510] Nardecchia S, Serrano MC, Garcia-Arguelles S, Maia Da Costa MEH, Ferrer ML, Gutierrez MC. Ice as a green-structure-directing agent in the synthesis of macroporous MWCNTs and chondroitin sulphate composites. Materials 2017;10:355/1-16.

[511] Aliramaji S, Zamanian A, Mozafari M. Super-paramagnetic responsive silk fibroin/chitosan/magnetite scaffolds with tunable pore structures for bone tissue engineering applications. Mater Sci Eng C 2017;70:736-44.

[512] Jana S, Cooper A, Zhang M. Chitosan scaffolds with unidirectional microtubular pores for large skeletal myotube generation. Adv Healthc Mater 2013;2:557-61.

[513] Riblett BW, Francis NL, Wheatley MA, Wegst UGK. Ice-templated scaffolds with microridged pores direct DRG neurite growth. Adv Funct Mater 2012;22:4920-3.

[514] Wang D, Romer F, Connell L, Walter C, Saiz E, Yue S, Lee PD, McPhail DS, Hanna JV, Jones JR. Highly flexible silica/chitosan hybrid scaffolds with oriented pores for tissue regeneration. J Mater Chem B 2015;3:7560-76.

[515] Pourhaghgouy M, Zamanian A, Shahrezaee M, Masouleh MP. Physicochemical properties and bioactivity of freeze-cast chitosan nanocomposite scaffolds reinforced with bioactive glass. Mater Sci Eng C 2016;58:180-6.

[516] Gutiérrez MC, García-Carvajal ZY, Jobbágy M, Rubio F, Yuste L, Rojo F, Ferrer ML, del Monte F. Poly(vinyl alcohol) scaffolds with tailored morphologies for drug delivery and controlled release. Adv Funct Mater 2007;17:3505-13.

[517] Gutiérrez MC, García-Carvajal ZY, Jobbágy M, Yuste L, Rojo F, Abrusci C, Catalina F, del Monte F, Ferrer ML. Hydrogel scaffolds with immobilized bacteria for 3D cultures. Chem Mater 2007;19:1968-73.

[518] Wicklein B, Aranda P, Ruiz-Hitzky E, Darder M. Hierarchically structured bioactive foams based on polyvinyl alcohol–sepiolite nanocomposites. J Mater Chem B 2013;1:2911-20.

[519] Munir N, Callanan A. Novel phase separated polycaprolactone/collagen scaffolds for cartilage tissue engineering. Biomed Mater 2018;13:051001/1-7.

[520] He F, Ye J. In vitro degradation, biocompatibility, and in vivo osteogenesis of poly(lactic-co-glycolic acid)/calcium phosphate cement scaffold with unidirectional lamellar pore structure. J Biomed Mater Res A 2012;100:3239-50.

[521] Schardosim M, Soulie J, Poquillon D, Cazalbou S, Duployer B, Tenailleau C, Rey C, Hubler R, Combes C. Freeze-casting for PLGA/carbonated apatite composite scaffolds: structure and properties. Mater Sci Eng C 2017;77:731-8.

[522] Wan AM, Inal S, Williams T, Wang K, Leleux P, Estevez L, Giannelis EP, Fischbach C, Malliaras GG, Gourdon D. 3D conducting polymer platforms for electrical control of protein conformation and cellular functions. J Mater Chem B 2015;3:5040-8.

[523] Xue J, Gao H-L, Wang X-Y, Qian K-Y, Yang Y, He T, He C, Lu Y, Yu S-H. Bioinspired unidirectional silk fibroin–silver compound nanowire composite scaffold via interface-mediated in situ synthesis. Angew Chem Int Ed 2019;58:14152-6.

[524] Hoogenkamp HR, Pot MW, Hafmans TG, Tiemessen DM, Sun Y, Oosterwijk E, Feitz WF, Daamen WF, van Kuppevelt TH. Scaffolds for whole organ tissue engineering: construction and in vitro evaluation of a seamless, spherical and hollow collagen bladder construct with appendices. Acta Biomater 2016;43:112-21.

[525] Bai H, Polini A, Delattre B, Tomsia AP. Thermoresponsive composite hydrogels with aligned macroporous structure by ice-templated assembly. Chem Mater 2013;25:4551-6.

[526] Chen D, Zhang Y, Ni C, Ma C, Yin J, Bai H, Luo Y, Huang F, Xie T, Zhao Q. Drilling by light: ice-templated photo-patterning enabled by a dynamically crosslinked hydrogel. Mater Horiz 2019;6:1013-9.

[527] Zhou L, Tang L-S, Tao X-F, Yang J, Yang M-B, Yang W. Facile fabrication of shape-stabilized polyethylene glycol/cellulose nanocrystal phase change materials based on thiol-ene click chemistry and solvent exchange. Chem Eng J 2020;396:125206/1-10.

[528] Wu J, Hu R, Zeng S, Xi W, Huang S, Deng J, Tao G. Flexible and robust biomaterial microstructured coloured textiles for personal thermoregulation. ACS Appl Mater Interfaces 2020;12:19015-22.

[529] Wang Y, Cui Y, Shao Z, Gao W, Fan W, Liu T, Bai H. Multifunctional polyimide aerogel textile inspired by polar bear hair for thermoregulation in extreme environments. Chem Eng J 2020;390:124623/1-8.

[530] Hwa Y, Yi E, Shen H, Sung Y, Kou J, Chen K, Parkinson DY, Doeff MM, Cairns EJ. Three-dimensionally aligned sulfur electrodes by directional freeze tape casting. Nano Lett 2019;19:4731-7.

[531] Dang D, Wang Y, Gao S, Cheng Y-T. Freeze-dried low-tortuous graphite electrodes with enhanced capacity utilization and rate capability. Carbon 2020;159:133-9.

[532] Kholmanov I, Kim J, Ou E, Ruoff RS, Shi L. Continuous carbon nanotube–ultrathin graphite hybrid foams for increased thermal conductivity and suppressed subcooling in composite phase change materials. ACS Nano 2015;9:11699-707.

[533] Geng H, Liu X, Shi G, Bai G, Ma J, Chen J, Wu Z, Song Y, Fang H, Wang J. Graphene oxide restricts growth and recrystallization of ice crystals. Angew Chem Int Ed 2017;56:997-1001.

[534] Bai G, Gao D, Liu Z, Zhou X, Wang J. Probing the critical nucleus size for ice formation with graphene oxide nanosheets. Nature 2019;576:437-41.

[535] Chen HB, Liu B, Huang W, Wang JS, Zeng G, Wu WH, Schiraldi DA. Fabrication and properties of irradiation-cross-linked poly(vinyl alcohol)/clay aerogel composites. ACS Appl Mater Interfaces 2014;6:16227-36.

[536] Wang P-C, Huang W, Liu B, Liu J-Y, Chen H-B. Post-irradiation crosslinking of silicone foam induced by 60Co gamma ray. Polym Degrad Stab 2019;160:73-9.